THE UNIVERSITY
of EDINBURGH

Improvement of modelling human exposure to NO_2 in cities in China – the case of Guangzhou

THE UNIVERSITY
of EDINBURGH

Baihuiqian He

A thesis submitted in fulfilment of the requirements

for the degree of Doctor of Philosophy

The University of Edinburgh

2020

Declaration

I declare that this thesis was composed by myself, that the work contained herein is my own except where explicitly stated otherwise in the text, and that this work has not been submitted for any other degree or professional qualification except as specified.

Chapter 3 and Chapter 4 of this thesis have been published in

He, B., Heal, M.R., Reis, S., 2018. Land-use regression modelling of intra-urban air pollution variation in China: current status and future needs. Atmosphere 9, 134. https://doi.org/10.3390/atmos9040134

He, B., Heal, M.R., Humstad, K.H., Yan, L., Zhang, Q., Reis, S., 2,019. A hybrid model approach for estimating health burden from NO_2 in megacities in China: a case study in Guangzhou. Environ. Res. Lett. 14, 124019. https://doi.org/10.1088/1748-9326/ab4f96

Chapter 5 of this thesis has submitted to Environmental Research Communications.

June 2020

Lay Summary

Nitrogen dioxide (NO_2) is an air pollutant identified as a public health concern. Studies show that it is related to respiratory diseases and premature deaths. It also contributes to formation of fine particles [1] ($PM_{2.5}$ particles with aerodynamic diameters <2.5 μm) in the presence of light and ozone (O_3). The World Health Organisation (WHO) specifies the guideline concentration of 40 μg m^{-3} (annual mean) to protect the public and Directive 2008/50/EC of the European Parliament on ambient air quality and cleaner air for Europe sets the same limit value. Governments all over the world use monitoring and modelling as part of the process of managing concentrations of NO_2.

Because NO_2 is emitted from all kinds of combustions in an urban area, and it has a relatively short atmospheric lifetime (due to its rapid chemical reactions), urban concentrations of NO_2 vary dramatically at different locations and time. A monitoring network can only measure concentrations at a limited number of discrete points which is inadequate to describe the spatial variability of NO_2, and hence also human exposure to NO_2 for estimating health impacts. For example, the concentration near busy roads can be several times higher than that at background locations. Modelling methods are therefore often used in most developed countries for estimating concentrations at locations without measurements in order to evaluate health impacts and to assess the effectiveness of mitigation approaches.

Rapid economic growth, industrialization, and urbanization in China are leading to substantial adverse air quality issues, including high levels of annual mean NO_2 concentrations. In China, air quality is primarily protected under the Environmental Protection Law (EPL) and the Law of the Prevention and

[1] Exposure to $PM_{2.5}$ is estimated to have been responsible for 4.2 million premature deaths worldwide in 2016.

Control of Atmospheric Pollution (LPCAP). Air quality management in China is largely driven by the ambition to attain the National Ambient Air Quality Standard (NAAQS) (GB3095-2012) and specific targets set by local governments under Chapter 2 of the LPCAP. Since 2013, China has been implementing a nationwide monitoring network for the routine measurement of ambient air pollutant concentrations including NO_2. Despite the wide coverage over the country, the number of sites in each city is limited—for example, the 22 monitoring stations covering a 50 km × 50 km area over Beijing equates to an average of 113 km^2 per station. The air pollution modelling is also in the early development stage with most modelling studies set up at regional scale and a deficiency of more spatially resolved urban/street level modelling.

Guangzhou is chosen as an exemplar geographic domain. It is the third largest city in China, with a population of 14 million and an area of 7,433 km^2, and does not currently meet the NAAQS for NO_2, which is set as the same as the WHO guideline. The Guangzhou Municipal People's Government has developed the Guangzhou Ambient Air Quality Compliance Plan (GAAQCP) which aspires to reach annual average NO_2 concentrations of 40 μg m^{-3} by 2020. Urban-scale air quality modelling is needed to fill the gaps of estimating human exposure of NO_2 and to investigate the ability of a range of example emission reduction scenarios to meet the GAAQCP.

The overall aim of this PhD project is to explore modelling approaches for better estimating intra-urban variability of NO_2 for human exposure research in China, given the obstacles in data availability of monitor data, emission inventories, and other high spatial resolved data in China.

Two modelling methods are widely used to simulate pollutant concentrations at relatively high spatial resolution within urban areas: dispersion modelling and land-use regression (LUR) modelling. Dispersion modelling aims to

simulate the physical chemical processes that link the emissions of pollutants from sources and their transport and dispersion. Recently, urban dispersion models have been developed for Beijing, Shanghai, Chongqing, Hangzhou, Kunming, Hong Kong, Harbin, Lanzhou, Urumqi, Liaoning province, Jinan, Fushun, and Macao, but substandard modelling results can arise due to insufficient monitor data and incomplete or inaccurate emission inventories.

LUR relies on existing measurements to derive the statistical relationship between pollutant concentrations at a given location and predictor variables representing the emission and dispersion of air pollutants. This relationship is extrapolated to predict concentrations at locations without measurements. For this reason, an appropriately sized and designed monitoring network is an important component for the development of a robust LUR model. LUR models are now being extensively applied to simulate pollutant concentrations in Chinese urban areas, but the quality of modelling results is currently constrained by a scarcity of input data, especially air pollution monitor data.

Given the limited number of monitoring sites in Guangzhou and the geographical scale of the domain, an integrated modelling approach combining dispersion modelling with ADMS-Urban [2] and LUR has been developed in this PhD work. Concentrations of NO_2 are simulated by ADMS-Urban at pre-selected 'virtual' monitoring sites spanning the six districts in Guangzhou and weighting towards population (since the overall focus is estimation of population NO_2 exposure). The LUR model is validated against both the virtual sites and independently against available observations. The modelled population-weighted long-term average concentration of NO_2 in the

[2] ADMS-Urban is a a widely-used dispersion model for simulating dispersion in the atmosphere of continuous releases from a range of explicit sources in an urban area developed by Cambridge Environmental Research Consultants (CERC) https://www.cerc.co.uk/

year 2017 across Guangzhou was 52.5 μg m^{-3}, which contributes an estimated 7,270 (6,960−7,620) attributable deaths.

This hybrid modelling approach is then applied to explore the scale of emissions reductions necessary within the Guangzhou domain to achieve compliance with a number of different interpretations of an NO_2 concentration target of 40 μg m^{-3}, since the GAAQCP does not explicitly state how to practically assess compliance. The modelling results show that achieving compliance required different levels of emission reductions, depending on how the concentration target was defined; for example, to reduce the average concentration at all monitoring sites below 40 μg m^{-3} requires a 60% reduction of emissions from all source sectors. In contrast, to attain ≤40 μg m^{-3} concentration across the whole of Guangzhou requires a 90% emissions reduction. The impacts of the emissions reductions on NO_2-atttributable premature mortality are also calculated and illustrate that use of a concentration value as a target does not fully convey the underlying health gains; what is fundamentally relevant to potential policy measures is not the change in proportion of locations with NO_2 concentrations ≤40 μg m^{-3}, nor the change in the numbers of people in locations with NO_2 concentrations ≤40 μg m^{-3}, but by how much the cumulative population exposure changes.

Whilst the results are based on detailed and consistent model results for the specific situation in Guangzhou, they are relevant for, and can provide evidence to, decision makers designing effective air pollution control policies in other fast-growing megacities in China and elsewhere globally. In the final part of this thesis, the findings and implications from the modelling studies are discussed. The hybrid modelling approach provides a step forward in modelling urban-scale air pollution concentrations for human exposure and policy analysis.

Abstract

Nitrogen dioxide (NO_2) is an air pollutant identified as a public health concern. Exposure to NO_2 is associated with a number of adverse respiratory health effects, and ultimately with premature mortality. It also contributes as a precursor to formation of tropospheric ozone (O_3) and ammonium nitrate fine particulate matter ($PM_{2.5}$, particles with aerodynamic diameters <2.5 μm).

Rapid economic growth, industrialization, and urbanization in China are leading to substantial adverse air quality issues, including high levels of annual mean NO_2 concentrations. It is important to quantify human exposure to NO_2 to evaluate its health impacts and to assess the effectiveness of mitigation approaches. Since 2013, the China National Environmental Monitoring Centre (CNEMC) has been implementing a nationwide monitoring network for the routine measurement of ambient air pollutant concentrations. Previous studies into population exposure used the monitor data as a proxy for human exposure. However, NO_2 concentrations within cities have shown high spatial variations. The monitoring network only provides concentrations at a limited number of discrete points, which is inadequate to describe the spatial variability of urban air pollution. New methods need to be developed to tackle these challenges. The overall aim of this PhD project is to explore modelling approaches for better estimating intra-urban variability of NO_2 for human exposure research in China, given the obstacles in data availability of monitored data, emission inventories, and other highly spatially resolved data in China.

Guangzhou is chosen as an exemplar geographic domain. It is the third largest city in China, with a population of 14 million and an area of 7,433 km^2, and does not currently meet the Chinese air quality standard (GB 3095-2012) for NO_2, which is set as 40 μg m^{-3} as an annual average. The Guangzhou local

government has an air quality compliance plan that aspires to annual average NO_2 concentrations of 40 μg m^{-3} by 2020.

Two modelling methods are widely used to simulate pollutant concentrations at relatively high spatial resolution within urban areas: dispersion modelling and land-use regression (LUR) modelling. Dispersion modelling aims to simulate the physical chemical processes that link the emissions of pollutants from sources and their transport and dispersion. Recently, urban dispersion models have been developed in Beijing, Shanghai, Chongqing, Hangzhou, Kunming, Hong Kong, Harbin, Lanzhou, Urumqi, Liaoning province, Jinan, Fushun, and Macao using ADMS and AERMOD. Substandard modelling results can arise due to insufficient monitor data and incomplete or inaccurate emission inventories. LUR relies on existing measurements to derive the statistical relationship between pollutant concentrations at a given location and predictor variables representing the emission and dispersion of air pollutants. An appropriately sized and designed monitoring network is an important component for the development of a robust LUR model.

LUR models are now being applied to simulate pollutant concentrations with high spatial resolution in Chinese urban areas. Current challenges and future needs in employing LUR approaches were identified first in this PhD work. Details of twenty-four recent LUR models for NO_2 and $PM_{2.5}$/PM_{10} (particles with aerodynamic diameters <10 μm) were reviewed. LUR modelling in China is currently constrained by a scarcity of input data, especially air pollution monitor data. There is an urgent need for accessible archives of quality-assured measurement data and for higher spatial resolution proxy data for urban emissions, particularly in respect of traffic-related variables. The rapidly evolving nature of the Chinese urban landscape makes maintaining up-to-date land-use and urban morphology datasets essential for LUR models.

Given the limited number of monitoring sites in Guangzhou and the geographical scale of the domain, an integrated modelling approach combining dispersion modelling with ADMS-Urban and LUR has been developed in this PhD work. ADMS-Urban was applied in Guangzhou using input data including emissions from the Multi-resolution Emission Inventory for China (MEIC), road geometry from OpenStreetMap, and hourly meteorological data from the European Centre for Medium-Range Weather Forecasts (ECMWF). Concentrations of NO_2 were simulated by ADMS-Urban at 83 'virtual' monitoring sites spanning the six districts in Guangzhou and weighted according to population (since the overall focus is estimation of population NO_2 exposure). The LUR model was validated against both the 83 virtual sites (adj R^2: 0.96, RMSE: 5.48 μg m^{-3}; LOOCV R^2: 0.96, RMSE: 5.64 μg m^{-3}) and, independently, against available observations (n = 11, R^2: 0.63, RMSE: 18.0 μg m^{-3}). The modelled population-weighted long-term average concentration of NO_2 across Guangzhou in 2017 was 52.5 μg m^{-3}, which contributes an estimated 7,270 (6,960−7,620) attributable deaths.

This hybrid modelling approach is then applied to explore the scale of emissions reductions necessary within the Guangzhou domain to achieve compliance with a number of different interpretations of an NO_2 concentration target of 40 μg m^{-3}. (The Guangzhou Ambient Air Quality Compliance Plan does not explicitly state how to practically assess compliance.) The modelling results show that achieving compliance requires different levels of emission reductions, depending on how the concentration target was defined; for example, to reduce the average concentration at all monitoring sites below 40 μg m^{-3}, requires a 60% reduction of emissions from all source sectors. In contrast, to attain ≤40 μg m^{-3} concentration across the whole of Guangzhou requires a 90% emissions reduction. The impacts of the emissions reductions on NO_2-atttributable premature mortality are also calculated and illustrate that use of a concentration value as a target does not fully convey the underlying health gains even when the target is not met.

In the final part of this thesis, the findings and implications from the modelling studies are discussed in the context of current air quality management system in China. Whilst the results are based on detailed and consistent model results for the specific situation in Guangzhou, they are relevant for, and can provide evidence to, decision makers designing effective air pollution control policies in other fast-growing megacities in China and elsewhere globally. The challenges and limitations for the development of a highly spatial revolved model for human exposure are discussed.

Acknowledgements

I have been interested in environmental pollution since I was in primary school, because I witnessed the disappearing natural world and the rising urbanization-related pollution. But before I met my supervisors, I had never thought that I could really do something about it. Everything started with my MSc project on the Contribution of Railway Emissions to Local Particulate Matter Concentrations, where working with Stefan made me able to appreciate the beauty and fun of research. But even before that, Mat's lecture on atmospheric chemistry led me into the beautiful and complex world of the atmosphere. I am fortunate enough to have met them and to have had the opportunity to pursue the questions I have always been interested with their support. I appreciated the weekly meetings with them to discuss issues and spark new ideas, as well as their fast and countless comments on drafts I sent. Thanks to them, this PhD has been a beautiful journey for me.

The groups in Edinburgh university and CEH have made this journey smooth and enjoyable. I would like to thank Chun Lin and Hao Wu for helping me learn R. Edward Carnell and David Leaver in CEH also gave me a lot of support in terms of data analysis and making plots. The MSc project student Kamilla H Humstad who helped me learn GIS. The MACAQUE group meeting with colleagues from the School of GeoSciences motivated me to produce present interesting results and discuss with them.

Thank you to the two venues where I sat and wrote most: my home-office and Room 275 in Joseph Black Building. I would also like to thank the websites which I acquired many skills from: Google, YouTube, and Lynda.

I am also grateful to the China Scholarship Council and the School of Chemistry. My life would be totally different without the funding provided by them.

Finally, I would like to thank my parents for their love and support.

Contents

List of Figures

List of Tables

Acronyms and Abbreviations

[3] NO_x emissions are always expressed as kt-NO_2 unless otherwise stated.

Chapter 1 Introduction

1.1 Air pollution

1.1.1 Sources of air pollution

The growth of population and the global economy drives industrialization and urbanization. The demand for energy consumption and transportation consequently also increases, which then imposes pressure on air quality. Most forms of anthropogenic energy use are based on combustion, which forms carbon dioxide (CO_2), and, depending on the nature of the fuel and the process, some or all of carbon monoxide (CO), unburnt hydrocarbons, nitrogen oxides (NO and NO_2, collectively termed NO_x), sulfur oxides (SO_x) and particulate matter (PM). The combustion process happens in all sectors: power generation, industry, domestic, transportation, and uncontrolled waste and agricultural residue burning. NO_x is formed in combustion systems mostly as nitric oxide (NO) by three mechanisms (Figure 1.1): thermal-NO (oxidation of atmospheric nitrogen, N_2, at high temperature), prompt-NO (oxidation of N_2 with radicals derived from fuel), and fuel-NO mechanisms (conversion of nitrogen chemically bound in certain fuels).

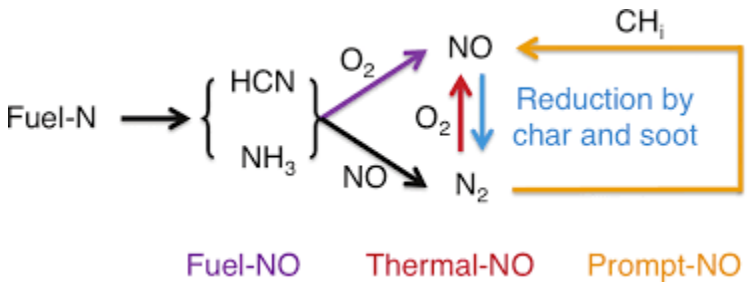

Figure 1.1 Schematic representation of NO formation in a coal combustion system (Vekemans and Chaouki, 2016).

Other air pollutants such as ammonia (NH_3), and methane (CH_4) also have large sources in the agriculture sector through fertilizer application, enteric fermentation, and livestock manure and manure storage. Natural sources of air pollution include forest fires, volcanoes and biogenic volatile organic compounds (VOCs) emitted from vegetation (Vallero, 2014).

1.1.2 Physical and chemical processes

The changes in atmospheric composition are caused by physical processes and chemical reactions. The physical movement of pollutants in the atmosphere are advection, dispersion, and deposition. Advection is the movement caused by the wind, which moves the pollution from a source to a receptor. Dispersion results from local turbulence, which exchange air parcels from the edges of the plume to the surrounding (Vallero, 2014; Watson et al., 1988). The pollutants are deposited in the atmospheric boundary layer (also known as planetary boundary layer PBL), lowest part of the atmosphere and where many chemical reactions happen. Deposition is the processes that cause removal of the pollutants to the ground surface and includes dry deposition, i.e., the uptake at the Earth's surface (soil, water, or vegetation), and wet deposition, i.e., absorption into droplets followed by precipitation (e.g., by rain) (Watson et al., 1988; Zannetti, 1990).

For example, in the PBL, the concentration of NO_2 at a given location is affected by the proximity of emissions sources, the rate of NO_x emissions, how the emissions are dispersed, and chemical coupling of NO_x with O_3 and VOCs. NO_x undergoes both photochemical and dark chemical cycles (Figure 1.2). The main reactions in NO_x cycle are:

(R 1-1) $NO_2 + h\nu \rightarrow NO + O$

(R 1-2) $O + O_2 + M \rightarrow O_3 + M$

(R 1-3) $NO + O_3 \rightarrow NO_2 + O_2$

where M is a non-reacting molecule (normally N_2) that removes reaction energy and the photolysis of NO_2 only happens at wavelengths < 424 nm. The primary pollutant NO is converted to NO_2 via the reaction with O_3 (R 1-3). This happens at locations close to the sources of NO_x, where NO is in large excess, and in the absence of VOCs. During daytime, NO_2 is converted to NO producing O_3 (R 1-1 and R 1-2).

However, in the presence of VOCs, the O_3 concentration increases after NO is converted to NO_2 due to the formation of radicals (R 1-4 and R 1-5).

(R 1-4) $HO_2 + NO \rightarrow OH + NO_2$

(R 1-5) $RO_2 + NO \rightarrow RO + NO_2$

In these reactions, HO_2 is a hydroperoxyl radical, a by-product of the oxidation of carbon monoxide (CO) and of hydrocarbons by the hydroxy radical (HO). RO_2 is a peroxy radical. HO, RO_2 and HO_2 (HO_x) radicals initiate and propagate the chain reactions that lead to O_3 formation in the troposphere.

At night, NO reacts with O_3 rapidly and NO_2 reacts with O_3 to produce the nitrate (NO_3) radical and generate nitrate aerosol (R 1-6 to R 1-8). During the day, NO_2 is removed by (R 1-9).

(R 1-6) $NO_2 + O_3 \rightarrow NO_3 + O_2$

(R 1-7) $NO_3 + NO_2 + M \leftrightarrows N_2O_5 + M$

(R 1-8) $N_2O_5 + H_2O \rightarrow 2HNO_3$

(R 1-9) $OH + NO_2 + M \rightarrow HNO_3 + M$

R 1-1 to R 1-3 form a null cycle whereby NO_2, NO, O and O_3 are in photochemical equilibrium. The net effect on production or loss of O_3 highly

depends on the amount of NO_x present in the atmosphere. In low emission regions, NO_x is the catalyst that produces O_3 (R 1-1 and R 1-2), whilst in urban regions with high NO levels, R 1-3 dominates leading to lower O_3 levels.

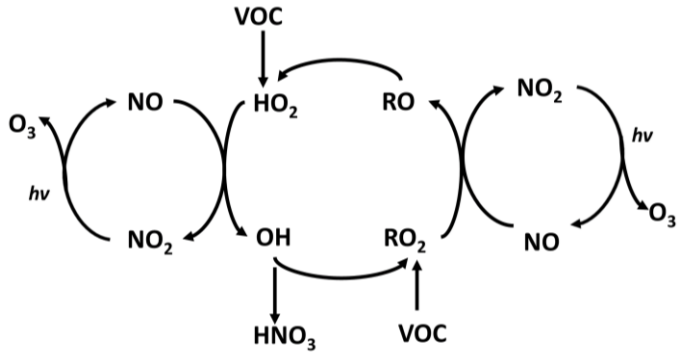

Figure 1.2 Diagram of NO_x cycle and RO_x ($RO_x = OH+HO_2+RO_2$) cycle. Adapted from (T. Wang et al., 2017)

Because of the way emission sources are physically distributed in an urban area and the relatively short atmospheric lifetime of NO_2, urban concentrations show high spatial and temporal (day-to-day and diurnal) variations (Cyrys et al., 2012).

1.2 Impacts of air pollution

1.2.1 Health impacts

Elevated levels of ambient air pollutants are the biggest environmental risk to human health globally (Babatola, 2018; WHO, 2018). Exposure to outdoor fine particulate matter ($PM_{2.5}$, particles with aerodynamic diameters <2.5 μm) is estimated to have been responsible for 4.2 million premature deaths worldwide in 2016, making it the fifth greatest risk factor globally for premature deaths, and to have contributed more than 100 million disability-adjusted life-years globally (Cohen et al., 2017). A recent comprehensive review indicates that air

pollution may damage every organ and tissue from pollutant toxicity or through inflammatory processes in the human body (Schraufnagel et al., 2019a, 2019b).

Due to its low water solubility, NO_2 can reach the lower respiratory tract, including the lung alveoli. The strong oxidizing property of NO_2 makes it irritable to respiratory system. NO_2 has been reported to be associated with respiratory inflammation (Jiang et al., 2019), which is widely considered to be a critical pathophysiological basis for impaired lung function (Lokwani et al., 2019). Short-term exposure to NO_2 (i.e. <24 h) is associated with increased hospitalisations, respiratory symptoms such as bronchitis and asthma, and mortality (Brunekreef and Holgate, 2002; Chiusolo et al., 2011; Weinmayr et al., 2010; WHO, 2013). Long-term exposure to ambient NO_2 is associated with premature mortality and hypertension (Brunekreef and Holgate, 2002; Cai et al., 2016; Crouse et al., 2015; Faustini et al., 2014; Hoek et al., 2013; WHO, 2013a).

However, it is uncertain whether the effects of NO_2 are independent from concomitant exposure to other air pollutants (COMEAP, 2018; Samoli et al., 2006). Correlations between NO_2 and other traffic pollutants such as primary combustion particles, particle number concentration, CO, or polycyclic aromatic hydrocarbons (PAHs) are likely to be very high. This would have made it difficult to interpret multi-pollutant models. There is also insufficient evidence to assess possible confounding of NO_2 associations by O_3 and noise. However, O_3 can be negatively correlated with NO_2 which might increase the estimated NO_2 coefficient after adjustment. Using measurements from fixed-site stations as surrogates for the exposure levels of NO_2 may result in considerable and uncertain exposure errors and lead to inconsistent results from previous epidemiological studies (Delfino Ralph J. et al., 2006)

1.2.2 Environmental impacts

In addition to the harm caused to human health, air pollution can also impair ecosystem function: for example, tropospheric ozone (O_3) formed in the air through reactions between VOCs and NO_x and sunlight causes damage to agricultural and horticultural crops and natural vegetation (Ashmore, 2005; Feng et al., 2015; Mills et al., 2018, 2016; The Royal Society, 2008; Wang et al., 2017a), whilst deposition of reactive nitrogen components (NO_2, HNO_3 and NH_3, and their dissolved equivalents) leads to eutrophication and consequently to biodiversity changes (Erisman et al., 2015; Stevens et al., 2010; Sutton et al., 2011).

1.3 Modelling air pollution

Atmospheric models can be divided into deterministic modelling, which is based on the fundamental description of atmospheric physical and chemical processes and stochastic modelling which is based on statistical analysis of data (Seinfeld and Pandis, 2016). Deterministic modelling involves describing emission patterns, meteorology, chemical transformations, and removal process and it is an essential tool for establishing emission fluxes and ambient concentrations for policy scenario analysis. The three basic components are species emissions, transport, and physicochemical transformations (Figure 1.3). Because a pollutant released from traffic or industries in a city may have a significant impact on the city or much further afield, according to the properties and atmospheric lifetime of the pollutant, atmospheric models can be divided into five scales (global; continental; regional: 5-50 km; urban: 1-5 km; local: 1 km and street) (Table 1.1). By far the main emphasis of research in past decades in atmospheric chemistry has been on the global and regional atmosphere. However, a large percentage of global population live in cities and that cities present a very special case as far as atmospheric composition and physics are concerned. The chemistry and physics are different at urban

scale. As a result, a range of street-scale-resolution air quality modelling techniques have recently emerged. Land-use regression (LUR) and dispersion modeling are widely used at street-scale-resolution and details of the two models will be discussed in Chapter 2 .

Table 1.1 Atmospheric models defined according to their spatial scale (Seinfeld and Pandis, 2016).

Model	Typical domain scale	Typical spatial resolution
Microscale (street)	200 m × 200 m × 100 m	5 m
Mesoscale (urban)	100 km × 100 km × 5 km	2 km
Regional	1,000 km × 1,000 km × 10 km	20 km
Synoptic (continental)	3,000 km × 3,000 km × 20 km	80 km
Global	40,000 km × 40,000 km × 20 km	5°

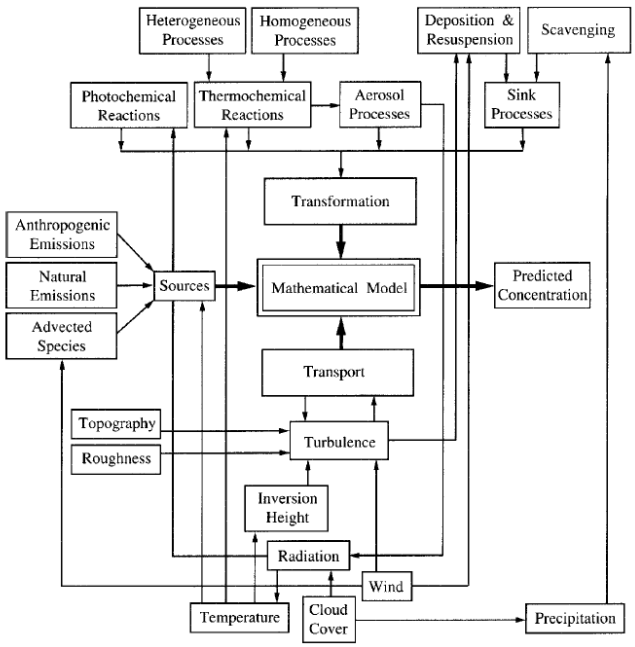

Figure 1.3 Elements of a mathematical atmospheric chemical transport model (Seinfeld and Pandis, 2016).

1.4 Air pollution and governments' responses in China

1.4.1 Air pollution in China

Rapid economic growth, industrialization, and urbanization are leading to substantial air pollution challenges in China (Chen et al., 2016; He et al., 2002; Liu and Diamond, 2005; Song et al., 2017; Vennemo et al., 2009; H. Wang et al., 2017; T. Wang et al., 2017; Zhang et al., 2012). In 2016, 81%, 62%, 46%, 38%, 4.1% and 1.4% of 74 main cities in China (including provincial capitals and prefectural and municipality-level cities) failed the Chinese air quality standards that are listed in Table 1.2 for $PM_{2.5}$, PM_{10}, NO_2, O_3, CO and SO_2, respectively (Ministry of Environmental Protection, 2018a). Furthermore, while the Chinese air quality standard for NO_2 is the same as the World Health Organization (WHO) air quality guideline, those for $PM_{2.5}$, PM_{10}, and O_3 are currently less stringent than the WHO equivalents (Table 1.2). The air quality problem is particularly serious in regions of rapid population growth such as Beijing, Shanghai, the Pearl River Delta (PRD)[4] (Wang and Hao, 2012). Ample evidence that air pollution leads to adverse health effects and economic losses, including recent studies in China (Chen et al., 2017; R. Chen et al., 2013b, 2013a, 2012; Y. Chen et al., 2013; Kan et al., 2009; Yin et al., 2017) underscores the need to quantify human exposure to air pollution in China in order to determine health impacts and monitor the effectiveness of mitigation policies.

[4] Pearl River Delta refers to cities that cover nine prefectures of Guangdong province (Guangzhou, Shenzhen, Zhuhai, Dongguan, Zhongshan, Foshan, Huizhou, Jiangmen, and Zhaoqing, Hong Kong, and Macau.), and their surrounding areas.

Table 1.2 Chinese air quality standards for concentrations of SO_2, NO_2, CO, O_3, Particulate Matter (PM_{10}, and $PM_{2.5}$) (Ministry of Ecology and Environment, 2012). Also shown for comparison are the World Health Organization (WHO) air quality guidelines, where they exist (WHO, 2005).

Pollutant	**Grade** [a]	**Annual Mean ($\mu g\ m^{-3}$)**	**24-h Mean ($\mu g\ m^{-3}$)**	**1-h Mean ($\mu g\ m^{-3}$)**	**Percentage of cities not meeting the guideline (Grade II) (2017)（%）**
SO_2	I	20	50	150	
	II	60	150	500	1.4
	WHO		**20**	**500** [b]	
NO_2	I	40	80	200	
	II	40	80	200	46
	WHO	**40**		**200**	
CO [c]	I		4	10	
	II		4	10	4.1
O_3	I		100 [d]	160	
	II		160 [d]	200	38
	WHO		**100** [d]		
PM_{10}	I	40	50		
	II	70	150		62
	WHO	**20**	**50**		
$PM_{2.5}$	I	15	35		
	II	35	75		81
	WHO	**10**	**25**		

[a] Grade I applies to special regions such as national parks; Grade II applies to all other areas, including urban and industrial areas. b 10-min mean. c The units of CO concentration limits are mg m-3. d Daily maximum 8-h mean.

1.4.2 Air quality management system in China

In order to prevent further deterioration caused by air pollution, governments at all levels have taken substantial measures. Environmental governance structure in China is summarized in Figure 1.4. In China, air quality is primarily managed through the Environmental Protection Law (EPL) which was initially proposed in 1979 and adopted in 1989. In addition, the Law on the Prevention and Control of Atmospheric Pollution (LPCAP) was adopted in 2016 (MEP, 2016). A new instalment of the EPL was passed by China's National People's

Congress (NPC) Standing Committee (Figure 1.4) in 2014 (Zhang et al., 2016) and the LPCAP was amended in 2018 (Ministry of Ecology and Environment of the People's Republic of China, 2018). Air quality management in China is largely driven by the ambition to attain the National Ambient Air Quality Standard (NAAQS) (GB3095-2012) (Ministry of Ecology and Environment formerly known as Ministry of Environmental Protection, 2012) and specific targets set by local governments under Chapter 2 of the LPCAP. Targets are implemented through specific instruments, which delegate responsibilities to lower levels of the state administration and allocate resources. The goal of reducing levels of air pollution is now included in the national and local Five-Year Plans (FYPs), which formerly were only for economic and social development. Institutionally, the Ministry of Ecology and Environment (MEE), which was formerly the Ministry of Environmental Protection, is responsible for the implementation of air pollution policies cooperating with other departments when necessary.

Over the past 20 years, the measures implemented have helped to improve overall air quality in China (UN Environment, 2019; Zhang et al., 2010; Zheng et al., 2017). However, annual mean NO_2 concentrations in densely populated cities remained almost unchanged during 2015-2017 (Guo et al., 2019). NAAQS (GB3095-2012) were firstly implemented in 74 cities since Jan 2013. About half of the 74 cities failed to meet Chinese NO_2 standards in 2017 (Ministry of Ecology and Environment, 2018). In addition, annual mean O_3 concentrations increased year by year during 2015-2017 (Guo et al., 2019; Ministry of Ecology and Environment, 2018).

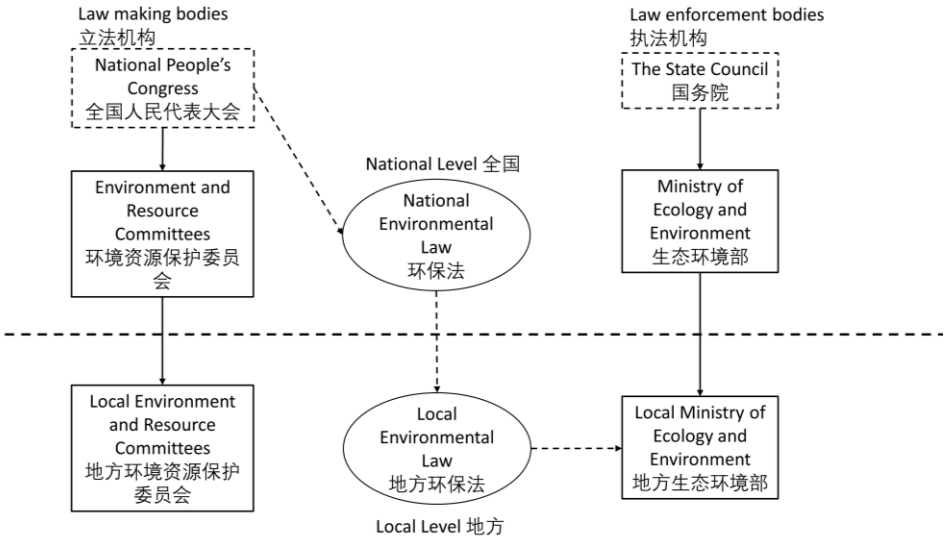

Figure 1.4 Environmental governance structure in China (with Chinese). Adapted from (Jin et al., 2016). The State Council is the chief executive body. The National People's Congress (NPC) is a legislative body consisting of delegates from provinces, municipalities, autonomous regions, and the armed forces.

1.4.3 Air quality monitoring network in China

Monitoring compliance is a key step of implementing pollution measures and estimating air pollution burdens. Since 2013, the China National Environmental Monitoring Centre (CNEMC) has been implementing a comprehensive nationwide monitoring network for the routine measurement of ambient air pollutant concentrations. At the end of 2016, 1,436 monitoring stations had been established in 338 cities (CNEMC, 2017). The networks comprise five types of monitoring sites: urban assessing stations, regional assessing stations, background stations, source impact stations, and traffic stations. The monitor data are published hourly and daily on local environmental agencies' websites with an Air Quality Index (AQI) calculated as well as raw concentration data. The rapid development and expansion of air quality monitoring networks provide useful data for compliance checking, annual environmental reports, public information, as well as some health impacts

assessments and epidemiological studies. However, the government needs to boost the ability to disseminate monitor data to stakeholders. Currently, collection of raw data is undertaken by monitoring departments. Although real-time concentration data are published on the National Air Quality Publication Platform (http://106.37.208.233:20035/), archived historical data are available only on a few official websites (EPA, 2017; EPG, 2017; EPW, 2017). Historical data are also collected and archived elsewhere by private companies without validation, for example https://data.epmap.org/ and https://beijingair.sinaapp.com/.

Despite the increase in the number of monitoring sites across China in recent years, the coverage of monitoring stations for urban sources is still limited—for example, the 22 monitoring stations covering a 50 km × 50 km area over Beijing equates to an average of 113 km^2 per station (Xie et al., 2017)—which is inadequate to describe the spatial variability of urban air pollution, particularly for NO_2. The concentrations of NO_2 are strongly spatially varying, due to its widespread sources and relatively short lifetime (Beirle et al., 2011; Cyrys et al., 2012; Gurung et al., 2017). The current air quality monitoring networks cannot provide the highly spatially resolved concentration fields needed to accurately evaluate the population health burden of exposure to NO_2. The misclassification of human exposure can lead to a loss of power in epidemiological studies and the attenuation of health risk estimates (Basagaña et al., 2012). Measurements also cannot provide the data needed to evaluate future mitigation scenarios that address the challenges of reducing population exposure to NO_2. There is an urgent need for modelling NO_2 concentration over cities in China.

1.5 Aims and structure of the thesis

The overall goal of this PhD project is to develop and implement improved methods for modelling NO_2 intra-urban variability, for the primary purpose of estimating health burdens, given the obstacles on data availability in China. The city of Guangzhou, the third largest city in China with a population of 14 million is chosen as an example. The specific aims are as follows:

1. What are the obstacles to quantifying human exposure to air pollution in China for the purposes of determining health impacts and monitoring the effectiveness of mitigation policies? (Chapter 3)
2. What can be done to improve estimation of human exposure to NO_2 for cities in China given the current obstacles with respect to data availability and city characteristics? (Chapter 3 and Chapter 4)
3. How does the improved modelling of NO_2 concentration in cities help to better understand its health burdens? (Chapter 4)
4. How does the improved modelling of NO_2 concentration in cities help to measure the effectiveness of potential mitigation policies? (Chapter 5)
5. What are the current problems and policy needs to support the assessment of mitigation opportunities and decision-making process? (Chapter 5)

Chapter 2 presents the key methods used in the thesis. The first question is addressed by reviewing current literature on LUR models in Chinese cities (Chapter 3). Based on the gaps and obstacles identified through studies in China, a hybrid modelling approach is developed and its applicability to cities in China is tested in Guangzhou (Chapter 4). The hybrid modelling approach

is used to investigate the impacts of NO_2 concentration on urban population health burden and the effectiveness of policy intervention (Chapter 5).

Chapter 2 Methodology

The overall goal of this PhD project is to develop and implement improved methods for modelling NO_2 intra-urban variability, for the primary purpose of estimating health burdens, in the context of limited data availability in China. This is achieved by firstly identifying gaps and barriers for modelling NO_2 concentrations in cities in China. Based on the current situation, an improved modelling approach is identified and developed. This improved approach is then applied to estimating human exposure and calculating health burdens as well as used for running different scenarios for investigating effectiveness of potential policies. The top-level methodology and workflow are summarized in Figure 2.1.

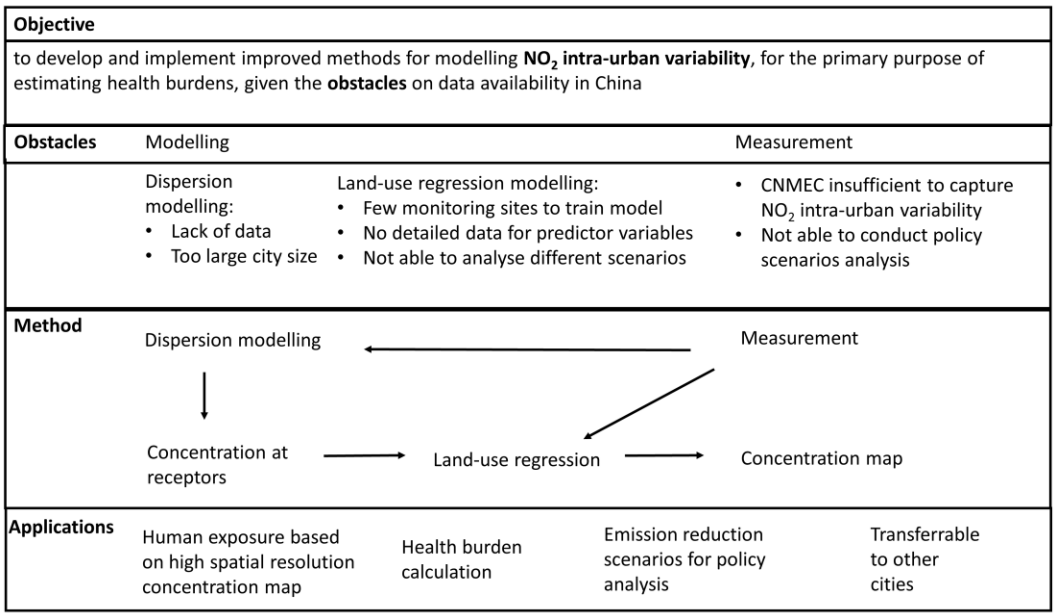

Figure 2.1 Summary of top-level methodology and workflow of the thesis.

2.1 Atmospheric dispersion modelling

Atmospheric dispersion modelling simulates how air pollutants disperse in the ambient atmosphere. It is based on mathematical equations that describe the source-to-receptor emissions and atmospheric transport, dilution, and fate processes (Figure 2.2). Key components in atmospheric dispersion models include:

(1) meteorological conditions (e.g., wind speed, wind direction, temperature, rainfall, the amount of atmospheric turbulence, cloud cover, and solar radiation);

(2) the terrain (e.g., buildings, hills, surface water), which affects the travel of the emitted plumes and determines the surface roughness;

(3) the source (e.g., stack height and diameter, stack gas temperature and velocity, emission rate of the pollutant), and the physical and chemical properties of the pollutant (reactivity, solubility).

The corresponding inputs of data required to apply a dispersion model in a city are listed in Table 2.1.

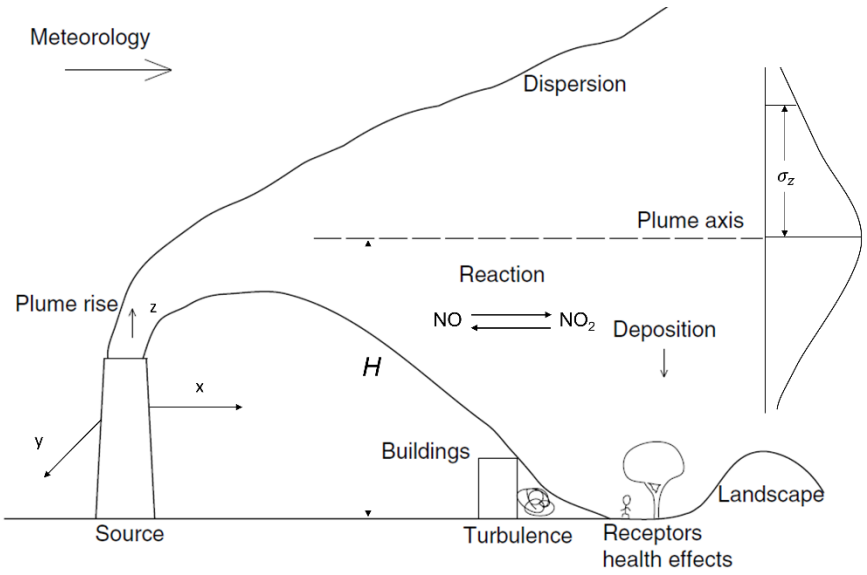

Figure 2.2 Diagram of plume dispersion adapted from (De Visscher, 2013) *H* is the effective source height and the stack is located at point x = 0; y = 0, z = h. The wind direction is along the x axis. The figure shows

the concentrations of air pollutants affected by the meteorology, the source, the terrain, and the physical and chemical processes.

Table 2.1 Summary of input data for the application of an urban dispersion model (De Visscher, 2013) .

Input	**Detailed components**
meteorology	wind field
	mixing height
	topography
	surface roughness
	solar insolation
	temperature
	relative humidity
emission inventory	road sources
	point sources
	line sources
	area sources
	volume sources
	grid sources
background condition	initial condition field
	boundary conditions

The Gaussian plume model is the most common dispersion model. The plume is described by a Gaussian distribution in lateral and vertical directions when the wind speed, wind direction and the propensity of atmosphere to disperse pollutant are considered to be constant (Figure 2.3). Though the reality does not fully satisfy these conditions, the hourly average concentration distributes as a Gaussian curve in many case (De Visscher, 2013). This is therefore routinely used to simplify the process and the equation can be written as:

Equation 2.1 $$c(x,y,z) = \frac{Q}{2\pi u \sigma_y \sigma_z} exp\left(-\frac{1}{2}\frac{y^2}{{\sigma_y}^2}\right)\left\{exp\left[-\frac{1}{2}\frac{(z-H)^2}{{\sigma_z}^2}\right] + exp\left[-\frac{1}{2}\frac{(z+H)^2}{{\sigma_z}^2}\right]\right\}$$

where c is the concentration at a given point, Q is the emission rate, u is the wind vector in the x direction (x = 0 at the source; x > 0 downwind), σ_y and σ_z are the standard deviations of the particle distribution in the perpendicular horizontal (y) and vertical (z) directions and H is the effective height of the plume (Figure 2.3) (Melli and Runca, 1979).

The NO_2 concentration is also significantly affected by R 1-1 and R 1-3 (Section 1.1.2), so reactions are embedded in dispersion models. Dispersion models are therefore highly dependent on the quality of the input data, particularly on emissions, but also detailed meteorological data, and background concentrations (Table 2.1).

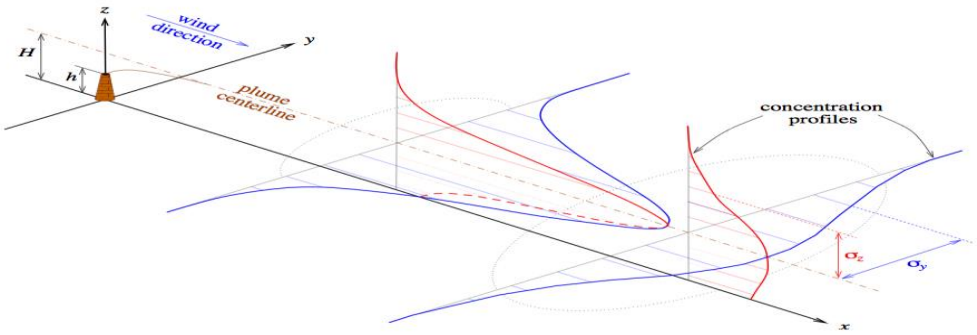

Figure 2.3 Diagram of Gaussian plume dispersion from a point source. H is the effective source height and the stack is located at point x = 0; y = 0, z = h. The wind direction is along the x axis and the concentration distribution resulting from the dispersion in the y, z plane is shown at two downwind locations (Brasseur and Jacob, 2017).

2.2 The ADMS-Urban dispersion model

The ADMS-Urban dispersion model (CERC, 2017; Carruthers et al., 1994) is a widely-used (Carruthers et al., 2000; Di Sabatino et al., 2007; McHugh et al., 1997; Righi et al., 2009) quasi-Gaussian model for simulating dispersion in the

atmosphere of continuous releases from a range of explicit sources in an urban area. The Gaussian distribution applies to stable and neutral conditions and when the boundary layer is convective the plume is skewed and non-Gaussian. The model can produce gridded concentrations or point concentrations hourly or annually.

2.2.1 Chemistry and emissions

The NO_x-NO_2 chemistry (described in Section 1.1.2) is simplified using the Generic Reaction Set (GRS) of Venkatram *et al*. (1994) that includes reactions with O_3 and hydrocarbons. This has been thoroughly evaluated against measurements (Carruthers et al., 2017; Tonnesen and Jeffries, 1994; Venkatram et al., 1994).

(R 2-1)	$ROC + h\nu \rightarrow RP+ROC$
(R 2-2)	$RP + NO \rightarrow NO_2$
(R 2-3)	$NO_2 + h\nu \rightarrow NO + O_3$
(R 2-4)	$NO + O_3 \rightarrow NO_2$
(R 2-5)	$RP + RP \rightarrow RP$
(R 2-6)	$RP + NO_2 \rightarrow SGN$
(R 2-7)	$RP + NO_2 \rightarrow SNGN$

In this reaction set, ROC represents reactive organic compounds, RP is the radical pool, SGN are stable gaseous nitrogen products and SNGN are the stable non-gaseous nitrogen products. Reactions producing particulate matter involving oxidation of SO_2 to form $(NH_4)_2SO_4$ (ammonium sulphate) are also included in the model. Pollutant emissions are represented as individual plumes dispersing from a range of explicitly represented sources, including point, road, area, and volume sources. Aggregated grid sources are used to account for additional emissions, such as non-explicitly modelled roads and

combustion processes in domestic, commercial and industrial settings, including cooking, and (where relevant) shipping.

2.2.2 Meteorology and surface roughness

The input meteorology data containing a variety of meteorological variables (Section 2.1) is processed hourly by the model to calculate PBL height (PBLH) and the Monin-Obukhov length (L_{MO}) which determines the stability of the PBL. Cloud cover measurements, along with the time of day and day of year, are used to calculate incoming solar radiation which generates surface sensible heat flux ($F_{\theta 0}$) and friction velocity (u_*) terms via the surface energy balance and L_{MO} is calculated from

Equation 2.2

$$L_{MO} = \frac{-u_*^3}{\left(\frac{kgF_{\theta 0}}{\rho c_p T_0}\right)}$$

where u_* is the friction velocity at the Earth's surface, k is the von Karman constant ($\approx$ 0.40), g is the gravitational acceleration (9.81 m s^{-2}), ρ and c_p are the density and specific heat capacity of air respectively and T_0 is the near-surface temperature. Alternatively, measurements of PBLH can be used if available. The ratio of PBLH to L_{MO} determines the vertical and horizontal spread extents of each emitted Gaussian plume, with the aggregate contribution from each individual emission source determining hourly simulated pollutant concentrations. In unstable conditions, an additional convectively driven turbulence component is calculated. This produces a skewed, non-Gaussian concentration distribution.

Differences between conditions at the meteorological site and the modelling area (Figure 2.4), largely caused by the large size of obstacles, are accounted

for through distinct definitions of surface roughness (Z_0). The Z_0 values of different land use types in the model are given in Table 2.2.

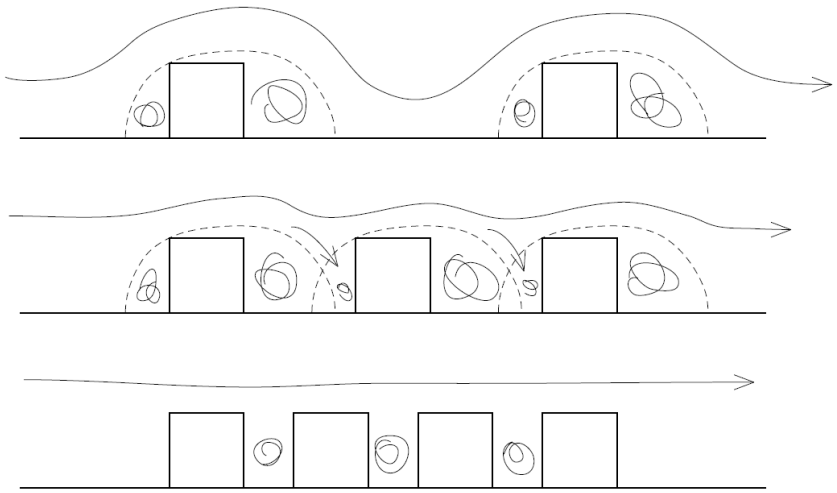

Figure 2.4 Wind flow around obstacles in urban terrain (De Visscher, 2013).

Table 2.2 The built-in surface roughness lengths for the different land uses in ADMS-Urban (CERC, 2017).

Land use	**Surface roughness (m)**
Large urban areas	1.5
Cities, woodlands	1
Parkland, open suburbia	0.5
Agricultural areas (max)	0.3
Agricultural areas (min)	0.2
Root crops	0.1
Open grassland	0.02
Short grass	0.005
Sea	0.0001

2.3 Land-use regression modelling

Land-use regression (LUR) is based on the principle that pollutant concentrations at any location depend on the environmental characteristics of the surrounding area. It uses a geographic information system (GIS) to regress spatially explicit predictor variables (e.g. land cover, traffic, and topography) against the dependent variable of monitored pollutant concentration at a subset of locations. The resulting relationship (Equation 2.3) of significant predictor variables is then used to predict pollutant concentrations at unmonitored locations (Briggs et al., 1997; Jerrett et al., 2005).

Equation 2.3 $$C_i = a + \sum_{j=1}^{n} b_j X_{ij} + \varepsilon$$

In this equation, C_i is the modelled concentration at location i, a is a constant (approximating to the regional background concentration), b_j is the weight attached to variable j, X_j is the value of variable j, computed around location i, and ε is the error term, representing the unexplained variation in concentrations. The process is illustrated in Figure 2.5 using road with different buffers as an example. LUR modelling normally requires observed pollutant concentrations, traffic and road networks, land-use classification, population density, and meteorological data (Table 2.3).

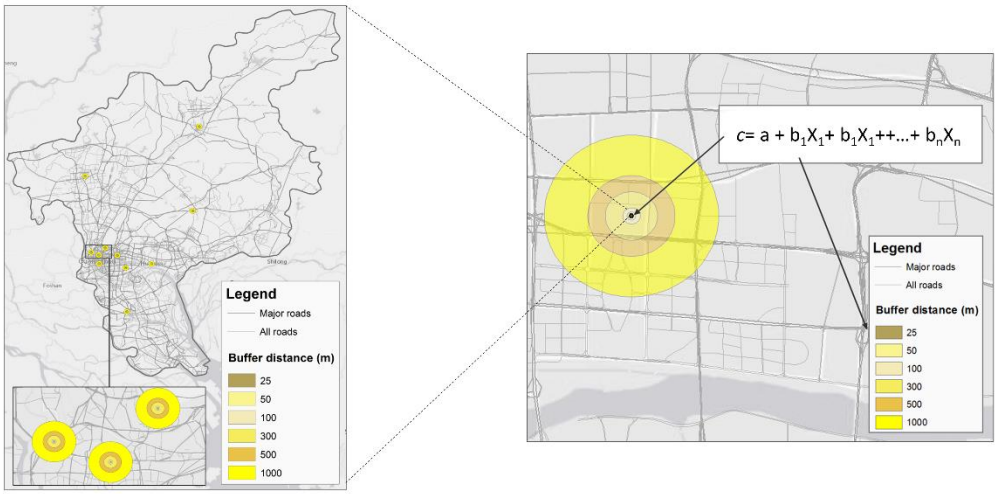

Figure 2.5 Schematic of LUR modelling process (Humstad, 2018). Predictor variables are often calculated for circles with various radii around the sampling points called buffer and the figure shows different buffers of major roads and all roads as predictor variables. The intercept (a) and coefficients (b_j) can be calculated at monitor sites with concentration values to form the model equation.

Table 2.3 Example input data that may be considered, if available for development of a land-use regression (LUR) model (Nieuwenhuijsen, 2015).

Input	**Detailed Components**
pollutant data	Regulatory(routine) monitoring data purpose designed campaign short-term or mobile measuring campaigns
land-use classification	residential land industrial land urban green space
traffic data	road network by road classification numbers and types of vehicles railways
census data	population density household density
meteorology	wind field temperature
physical geography	altitude distance to coast slope angle
emission data	emission inventory
remote sensing data	satellite data
street configuration	factors such as aspect ratio or sky view factor

2.3.1 Selection of sites

The number and type of measurement sites are critical to the final LUR model results. There is no rigorous methodology to determine the required number of monitoring locations given a certain study objective and setting. Based on previous studies in Europe and North America, Hoek *et al.* (2008) suggested the use of 40–80 monitoring sites for LUR models, though the required number of sites is dependent on the size of the population and city and heterogeneities in developed urban areas. Basagaña *et al.* (2012) recommended no less than 80 monitoring sites for accurate health impact assessment for an area of 45.7 km^2 in Spain. Gillespie *et al.* (2016) used hold-out validation (details of model evaluation in Section 2.4) and reported that exposure estimate precision improved with increasing number of training sites and suggests that the number of sites should be no less than 35 to ensure the predictability of the model for the Glasgow conurbation (368.5 km^2). Wu *et al.* (2017) studied the effects of different monitoring network design (roadside sites, high household density sites, and background sites) on the model results in Edinburgh (264 km^2). They reported that the improvement of model performance was insignificant when the number of sites is larger than 30 and not a single network design minimised error in simulating both the full range of concentrations across a city and the high concentration levels (hotspots) only in the city.

2.3.2 Selection of predictor variables

The predictor variables are selected based on prior knowledge or expectation that emission sources, dispersion, and physical geography may contribute to NO_2 concentration variation in urban areas (ESCAPE, 2008). Variables that represent emission sources should be positively associated with pollution; variables representing distance from, or absence of, emission sources or the effectiveness of dispersion/mixing processes can be expected to have

negative associations. The inclusion of different buffer sizes allows for potential different influences of predictor variables over different distances from the receptor (Beelen et al., 2013; Su et al., 2009). Sky View Factor (SVF) is defined as a ratio that has a value ranging from zero (zero view of the sky) to one (a full 360° unobstructed view of the horizon) (L. Chen et al., 2012; Ma et al., 2019). This variable is related to surface roughness and urban climate of a city.

2.3.3 Model development process

The model development processes include (1) pre-processing of monitor data and predictor variables, (2) development of model, (3) diagnostic testing, and (4) model evaluation (the latter is discussed in Section 2.4.2).

(1) Collect and pre-process data for a selection of monitoring sites to set monitor sites and predictor data in the same projected coordinate system. Define the list of predictor variables, including zones of influence (buffer/neighbourhood size) and direction of effect. Specify the zones of influence to reflect the scale of environmental processes appropriate for each variable.

(2) Export the monitoring data and extracted predictor variables from the GIS and import into the statistical package and develop the LUR model using linear regression. A stepwise multiple regression approach is used to select the potential predictor variables to maximize the adjusted percentage explained variance (R^2) and minimize the root mean square error (RMSE) (ESCAPE, 2008). First, all predictor variables are individually regressed against the dependent variable data. The predictor variable with the highest R^2 and with a coefficient which conforms to the expected direction of effect forms the initial model. The univariate linear regression process is repeated with the remaining variables. The variable with the highest increase in adjusted R^2 is added

into the initial model if it meets the following criteria: (1) the increase in adjusted R^2 is greater than 0.01; (2) the coefficients of this variable and the variables already in the model are in accord with the *a priori*-defined direction. This process is repeated until no further variable satisfied the criteria. In the final step, variables with *p*-value greater than 0.1 are removed from the model starting from the variable with highest *p*-value. The univariate regression analysis is the first step of the LUR function where a looping function regressed each of the predictor variables against the dependent variable.

(3) Diagnostics tests are then performed to check multicollinearity and influential observations. Multicollinearity in the variables is checked using Variance Inflation Factor (VIF). The VIF (Equation 2.4) shows the effects of R^2 on the variance of the estimated regression coefficient for the independent variable (O'Brien, 2007). Variables with VIF values greater than three are removed from the model. Cook's distance is the normalized change in the fitted response values due to the deletion of an observation. Extreme values or many zero values in a variable data can skew the final model and this can be indicated by a Cook's distance >1 (Olive, 2017).

Equation 2.4 $$VIF = \frac{1}{1-R^2}$$

2.4 Model evaluation

Model evaluation implies a broad assessment of model results, considering possible positive and negative outcomes, to understand the value of the model. Table 2.4 summarises different statistical metrics for paired comparisons of model to observed values that are used to test the skill of models. Explained variance (R^2, called Coefficient of Determination in regression analysis) quantifies how well a linear regression explains the

variance in the measurement data. It shows the part of the model's total variance that is explained by the predictor variables included. Higher percentages of explained variance indicates a stronger strength of association and means that the model makes better predictions (Rosenthal and Rosenthal, 2011). The agreement between predicted and observed concentrations is usually assessed using the adjusted R^2, which is a modified version of R^2 adjusting for the number of predictors in the model. The root-mean-square error (RMSE), which quantifies the differences between the model-predicted and observed concentrations. Hold-out validation and leave-one-out cross-validation (LOOCV) are the most commonly used validation tests for LUR models. In hold-out validation, the dataset is separated into a training set and a testing set. The training set is used to develop the model and the testing set is used to evaluate the model by using the model to predict the output values for the data in the testing set. In *k*-fold cross validation, the data set is divided into *k* subsets and the holdout method is repeated *k* times. LOOCV uses the variables in the final model to develop a regression model using $n - 1$ sites, where *n* is the total number of observations in a monitoring network. The predicted concentrations are then compared with the actual measured concentrations at the left-out site. The procedure is repeated *n* times. LOOCV can be used in studies with a small number of monitoring data that prevents division into training and testing datasets. However, LOOCV does not sufficiently address the overestimation of the predictive ability of regression models, especially for smaller numbers of sites (Basagaña et al., 2012; Johnson et al., 2010; Wang et al., 2012; H. Wu et al., 2017).

Table 2.4 Different statistical metrics for comparison of model to observed values. (M =predicted concentration, O = observed concentration, σ = standard deviation)

Name	Formula
Mean Bias	$\frac{1}{n}\sum_{1}^{n}(M-O)$
Mean Error	$\frac{1}{n}\sum_{1}^{n}\lvert M-O\rvert$
Root Mean Square Error	$\sqrt{\frac{\sum_{1}^{n}(M-O)^2}{n}}$
Normalised Mean Bias	$\frac{\sum_{1}^{n}(M-O)}{\sum_{1}^{n}O}$
Normalised Mean Error	$\frac{\sum_{1}^{n}\lvert M-O\rvert}{\sum_{1}^{n}O}$
Fractional Bias	$\left(\frac{\sum_{1}^{n}(M-O)}{\sum_{1}^{n}(\frac{M+O}{2})}\right)$
Fractional Error	$\frac{1}{n}\left(\frac{\sum_{1}^{n}\lvert M-O\rvert}{\sum_{1}^{n}(\frac{M+O}{2})}\right)$
Correlation	$\frac{1}{n}\sum_{1}^{n}\left(\left(\frac{O-\overline{O}}{\sigma_o}\right)*\left(\frac{M-\overline{M}}{\sigma_m}\right)\right)$

2.5 Measurement of NO_2 concentrations

NO_2 can be measured after conversion to NO by passage over a heated molybdenum surface or via photolysis using UV lamp (Ridley et al., 1988). NO is usually measured by detecting chemiluminescence from the electronically excited NO_2 product of the reaction of NO and O_3 (R 1-3). NO is unaffected by such converters, and the concentration of NO_2 in a sample containing NO and NO_2 can be inferred from the difference between readings when samples are passed through, or bypass, the converter. Nitrogen-containing compounds

other than NO_2 that can be reduced to NO by the converter can interfere the results (Kleffmann et al., 2013). Conversion to NO and detection via chemiluminescence is in widespread use to measure emissions and atmospheric concentrations of NO_2. NO_2 has also been monitored using passive diffusion samples, e.g. the Palmes diffusion tubes (PDT) and the Ogawa badge (Aguilera et al., 2007; Gilbert et al., 2005; Palmes et al., 1976)

The chemiluminescence method is used for measuring the ambient NO_2 concentration in China. The monitoring specification HJ654-2013 (Ministry of Environmental Protection, 2018b) specifies detailed calibration procedures for each instrument such as zero and span checks, but documentation of the processes applied for data quality control and assurance (QA/QC) and the operating principles at each monitoring site is not publicly available. Overestimation of NO_2 concentrations using instruments based on the chemiluminescence method (TEI Model 42i from Thermo Fisher Scientific Inc., USA) ranged from 6% to 280% depending on the composition of the oxidation products of NO_x has been reported (Xu et al., 2013). In Europe directives, the chemiluminescence method required to measure NO_2 concentration within an error of ±15% (Gerboles et al., 2003). Measurement errors have been reported previously in China but more recent literature indicates that data is more reliable since 2013 (Ghanem and Zhang, 2014; Stoerk, 2016; Yuyu et al., 2012).

2.6 Epidemiological studies and health burden calculation

2.6.1 Air pollution epidemiological studies

Epidemiological studies of air pollution are used to determine the relationship between the pollutant concentration, the exposure, and the health outcome

(morbidity and /or mortality). Many studies have been conducted to estimate the link between short-term (acute) and long-term (chronic) exposure to air pollution in different populations to a range of health outcomes. Statistical modelling is used to quantify the relationship and the relationship is described by as the concentration-response function (CRF) which is then used to derive the relative risk (RR). The RR is the ratio of the health outcome occurring in the exposed population to the health outcome occurring in the unexposed population.

2.6.2 Health burden calculation

The CRFs derived from epidemiological studies (Section 2.6.1) are used to calculate estimates of population exposure in terms of air pollutant concentrations into health impacts estimates. The attributable burden (AB) due to long-term exposure to the air pollutant is estimated by multiplying the attributable fraction of mortality (AF) by burden of disease (BoD) (Equation 2.5). The attributable fraction of disease burden is the expected percentage reduction in the number of cases following elimination of the exposure in population and is calculated from Equation 2.6,

$$\textbf{Equation 2.5} \qquad \boldsymbol{AB = BoD \times AF}$$

$$\textbf{Equation 2.6} \qquad \boldsymbol{AF = \frac{R - R_0}{R}}$$

where R represents the risk or rate of disease in the population as a whole (i.e. both exposed and non-exposed group) and R_0 is risk of disease in non-exposed only. R can be calculated from Equation 2.7:

$$\textbf{Equation 2.7} \qquad \boldsymbol{R = p\,R_1 + (1 - p)R_0}$$

where R_1 is risk of disease in exposed and p represents the proportion of the population exposed ($0 \leq p \leq 1$). RR is the ratio of the probability of an outcome in an exposed group to the probability of an outcome in an unexposed group Equation 2.8.

Equation 2.8 $$RR = \frac{R_1}{R_0}$$

From Equation 2.6 to Equation 2.8, AF can be calculated as Equation 2.9.

Equation 2.9 $$AF = \frac{p(RR-1)}{p\,(RR-1)+1}$$

For outdoor air pollution, the whole population is assumed to be exposed (p =1), so

Equation 2.10 $$AF = \frac{RR-1}{RR}$$

The RR corresponding to an air pollution increment of 10 μg m^{-3} is scaled to a new relative risk for the appropriate population-weighted average concentration. The equation used is:

Equation 2.11 $$RR\,(x) = \beta^{\frac{x}{10}}$$

In this equation, x is the population-weighted average concentration of interest and β is the concentration-response coefficient for the pollutant (per 10 μg m^{-3}). For the example in Guangzhou, the concentration-response coefficient for all-cause mortality attributable to NO_2 is 1.0245 and the population-weighted average concentration is 52.5 μg m^{-3} (Section 4.6).

Chapter 3 Modelling intra-urban variability of air pollution in China: current status and future needs

This chapter is based on a review paper published in 'Atmosphere' (He, B.; Heal, M.R.; Reis, S. Land-Use Regression Modelling of Intra-Urban Air Pollution Variation in China: Current Status and Future Needs. Atmosphere 2018, 9, 134. 10.3390/atmos9040134) I researched and tabulated the literature and wrote the first draft of the paper. Mathew Heal and Stefan Reis contributed revisions to the paper.

3.1 Introduction

The expansion of the CNMEC (and other) monitoring networks is driving a growing number of LUR studies in China. As the nature of urban areas in China, it is timely to assess the present status of LUR modelling in China in the context of identifying what lessons can be learned to advance this field from the similarities and differences with LUR studies applied elsewhere. The objectives of this paper are therefore: (i) to briefly summarize differences between Chinese urban areas and those in Europe and North America in the context of LUR modelling of air pollution concentration; (ii) to summarize the state-of-the-art of LUR air pollution modelling in China; and (iii) to highlight the current gaps in LUR modelling in China in comparison with LUR models in Europe and North America and make recommendations on future needs for China. The majority of applications of LUR have been for NO_2 and PM, since these pollutants are a priority for regulatory monitoring and interventions due to their public health effects. This paper therefore focuses on LUR studies for NO_2 and PM only. Twenty-four such studies in China were identified from the peer-reviewed English-language literature and their details used as the basis for discussion in this paper.

3.2 Urbanization in China

3.2.1 Pace of urbanization

China's rapid economic development has led to extremely rapid urban population growth. At the end of 2011, China's urban population exceeded that of rural dwellers for the first time (National Bureau of Statistics of China, 2016a, 2012) and the trend is continuing—the proportion of urban population in China is expected to reach approximately 70% by 2025 (Qiu, 2012). The extent of built-up area in China has expanded correspondingly rapidly. The growth rate of built-up land from 2000 to 2010 was 2.14 times higher than in the previous decade (Liu et al., 2014). Between 2010 and 2016 the area of land undergoing urban construction increased from 39,760 km^2 to 52,750 km^2 and possession of private vehicles increased from 59.4 to 163.3 million (National Bureau of Statistics of China, 2016b). The pace of change is a challenge for generating and maintaining up-to-date land-use datasets.

3.2.2 Magnitude and density of urbanization

Urban areas in China are characterized by populations of several million (United Nations, 2017), with considerably higher population densities than the vast majority of urban areas in Europe and North America. The average urban population density in China across all built-up areas with a population >500,000 is 5,100 per km^2, compared with equivalent values of 2,900 per km^2 for the European Union (3,100 per km^2 for all of Europe including Russia) and 1,600 per km^2 for North America (1,200 and 2,500 per km^2 for the USA and Canada individually) (Demographia, 2019).

3.2.3 Urban topography

The higher urban population density in China is a consequence of the greater proportion of multi-story residential and commercial buildings. In 2016, China completed the most high-rise buildings (84) with heights exceeding 200 m of any country in the world. It was the ninth year in a row that China topped this list. Thirty-one cities in China had at least one 200-m-plus building completion in 2016 (Gabel et al., 2016). The greater urban 'roughness' and extent of street canyons impact the dispersion of air pollutants both directly and indirectly via differential changes in surface albedo and surface temperatures.

3.3 Emissions of air pollutants in China

Greater population density leads to increased emissions of air pollutants in a given area. The sectorial contributions to NO_x, $PM_{2.5}$ and PM_{10} emissions presented in Figure 3.1 for three illustrative urban areas (Beijing, Shanghai, and Guangdong province) show that power generation, industry and transportation all contribute substantially to NO_x emissions. Industrial sources dominate the contributions to emissions of PM, although residential combustion (heating and cooking) also contributes substantially to emissions of fine PM ($PM_{2.5}$).

Greater emissions density in China can also derive from a lag in implementation (International Council on Clean Transportation, 2017) and/or in compliance (Jin et al., 2016) with industrial and vehicle emissions standards compared with that in Europe and North America. Poorer fuel quality has also been reported as contributing to greater per vehicle emissions in China (Yue et al., 2015).

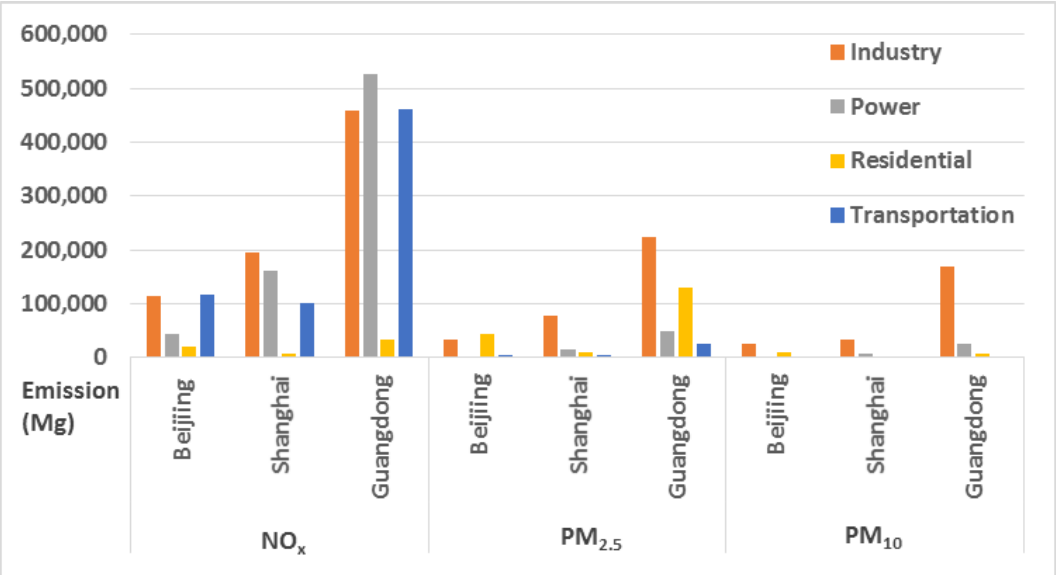

Figure 3.1 Emissions of NO_x, primary PM ($PM_{2.5}$ and PM_{10}) from industry, power, residential, and transportation sectors in Beijing, Shanghai, and Guangdong province in 2012. Data are from the Multi-resolution Inventory for China (MEIC) (Center for Earth System Science, 2012). Mg (megagram) = 10^6 g.

3.4 LUR models for Chinese urban areas

Twenty-four LUR studies were identified from Web of Science and Google Scholar, using the following search phrases and keywords: land-use regression; LUR; China; Hong Kong; Taiwan; air pollution; NO_2; $PM_{2.5}$, and PM_{10}. A first search was undertaken on 11 November 2017, with a follow-up search for any new literature on 3 February 2018. Language was limited to English but there was no restriction on publication date. Characteristics of these studies are summarized in Table 3.1 . LUR models for NO_2 and/or PM have been developed for individual Chinese cities (Hong Kong, Nanjing, Tianjing, Shanghai, Beijing, Changsha, Wuhan, Jinan, and Kaohsing) or regions (PRD, Taipei Metropolitan area, and Liaoning Province). The recent dates of the publications demonstrate the recent impetus for LUR modelling in China.

3.4.1 Monitor data

Table 3.1 shows that 16 of the 24 Chinese LUR studies used fixed-site, regulatory air pollutant monitoring data from CNEMC. The selection of monitor sites are discussed in Section 2.3.1. Apart from a study in Hong Kong that utilized potable sensors to collect PM_{10} and $PM_{2.5}$ data at 222 ad hoc monitoring sites and a study in Changsha with 80 ad hoc sites for NO_2. Table 3.1 shows that the remaining Chinese LUR studies all had fewer than 80 monitoring sites.

As is pointed in Section 1.4.3, it's difficult to get access to archived historical data from CNEMC, fixed-site monitoring data used in these studies were derived from hourly and daily concentrations published on websites of local environmental agencies. Other studies seeking to construct LUR models have collected their own campaign data (Ho et al., 2015; Lee et al., 2014, 2017; Li et al., 2015; Liu et al., 2015; Shi et al., 2016). While this approach provides freedom in the allocation of sites (both locations and heights), it costs both time and money and provides only short-term measurements of concentration at a given location and non-contemporaneous measurements across the full set of locations.

3.4.2 Predictor variables

The predictor variables in the final LUR models for the studies in Table 3.1 are presented in Table 3.2 for NO_2 LUR models and in Table 3.3 for PM LUR models. The most-used variables in the final LUR models for NO_2 were traffic-related variables or proxies of traffic variables such as road lengths or distance to the nearest roads (Table 3.2). This is consistent with LUR models for NO_2 developed elsewhere and of course reflects traffic being a major emission source for NO_x. However, it is important to note that only 4 of the 24 studies

summarized in Table 3.1 were able to obtain traffic data, and three of these were based in Hong Kong, not mainland China (Lee et al., 2017; Shi et al., 2017, 2016). A study in Jinan was able to obtain traffic data for major roads only (Chen et al., 2010b). For the rest of the studies, lack of traffic data meant that road lengths were used as a proxy for traffic counts. Some studies used bus stop density and gridded traffic emission estimates as predictor variables to represent the influence of road emissions (J. Wu et al., 2015; Yang et al., 2017). Ideally, variables based on traffic intensity (motor vehicles per day) multiplied by road length and divided by distance to the road would be used, as recommended by the European Study of Cohorts for Air Pollution Effects (ESCAPE), since these incorporate both emission and dispersion effects (ESCAPE, 2010).

The second most common category of variables for the LUR models in Table 3.2 were land-use variables, which indirectly represent the NOx emissions from power plants, industrial sites, or residential areas. Land-use variables for greenspace are also used, since these are negatively related to NO_2 concentrations. Most studies incorporating such variables were derived from 2010 Landsat TM5 data [5], which classifies into agricultural land, industrial land, commercial and residential land, green space and water area, at 30 m resolution. The monthly global Moderate Resolution Imaging Spectroradiometer (MODIS) Normalized Difference Vegetation Index (NDVI), a satellite-based greenness index that measures and monitors plant growth and vegetation density has also been used as a predictor.

In general, the same set of variables used in NO_2 LUR models were used to develop the PM models (Table 3.3). However, while traffic or traffic proxy variables were selected in all LUR models for NO_2—except for the study in Nanjing (Huang et al., 2017), this was not the case for PM models. Variables

[5] Landsat TM5 website : www.globallandcover.com/home/Enbackground.aspx

related to industrial emissions, artificial lands (such as residential, industrial, and public facilities lands), greenspace (such as forests, natural vegetation, and parks), and water lands were selected in the models as well. This is due to the complexity of the sources for PM emissions compared to NO_2. LUR models in the Taipei metropolitan area and Kaohsiung City included location height-related variables to simulate vertical variation of $PM_{2.5}$ (Ho et al., 2015; Wu et al., 2014). Sampling height had a larger predictive influence in Kaohsiung City than in the Taipei metropolitan area, which may be due to differences in the terrain between the two study areas. Other different predictor variables incorporated into $PM_{2.5}$ LUR models were related to Chinese restaurants and the burning of joss paper and incense in temples (C.-D. Wu et al., 2017).

3.4.3 Model performance

Table 3.2 and Table 3.3 also summarize the model performance statistics for the Chinese NO_2 and PM LUR models. An important observation is that not all studies reported formal validation, which is highlighted here as a shortcoming for those studies that did not do so.

The adjusted R^2 values for the 15 studies in Table 3.2 that provided quantitative validation results ranged from 0.42 to 0.87. For comparison, Hoek *et al.* (2008) suggested R^2 values for usable models are typically in the range 0.6–0.7. The variability in R^2 values in the Chinese studies is likely related to variable quality in the measured concentrations and predictor variables, and the complexity of the city, for example, in terms of differences in topography and emission sources. The highest R^2 value was for a study in Hong Kong (Shi et al., 2017). The high R^2 in this model may be due to the inclusion also of topographical and building-morphological variables. These predictors act as surrogates for the complex wind conditions in a mountainous high-density city

like Hong Kong. An approximately 20% increase in prediction performance was observed in the LUR model, which included these parameters compared to those without (Shi et al., 2017). However, this study only included 15 monitoring sites, so the high R^2 could also be a result of overfitting, where a statistical model begins to describe the random error in the data rather than the relationships between variables. Of the studies that utilized more than 40 monitoring sites, the model developed in Taipei had the highest explained variance for NO_2 (Lee et al., 2014) (Table 3.1 and Table 3.2). The authors of this study conducted 2-week campaigns of NO_2 measurement by Ogawa passive samplers during 3 seasons.

The adjusted R^2 values for the 12 models for $PM_{2.5}$ and 11 models for PM_{10} that reported model performance statistics ranged from 0.19 to 0.89 (Table 3.3). Compared with NO_2 studies, fewer $PM_{2.5}$ and PM_{10} monitoring data were available from CNEMC for developing LUR models and there was no regulatory monitoring data of $PM_{2.5}$ in China before 2012. The development of portable sensors makes collecting campaign data relatively easy for PM, albeit subject to the greater measurement uncertainties typically associated with portable monitors compared with fixed-site network analysers (Lin et al., 2017). In Hong Kong, transient measurements of $PM_{2.5}$ and PM_{10} at 222 locations were collected non-contemporaneously by portable monitor. This made it possible to estimate concentrations of PM in deep street canyons formed by compact urban development (Shi et al., 2017). As for NO_2, the LUR models for PM with urban-morphology-related variables were important for modelling the variability of pollutants in complex urban areas like Hong Kong. Another study in Hong Kong, which did not use the mountainous topographical and building morphological parameters, only had an R^2 value of 0.46, based on 97 campaign measurements (Lee et al., 2017).

The nature of the monitoring locations also affected LUR model performance. The study in PRD resulted in a high R^2 value (0.884) and low RMSE (2.754 μg

m^{-3}) for $PM_{2.5}$ but the monitoring network only included 5 sites located within 500 m of a major freeway and 1 site within 200 m of a freeway. The predictor variables included in the final models were latitude, longitude, and artificial land and water areas (Table 3.3). These variables could only explain the strong northwest-southeast trend of the variability of $PM_{2.5}$ due to the change of wind directions, emissions from human activities and emissions from international and domestic ports but failed to estimate more detailed street-level variation. The final model was therefore not able to satisfactorily explain the intra-urban variability of $PM_{2.5}$.

Table 3.1 Characteristics of recent air pollution land-use regression studies in China that include NO_2 or PM as a modelled pollutant.

Reference	Study Area	Area (km^2)	Population (million)	Type of Sites Used	No. of Monitoring Sites	Pollutants	Sampling Period [1]	Predictor Variables Collected
Yang et al., 2017	PRD	56,000	57.6	regulatory monitoring sites	69	NO_2, $PM_{2.5}$	01/12/2013 to 30/11/2014	geographic character, land use type, traffic indicator, urbanization indicator, wind field, satellite remote sensing, air quality model
Wu et al., 2017	Taipei Metropolitan area	2327	6.6	regulatory monitoring sites	17	$PM_{2.5}$	2006 to 2012	annual average of SO_2 and NO_x, land use type, land mark, road network, Normalized Difference Vegetation Index (NDVI)
Shi et al., 2017	Hong Kong	1100	>7	regulatory monitoring sites	15	CO, NO_2, NO_x, O_3, SO_2, $PM_{2.5}$, PM_{10}	2011 to 2015	traffic network/volume, urban land use, population density, geo-location and physical geography of monitoring points, wind availability
Lee et al., 2017	Hong Kong	1104	7.24	sampling campaign	43, 97, 63, 84	NO, NO_2, $PM_{2.5}$, BC	24/04/2014 to 30/05/2014, 18/11/2014 to 06/10/2015	annual average traffic density, road length, traffic loading, urban build-up, land use, point feature, value extracted at point, distance
Huang et al., 2017	Nanjing	6596	8.27	regulatory monitoring sites	9	$PM_{2.5}$, SO_2, NO_2, O_3	01/01/2013 to 31/12/2013	industrial emission, population density, topography, meteorological variables, road network, land use
L. Chen et al., 2017	Tianjin	11,760	>12	regulatory monitoring sites	28	$PM_{2.5}$	2014	population, land use, road network, distance to coast
Anand and Monks, 2017	Hong Kong	1104	7.35	regulatory monitoring sites	11	NO_2	2005 to 2015	vehicle emissions, industrial emissions, residential emissions, dry deposition, ocean deposition, surface elevation, surface temperature, wind advection, location

Xu et al., 2016	Wuhan	8494	>10	regulatory monitoring sites	9	SO_2, NO_2, PM_{10}	2007 to 2014	land use, socio-economic development, energy use, road density, industry emission, meteorological condition
Shi et al., 2016	Hong Kong	1104	7.35	mobile	222	$PM_{2.5}$, PM_{10}	14 days May to September 2015	traffic and transport, land use, physical geography, population, urban/building morphology
Meng et al., 2016	Shanghai	6300	23	regulatory monitoring sites	28	PM_{10}	2008	land use, road network, emission, population
Liu et al., 2016	Shanghai	6341	23.8	regulatory monitoring sites	53	$PM_{2.5}$, NO_2	2014	land use, road networks, distance to the ocean, longitude and latitude, distance to major air pollution sources, suburban and urban area
Hu et al., 2016	Beijing	16,411	21.69	regulatory monitoring sites	35	$PM_{2.5}$	2014	land use, terrain, transportation, population, polluting enterprises, points of interest, distance to the city center, buildings, natural landscape
Gong et al., 2016	Liaoning Province	145,900	42.21	regulatory monitoring sites	34	SO_2, NO_2, PM_{10}	2013	canyon indicator, elevation, normalized difference vegetative index, distance to air pollutant point source emissions, road density, population density, Gross Domestic Product
Wu et al., 2015	Beijing	16,411	21.69	regulatory monitoring sites	35	$PM_{2.5}$	04/03/2013 to 05/03/2014	road length, land cover, population density, catering services, bus stop density, intersection density, others
Meng et al., 2015	Shanghai	6300	23	regulatory monitoring sites	38	NO_2	2008–2011	population, road network, land use, industrial emissions, coastline
Liu et al., 2015	Changsha	1917	7	sampling campaign (regulatory monitoring sites)	74 (9), 36 (9)	NO_2, PM_{10}	14 days in each season of 2010	road network, land use, meteorology,
Li et al., 2015	Changsha	1917	7	sampling campaign	80, 40	NO_2, PM_{10}	14 days in each season	road length, land use, green space, water area
Ho et al., 2015	Taipei Metropolitan area	2327	6.5	sampling campaign	25	$PM_{2.5}$, Si, S, Ti, Mn, Fe, Ni, Cu, Zn	01/2010 to 10/2010	land use, road network, floor level, population
Wu et al., 2014	Kaohsiung City	2952	2.27	sampling campaign	29	$PM_{2.5}$, Si, S, Ti, Mn, Fe, Ni, Cu, Zn	03/2011 to 12/2011	land use, road network, sampling height, population

Lee et al., 2014	Taipei Metropolitan area	786	6.5	sampling campaign	40	NO_x, NO_2	10/2009 to 09 2010	road length, land use, population and household density, altitude
L. Chen et al., 2012	Tianjin	11,920	>10	regulatory monitoring sites	30	SO_2, NO_2, PM_{10}	2006	road network, traffic volume, land use, population density, meteorology, physical variables, pollution sources
Yu et al., 2011	Taipei	271.8	2.7	regulatory monitoring sites	18	$PM_{2.5}$	2005 to 2007	land use, road network
Chen et al., 2010b	Jinan	8177	60.485		14	SO_2, NO_2, PM_{10}	01/08/2008 to 31/07/2009	traffic, land use, population density, physical condition, meteorological condition, others
Chen et al., 2010a	Tianjin	11,920	>10	regulatory monitoring sites	30	NO_2, PM_{10}	heating season: 15/11/2006 to 15/03/2006; non heating: 16/03/2006 to 14/11/2006	major roads, land use, population, meteorological variables and distance to sea

[1] The form of the dates are DD/MM/YYYY and MM/YYYY.

Table 3.2 Predictor variables and performance statistics of land-use regression models for annual-average NO_2 concentrations in China.

Reference	Study Area	Predictor Variables in Final Model (Buffer in Unit m)	Adjusted R^2 of Model	RMSE (μg m^{-3})	R^2 Validation	RMSE Validation (μg m^{-3})
Yang et al., 2017	PRD	NO_2 emission from traffic (2000), urban road (2000), latitude			0.56	7.208
Shi et al., 2017	Hong Kong	skyview factor (100), private and government vehicles (750)	0.871			8.655
Lee et al., 2017	Hong Kong	express way length (1000), main roads (50), elevated roads (5000), open area (300)	0.43	27.7	0.39	29.5
Huang et al., 2017	Nanjing	residential (5000), population (3000)	0.87	2.69	0.7	2.13
Anand and Monks, 2017	Hong Kong	tertiary road length (300, 500, 3500, 7000), longitude	0.419		0.419	19.1
Xu et al., 2016	Wuhan	built-up land (4000), vegetation (1000), road density (2000), precipitation	0.575	5.51 [1]		
Liu et al., 2016	Shanghai	residential (1000), distance to coast, industrial (3000), urban or not urban, highway intensity (1000)	0.621			
Gong et al., 2016	Liaoning	Gross Domestic Product, population in a buffer, density of major roads in a buffer (200–2000), distance to the nearest industrial emission	0.42	6.9	0.37	8.42
Meng et al., 2015 [2]	Shanghai	major road length (2000), count of other industrial sources (10,000), agricultural land area (5000), population (in cell of 1000 × 850)	0.82		0.75	4.46
Liu et al., 2015	Changsha	major road (1200), residential land (600), residential land (1200), public facilities land (1200), green space (300)	0.51	7.10	0.61	
Li et al., 2015	Changsha	total length of urban expressways and freeways (300), residential (1200), total area of commercial, recreation, governmental and education lands (1200)	0.55		0.51	
Lee et al., 2014	Taipei	natural area (500), major road length (25), low density residential area (500), urban green area (100)	0.74	6.36	0.63	
Chen et al., 2012	Tianjin	point source index (10,000–5000), line source index, distance to expressway, greenness	0.89	0.18		
Chen et al., 2010	Jinan	length of major roads (2000), distance to express way, area of residential land (2000)	0.64			
Chen et al., 2010 [3]	Tianjin	major roads (2000), residence (500), population density, wind index	0.74	0.012 [4]		

[1] This is standard error of estimate. [2] This LUR model used data of 4 year average. [3] This LUR model was for the non-heating season. [4] This is standard error.

Table 3.3 Predictor variables and performance statistics of land-use regression models for annual-average particulate matter (PM) concentrations in China.

Reference	Study Area	Pollutants	Predictor Variables in Final Model (Buffer in Unit m)	Adjusted R^2 of Model	RMSE (μg m^{-3})	R^2 Validation	RMSE Validation (μg m^{-3})
Yang et al., 2017	PRD	$PM_{2.5}$	latitude, longitude, artificial land (2000), water land (200)	0.884		0.872	2.754
Wu et al., 2017	Taipei Metropolitan area	$PM_{2.5}$	concentration of NO_x, concentrations of SO_2, length of local roads (750), number of Chinese restaurants (1750), number of temples (750), average NDVI (1750)	0.89	1.66	0.83	1.58
Shi et al., 2017	Hong Kong	$PM_{2.5}$	commercial (300), public transport vehicles (50)	0.671			2.62
Shi et al., 2017 [1]	Hong Kong	$PM_{2.5}$ summer	commercial (300), public transport vehicles (100)	0.771			2.714
Shi et al., 2017 [2]	Hong Kong	$PM_{2.5}$ winter	primary road (400), tertiary road (1000), open space (100)	0.422			3.758
Shi et al., 2017	Hong Kong	PM_{10}	sky view factor, public transport vehicles (50), frontal area annual (200)	0.854			3.544
Shi et al., 2017 [3]	Hong Kong	PM_{10} summer	elevation above Hong Kong Principal Datum, public transport vehicles (50)	0.895			3.522
Shi et al., 2017 [4]	Hong Kong	PM_{10} winter	count of bus stops (50), open space (100)	0.634			5.138
Lee et al., 2017	Hong Kong	$PM_{2.5}$	expressway (25), distance to Shenzhen, car park density (1000), car park density (25), government land use (100), industrial land use (25)	0.54	4	0.43	4.7
Huang et al., 2017	Nanjing	$PM_{2.5}$	road length (300), residential (100), wind index,	0.72	2.1	0.38	2.58
Chen et al., 2017	Tianjin	$PM_{2.5}$	population density, road length (1000), industrial area (2000), distance to the coast			0.73	6.38
Xu et al., 2016	Wuhan	PM_{10}	water bodies (1000), Gross Domestic Product, energy consumption, industrial waste gas emission, precipitation	0.594	7.35 [5]		
Shi et al., 2016	Hong Kong	$PM_{2.5}$	primary road line density (300), ordinary road line density (400), traffic volume of public transport vehicles (500), frontal area index (400)	0.633	6.516	0.613	
Shi et al., 2016	Hong Kong	PM_{10}	primary road line density (300), traffic volume of private and government vehicles (200), government land use area (1000), frontal area index (400)	0.707	6.948	0.692	

Meng et al., 2016	Shanghai	PM_{10}	distance to the coast, emission (7000), green space (1000), road lengths (5000)	0.8	4.2	0.73	5
Liu et al., 2016	Shanghai	$PM_{2.5}$	longitude, distance to the coast, highway intensity (300), water (500), industrial (300)	0.877			
Hu et al., 2016	Beijing	$PM_{2.5}$	crop land (1000), forest (5000), water (3000), elevation (5000), railway and subway (2000), distance to city center	0.679			
Gong et al., 2015	Liaoning Province	PM_{10}	Gross Domestic Product, elevation, distance to the nearest industrial emissions	0.34	23.1	0.33	23.63
Wu et al., 2015	Beijing	$PM_{2.5}$	natural vegetation (3000), major roads (1000), water body (50)	0.58			9.3
Liu et al., 2015	Changsha	PM_{10}	expressway (1200), residential land (900), residential land (1200), industrial land (1200), public facilities land (1200), water area (1200)	0.62	9.00	0.58	
Li et al., 2015	Changsha	PM_{10}	total length of urban expressways and freeways downwind semicircular buffer (600), residential upwind semicircular buffer (300), total area of commercial, recreation, governmental and education lands downwind semicircular buffer (600)	0.51	5.6	0.60	
Ho et al., 2015	Taipei Metropolitan area	$PM_{2.5}$	floor level, total length of major roads (50), total length of all road segments (50), the surface area of industry (300)	0.75		0.62	
Wu et al., 2014	Kaohsiung City	$PM_{2.5}$	mid-level site, high-level site, total length of all major roads (500), total length of all roads (25), gravel plant (5000), agriculture (500)	0.55		0.28	11.48
Chen et al., 2012	Tianjin	PM_{10}	population density, point source index (10,000–5000), line source index, distance to sea	0.84	0.21		
Yu et al., 2011	Taipe	$PM_{2.5}$	road (500–1000), forest (500–1000), industry (300–500), park (500–1000), railroad (0–50), government institutions (100–300), park (300–500), public equipment (100–300), bus (0–50), public equipment (100–300), port (500–1000)				2.5685 [6]
Chen et al., 2010	Jinan	PM_{10}	area of residential land (1500), area of industrial land (1500), distance to sea	0.19			
Chen et al., 2010 [7]	Tianjin	PM_{10}	major roads (2000), residential area (500), population density, wind speed,	0.72	0.010 [8]		
Chen et al., 2010 [9]	Tianjin	PM_{10}	major roads (1000), residential area (500), wind speed	0.49	0.008 [10]		

[1,3] The LUR models were for summer. [2,4] The LUR models were for winter. [5] This is standard error of estimate. [6] This is standard deviation. [7] This LUR model was for the heating season. [8,10] These are standard errors. [9] This LUR model was for non-heating season.

3.5 Summary of application of LUR models for Chinese cities

3.5.1 Modelled pollutants

In some of the PM LUR studies, the intercept values of the resultant models are close to the mean observed/predicted values of the PM concentrations (Huang et al., 2017; C. Liu et al., 2016; Meng et al., 2016; Yang et al., 2017). The reason for these large intercepts is that longer-range transport and secondary formation within the atmosphere are more influential for PM_{10} and $PM_{2.5}$, compared with pollutants emitted locally and with shorter atmospheric lifetimes such as NO_x. LUR models for PM are therefore more likely to fit with noise rather than capturing the spatial variation. In contrast, LUR is more effective for modelling NO_2, which is derived mainly from traffic and domestic and other local combustion sources through the rapid reaction of NO and therefore has more pronounced spatial variability that the LUR model can capture.

3.5.2 Data availability/accessibility challenges

Although an increasing number of LUR models have been developed at the intra-urban scale in China, they remain constrained by the availability of key input data needed for LUR models (Table 2.3), especially air quality monitoring data. Measurement networks are sparser to date compared to those in Europe, and the cities in China are larger, denser and more complex and often also expanding rapidly. The number of monitoring sites from CNEMC often do not reach that recommended for developing LUR models for health studies (Basagaña et al., 2012; Hoek et al., 2008), so the expansion of monitoring (regulatory and/or 'low cost' and/or passive) is needed. Quality-assured historical data are not often available. Therefore, as well as the archiving of network data, there is also an urgent need for nationally-applied QA/QC

protocols to improve and document the quality of the data to ensure that Chinese networks comply with international standards (Y. Chen et al., 2012; Ghanem and Zhang, 2014).

Aside from carrying out additional targeted ground-based measurement campaigns to support LUR model development, satellite data have recently been used in LUR modelling applications to compensate for the lack of measurement data. Example datasets are the Ozone Monitoring Instrument NO_2 vertical column density (VCD) and aerosol optical depth (AOD) for PM (Duncan et al., 2014). As with studies in Europe (de Hoogh et al., 2016; Kloog et al., 2012, 2011; Novotny et al., 2011; Vienneau et al., 2013), studies in China have reported that incorporating satellite-based estimates improved model performance of regional LUR models for NO_2, PM_{10}, and $PM_{2.5}$ (Gong et al., 2016; Yang et al., 2017). More temporally-resolved models have also been reported; for example, using satellite AOD and VCDs, LUR models have been used to estimate daily average concentration of PM_{10} (Meng et al., 2016) and NO_2 (Anand and Monks, 2017). Details of temporally-resolved models will be discussed in Section 3.5.3.

Nevertheless, current satellite data are not currently suitable for modelling the intra-urban variability of ground-level pollutants within a LUR modelling framework for the following reasons: First, ground-level concentrations cannot be detected directly from satellite instruments but must be derived by removing satellite responses to the rest of the column using complex algorithms and modelling (Duncan et al., 2014). For example, high AOD values do not necessarily translate to high surface $PM_{2.5}$ levels due to the relationship between AOD, relative humidity, and $PM_{2.5}$ (Ziemba et al., 2013); secondly, the satellite-derived estimates are area-averaged concentrations, which are normally much too coarse to capture spatial contrast within cities. The pixel sizes of current instruments are around several hundred km^2 (OMI Team,

2012); and thirdly, the availability of some satellite data are subject to meteorological conditions; for example, cloud cover can influence the quality of the retrievals of many variables (e.g., AOD) that are sensitive to atmospheric optics. In addition, satellite data can have systematic seasonal errors (Gong et al., 2016; Yang et al., 2017). For example, Yang *et al.* (2017) reported that satellite remote sensing tended to overestimate concentrations of $PM_{2.5}$ in summer and underestimate in winter.

Another approach to overcoming a lack of monitoring data is to integrate dispersion models with LUR models. Typically, dispersion models compute concentrations of air pollutants with high spatiotemporal resolution at specific background, roadside, and kerbside receptors. The concentrations at these receptors can then be used as pseudo-observations in the LUR model and eventually simulate the concentration variation over the city without applying a computationally-intensive dispersion model over the whole area. The integrated modelling approach also has the flexibility of developing more temporally-resolved models. The approach has been exemplified in the USA (Johnson et al., 2010) and in the UK (Mölter et al., 2010). However, it must be remembered that the pseudo-observations are not real monitor data. Importantly also, a fundamental drawback to the application of dispersion models in China is that they require very detailed input data on emissions (particularly traffic emissions such as fleet composition, emission factors, road width, canyon height, and time factors), meteorological variables (such as wind field, cloud cover, and precipitation) and boundary conditions—datasets, which as discussed above, are largely currently lacking in China.

As well as the challenges noted above in respect of pollutant data, another important challenge for Chinese LUR studies is capturing the rapidly changing urban landscape. The study by Xu *et al.* (2016) interpreted Landsat series images from 2007 to 2014 to account for urban land-use change during that period.

3.5.3 Temporal variability

LUR models are often used in epidemiological studies to estimate the long-term effects of air pollutants. LUR models for previous years were developed (C.-D. Wu et al., 2017; Xu et al., 2016). Xu *et al.* (2016) used Landsat series images over different years and modified traffic emissions and industrial emissions by the number of registered motor vehicles and the numbers of enterprises to account for the temporal variation over the years.

Greater temporal-resolution modelling data are needed for shorter-term-exposure epidemiology. Some studies in China have developed several unique models in different seasons (Chen et al., 2010a; Li et al., 2015; Shi et al., 2016; J. Wu et al., 2015; Yang et al., 2017). Both NO_2 and PM concentrations during the winter tended to be higher than in the summer, particularly over urban areas, which may be caused by a change of boundary layer and increased emissions from heating and other activities, such as setting off fireworks in the winter (ESCAPE, 2010). Under the influence of the East Asian monsoon, wind and precipitation patterns substantially change seasonally in much of China. Localized wind direction and speed data are needed as predictors to help characterize these temporal changes (Chen et al., 2010a; Liu et al., 2015; Shi et al., 2017).

Since $PM_{2.5}$ and NO_2 have shown high day-to-day and diurnal temporal variations (Cyrys et al., 2012; Lin et al., 2016; H. Wu et al., 2015), more detailed temporal resolution would benefit short-term epidemiological studies. Two studies in China achieved this by using a linear mixed effects (LME) model (Equation 3.1) approach including satellite data (Anand and Monks, 2017; Meng et al., 2016). LUR models are typically fixed-effect models (Equation 2.3), in which the predictor variables are temporally invariant. LME combines both fixed and random effects. In LME, additional time-dependent variables

are used to model daily concentrations of pollutants. For example in Meng *et al.* (2016), AOD data, meteorological data, and NDVI are time-dependent variables. Liu *et al.* (2015) used meteorological factors to build neural network models to explain the nonlinear relationship between meteorological factors and concentrations of NO_2 and PM_{10}.

Equation 3.1 $$C_{i,t} = a + \sum_{j=1}^{n} b_j X_{ij} + c_t + \sum_{t=1}^{m} \sum_{j=1}^{n} d_{jt} Y_{ijt} + \varepsilon_{it}$$

In this equation, $C_{i,t}$ is the modelled concentration at location i at time t, a is the fixed intercept for the regression model and c_t is the random intercept for time t, b_j is the fixed slope and d_{jt} is random slope. X_{ij} and Y_{ijt} are the fixed predictor and the random predictor, respectively, ε_{it} is the error term, representing the unexplained variation in concentrations.

3.6 Dispersion models for Chinese urban areas

Atmospheric dispersion modelling (Section 2.2) has been used for many years in local air quality management in China. Previous applications of ADMS-Urban (Cai and Xie, 2011; Chen et al., 2009; McHugh et al., 2005; Owen et al., 2000) and American Meteorological Society-Environmental Protection Agency Regulatory Model (AERMOD) (Cimorelli et al., 2005; Ma et al., 2013) in China have largely focussed on evaluating the impact that emission control schemes targeting individual sources have on the immediate environment. Chen *et al.* (2009) combined pollutant concentrations simulated by ADMS-Urban with population data to investigate the impact of traffic control policies in Shanghai. Cai and Xie (2011) used the ADMS-Urban model to quantify the effects of the odd–even traffic restriction (restricting vehicles with odd or even number plates) during the 2008 Olympics on emissions from a selection of major roads. The study finds that some of the previously most polluted areas subsequently complied with the NAAQS. Ma *et al.* (2013) applied AERMOD for future scenario simulation for SO_2 and NO_x in Xuanwei (Yunnan Province)

to study the effectiveness of emission control policy (emission reduction targets in the national 12th FYP) on the air quality. Substandard modelling results are due to insufficient monitored data and incomplete emission inventories.

3.7 Comparison of dispersion and LUR modelling

Compared to LUR, dispersion modelling has the advantage of grounding simulations of pollutant concentrations for different scenarios in a process-based simulation of the controlling processes; but the approach requires detailed input data on emissions (e.g. emission inventories), meteorological parameters, and background concentrations, which are currently not fully available/accessible in most cities in China. LUR is an efficient modelling approach, but in areas with limited monitoring sites such as Guangzhou, with only 11 monitoring sites, the selected variables may overfit the model and hence cause bias in health-effect estimates (Basagaña et al., 2012). LUR is also limited to modelling measured air pollutants and cannot predict air pollutant concentrations under potential future emissions scenarios. However, despite the disadvantages mentioned above, LUR is relatively cheap and easy to implement; and once input datasets are assembled, LUR models can be readily adapted to new 'measurement' data without needing to consider complex physicochemical processes.

3.8 Future research needs

3.8.1 Improvement of data quality/accessibility

LUR models require monitored pollutant concentrations, road networks and traffic data, land-use classification, population density and meteorological data

(Table 2.3). Foremost amongst these are the air pollutant monitoring data. Attempts have been made to improve the quality and the number of regulatory monitoring sites by the Ministry of Environmental Protection (China National Environmental Monitoring Centre, 2016) but formal archived historical data available to the public, together with nationally-applied QA/QC approaches to improve data quality, are still urgently needed.

In terms of predictor variable data, as summarized in Section 3.2, urban land-use in China is rapidly changing so regularly updated land-use classification data are needed now and going forward. In order to model the effects of high-rise buildings, detailed building height and street width datasets are required as a model proxy for potential street canyon effects. As discussed in Section 3.4.2, most LUR studies in China have used road lengths as a proxy for traffic counts due to unavailable traffic data. Thus, traffic counts and fleet data are also indispensable. At present, all the data mentioned in Table 2.3 are produced by different organizations and archived (if at all) on various platforms. It would save time and effort if these data were systematically collected and stored.

3.8.2 Integration of modelling approaches and fusion of sensor data

As shown by studies in both the UK and the USA (Johnson et al., 2010; Mölter et al., 2010), the integration of dispersion and LUR modelling can provide an alternative to simulating high spatial resolution pollutant concentration fields with insufficient monitoring data. As discussed in Section 3.5.2, the integrated approach makes it possible to design optimal monitoring sites network within the dispersion modelling domain. Because the scale of Chinese cities, running high spatially resolved processed based models can be computationally expensive, the integration of dispersion and LUR modelling can solve this issue by using statistical cheap LUR model to emulate the behaviour of

dispersion model. Future research should use this approach to explore the number of sites required to develop spatial models in Chinese urban areas and how the design of monitoring networks affects the modelling results, as demonstrated elsewhere (H. Wu et al., 2017). However, progress on this front is contingent on the availability of detailed, temporally-resolved emissions and meteorological data, which is lacking at present.

The integration of satellite and ground-based lower-cost sensing also has potential for overcoming the limitation of monitoring data scarcity in China. Data collected by sensors at different spatiotemporal scales may be used to develop models and also to calibrate and validate them. Example studies discussed in Sections 3.4.3 and 3.5.2 illustrate the benefits of incorporating sensor data, despite remaining challenges in relation to data QA/QC, metadata, access, spatiotemporal resolutions and data management (Reis et al., 2015).

3.8.3 LUR model standards

Rigorous standards and requirements specific to cities in China need to be set for LUR model development and validation to prevent substantial bias in estimated concentrations and to improve applicability in health burden research. Relevant standards could relate to a minimum number of monitoring sites, the ratio of roadside sites to residential sites, key predictor variables and published model-validation statistics.

3.9 Conclusions

China is at the forefront of this trend of rapid economic development and urbanisation, which has led to the emergence of megacities (>10 million

people) and megacity clusters and concomitant problems of poor air quality. Two modelling methods are widely used to simulate pollutant concentrations at relatively high spatial resolution within urban areas: dispersion modeling and LUR.

Although an increasing number of LUR models have been developed at the intra-urban scale in China, they remain constrained by the availability of air quality monitor data. The quality of LUR modelling studies of intra-urban air pollution concentrations in China is currently constrained mainly by the scarcity of input data, especially monitoring pollution data. There is an urgent need for the continued expansion of monitoring (including via passive and miniaturized sensors), the application of minimum standards of measurement assurance and accessible, long-term archiving of the data. There is a similarly urgent need for higher spatial resolution proxy data for urban emissions, particularly in respect of traffic-related variables. The rapidly evolving nature of the Chinese urban landscape makes generating and maintaining up-to-date land-use and urban morphology datasets a challenge but one that must be met to support researchers, planners and policy decision-makers. It is important that Chinese LUR models are subject to appropriate validation statistics. As is the case elsewhere, the integration of LUR modelling with portable air pollution monitor data, satellite data, and dispersion modelling has the potential to enhance the derivation of spatially-resolved urban pollution maps.

Gaussian plume dispersion models, capable of simulating dispersion from an array of explicitly represented emission source types, including road and point sources, are instead often implemented to represent pollutant concentrations at the scale needed to fully assess human health impacts and simulate the fundamental physical-chemical processes in the atmosphere from emission source to all selected receptor locations. Applications of either approach in China have so far been limited by the city size and data availability (He et al., 2018).

Given the obstacles in availability of monitor data, emission inventories, and other highly spatially resolved data, and the challenges in applying high spatially resolved models in large domains, a novel method for estimation of highly spatially resolved human exposure to atmospheric pollutants for health burden calculation in cities in China is developed and implemented. The approach combines the advantages of dispersion modelling and LUR modelling. Details of development of the hybrid model and application of the hybrid model are in Chapter 4 and Chapter 5 .

Chapter 4 Modelling intra-urban variability of NO_2 in Guangzhou

This chapter is based on a research paper published in 'Environmental Research Letters' (He, B.; Heal, M.R.; Humstad, K.H.; Yan, L.; Zhang, Q.; Reis, S. A hybrid model approach for estimating health burden from NO_2 in megacities in China: a case study in Guangzhou. Environmental Research Letters 2019, 14, 124019. https://doi.org/10.1088/1748-9326/ab4f96 *) I, in discussion with Stefan Reis and Mathew Heal, conceived the aims and methodology of the research. Liu Yan and Qiang Zhang assembled and advised on Guangzhou emissions inventories. I and Kamilla H Humstad assembled additiona l datasets. I, with some assistance from Kamilla H Humstad, undertook the modelling, mapping and calculations, plus all table and figure presentations. I wrote the full first draft of the paper. Other co-authors supplied further suggestions and revisions to the text.*

4.1 Introduction

In this work, we demonstrate a practical approach to simulating annual-average concentrations of NO_2 in Chinese megacities in which we combine the advantages of both dispersion and LUR modelling (Mölter et al., 2010). We use an urban dispersion model to simulate annual-average NO_2 concentrations at strategically chosen 'virtual' sites. This network of virtual measurements is then used to develop an LUR model to estimate NO_2 concentrations over the whole region at 25 m $\times$ 25 m resolution, from which mortality health burdens can be calculated. A particular advantage of this approach is that it can be used to derive spatially-resolved LUR models for future scenarios that are rooted in process-based dispersion model simulations of those scenarios. Here we apply our methodology in the megacity of Guangzhou, which is the third largest city in China. We use our hybrid model to estimate the scale of long-term health burden currently existing in Guangzhou due to the spatially varying NO_2 concentrations.

4.2 Study design

The city of Guangzhou is located on the north side of the Pearl River Delta (Figure 4.1). It has a total area of 7,434 km² and a population of 14 million, divided into six districts (Conghua, Guangzhou city centre, Huaxian, Nansha, Panyu, and Zengcheng) (Table 4.6). Concentrations of NO_2 are measured at 11 sites (Figure 4.1 and Table 4.1). The workflow for this study is shown in Figure 4.2. The ADMS-Urban dispersion model v4.1 (CERC, 2017) was used to derive NO_2 concentrations at 83 additional strategically-selected receptors locations across Guangzhou, which were then used to develop an LUR model for NO_2 concentrations across the whole city. The sources of data for the ADMS-Urban and LUR modelling are summarised in Table 4.2.

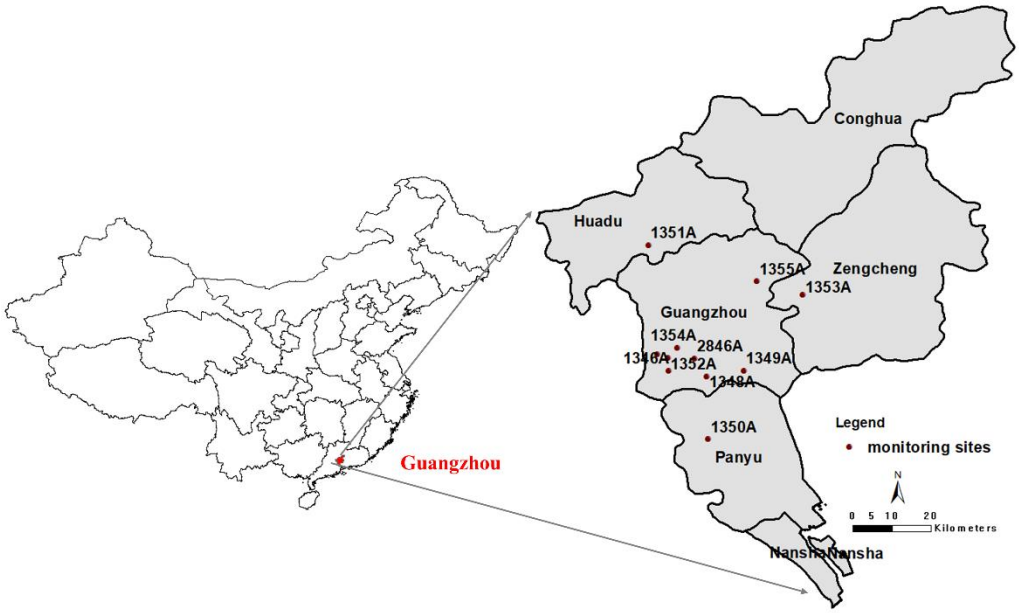

Figure 4.1 The location of Guangzhou in China and the locations of the 11 monitoring sites (red dots). The labels are the Guangzhou codes for the monitoring sites. Shapefiles of the city-wide and district administrative boundaries were obtained from the GADM database (GADM, 2019).

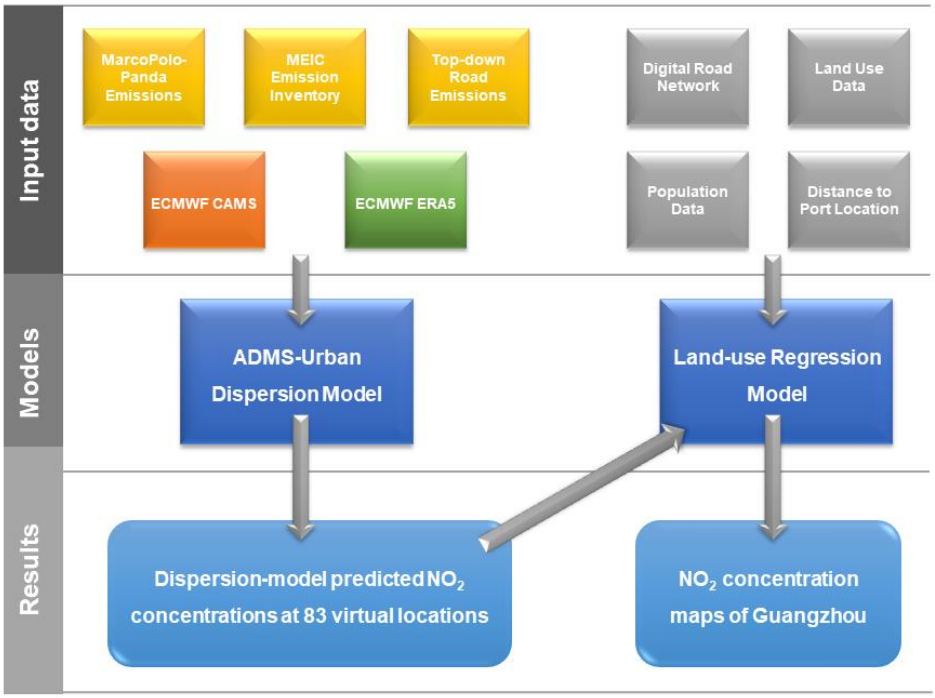

Figure 4.2 Schematic of the integration of ADMS-Urban model results into an LUR model. The methodology for selection of the 83 receptor locations is described in the text.

Table 4.1 Descriptions and coordinates of the 11 automatic chemiluminescence monitoring sites in Guangzhou.

Code	Name	Long (°)	Lat (°)
1,345A	Guangdong Guangya Middle School	113.24	23.14
1,346A	Guangzhou No.5 Middle School	113.26	23.11
1,348A	Guangdong University of Finance and Economics	113.35	23.09
1,349A	Guangzhou No.86 Secondary School	113.43	23.11
1,350A	Guangdong Panyu Middle School	113.35	22.95
1,351A	Huadu District Normal School	113.21	23.39
1,352A	City monitoring station	113.26	23.13
1,353A	Kowloon Town/Zhenlong	113.57	23.28
1,354A	Wuhu (Luhu)	113.28	23.16
1,355A	Maofengshan Forest Park	113.46	23.31
2,846A	Sports West	113.32	23.13

Table 4.2 Sources of data for the ADMS-Urban modelling and LUR modelling.

Data	Year	Source
Multi-resolution Emission Inventory for China (MEIC)	2016	http://meicmodel.org/cloud/
marcopolo-panda	2014	http://www.marcopolo-panda.eu/products/toolbox/emission-data/
openstreet map road, river, coast, port	2018	https://digimap.edina.ac.uk/
Land use GlobeLand30	2010	http://www.globallandcover.com/GLC30Download/index.aspx
ECMWF-ERA5	2017	https://apps.ecmwf.int/datasets/
ECMWF-CAMS	2017	https://apps.ecmwf.int/datasets/
Measured NO_2 concentration	2017	http://beijingair.sinaapp.com/
Altitude SRTM 90m	2014	https://cgiarcsi.community/data/srtm-90m-digital-elevation-database-v4-1/
UN adjusted population data	2015	https://www.worldpop.org/project/categories?id=3

4.3 The ADMS-Urban model set-up

The ADMS-Urban dispersion model v4.1 (detailed description is in Section 2.2) is used in this study. The input data and set up for Guangzhou is in Table 4.2 and Table 4.3. Hourly wind speed, wind direction, air temperature and cloud cover data at 10 m above the ground from ECMWF-ERA5 (ECMWF, 2019) were used because the meteorological measurement data from the only weather station in Guangzhou was incomplete. Surface roughness in Beijing has been reported mainly in 1-3 m (Zhang et al., 2017) and 2 m was chosen based on results of sensitivity tests. Since there was one site (1355A) located at hilly place, terrain file was used and prepared from altitude data. Gridded emissions of NO_x and VOCs for the year 2016 were obtained from the Multi-resolution Emission Inventory for China (MEIC) (Zheng et al., 2018a) and

downscaled to 4 km × 4 km horizon resolution using various spatial proxies (Geng et al., 2017; Zheng et al., 2018b). Detailed traffic flow and speed were not available, hence daily vehicle NO_x emissions on different road types in Beijing had to be used to estimate emissions on different roads in Guangzhou. Shipping emissions were taken from MarcoPolo-Panda for the year 2014 (MarcoPolo-Panda, 2017) due to shipping activities. The model was evaluated using the NO_2 concentrations at the 11 monitoring sites shown in Figure 4.1. State-controlled sites were used in this study, but no information about monitoring site heights was available other than they range in elevation from 2–20 m, 11.5 m was used as an estimation to validate the concentration with the observations. When the model simulated concentrations at receptors to estimate human exposure, 1.5 m was used assuming at this height human beings inhale contaminated air.

Table 4.3 The parameters used in the ADMS-Urban for Guangzhou.

Dispersion model parameters	**Parameters in ADMS-Urban**	**Set-up**
meteorological conditions	wind speed and direction	2 m temperature, 10 m u-component of wind,10 m v-component of wind, instantaneous surface sensible heat flux, total cloud cover, boundary layer height (ERA5)
	surface roughness	2 m
terrain		terrain file for 1355A
emissions	gridded	MEIC 4 km and macro panda shipping
	road	assigning MEIC transportation emission to each road
background concentration		CAMS at 114.4, 24.7 (lat, lon)
receptor height	for validation	11.5 m
	virtual receptors	1.5 m
chemistry		Chemistry with trajectory

4.3.1 Emission inputs

Gridded emissions of NO_x and VOCs for the year 2016 were obtained from the Multi-resolution Emission Inventory for China (MEIC) (Zheng et al., 2018a) and downscaled to 4 km × 4 km horizon resolution using various spatial proxies (Geng et al., 2017; Zheng et al., 2018b). Shipping emissions were taken from MarcoPolo-Panda for the year 2014 (MarcoPolo-Panda, 2017). A map of the total NO_x emissions is shown in Figure 4.3.

Motorway, trunk, primary, secondary, and tertiary roads, as defined by OpenStreetMap, were explicitly modelled as road sources (OpenStreetMap, 2018). Emissions from roads were calculated by assigning total on-road traffic emissions to the explicitly modelled roads according to road type and total length of each road. NO_x and VOC emissions from the transportation sector were obtained from MEIC. The proportion of these emissions assigned by MEIC as on-road is given in Table 4.4. To allocate the on-road NO_x and VOC emission to different road types (and for weekdays vs weekend), the relative emissions from the three types of roads – urban freeway, artery, and local – reported by Jing *et al.* (2016) and given in Table 4.5 was used. Since OpenStreetMap classifies roads into motorway, trunk, primary, secondary, and tertiary roads (OpenStreetMap, 2018) the following assignments were made: motorway was assigned as urban freeway; trunk, primary, and secondary roads were assigned as artery road; and tertiary road was assigned as local road. For each road type, the emission from each road in each grid for Guangzhou was calculated by using the total emission from that road type in that grid multiplied by the ratio of the road length to total road length in that grid (Equation 4.1).

Equation 4.1

$$\mathbf{E_{road}} = \mathbf{E_{grid\ road}} \times \frac{\mathbf{L_{road}}}{\mathbf{L_{tot}}}$$

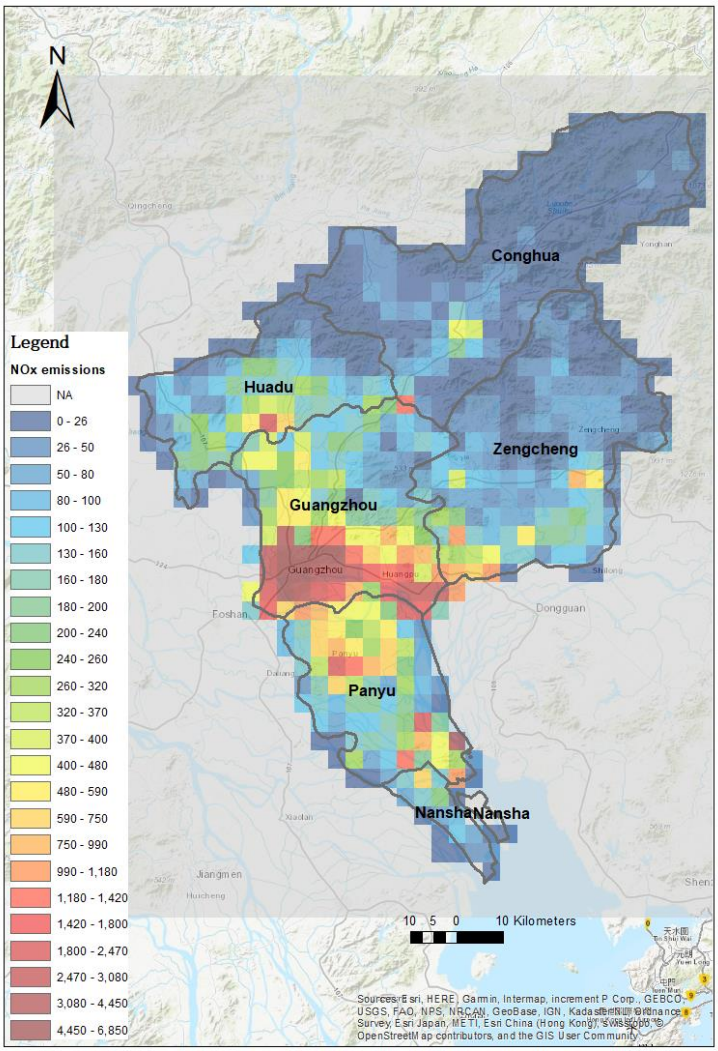

Figure 4.3 Total 2016 annual NO_x emission for each 4 km × 4 km emission grid in Guangzhou. Unit is Mg/grid. Data from Zheng et al. (2018a) and MarcoPolo-Panda (2017).

Table 4.4 Split between on-road and off-road emissions from the transportation sector in Guangzhou in 2,016 (Zheng et al., 2018a).

Type	NO_x	VOC
on-road	0.840118	0.986973
off-road	0.159882	0.013027

Table 4.5 Daily vehicle NO_x emissions on different road types in Beijing (unit: Mg day $^{-1}$) (Jing et al., 2016).

Date	Road type	NO_x	VOCs
Weekdays	Urban freeway	111.09	22.40
	Artery road	124.53	25.16
	Local road	56.49	11.42
Weekends	Urban freeway	95.39	19.21
	Artery road	110.81	22.36
	Local road	74.04	14.97

4.3.1 Meteorological inputs and background concentrations

Wind speed and direction at 10 m above the ground, and cloud cover, at a horizontal resolution of 31 km, were obtained from ECMWF-ERA5 (ECMWF, 2019). As the prevailing wind direction in Guangzhou was from the northeast (Figure 4.4), the background site for pollutant concentrations for the model was chosen to be a rural location to the northeast of the model domain (Figure 4.5), though south-easterly wind mainly occurs in summer. Background concentrations of NO_2, NO_x, and O_3 were obtained from the Copernicus Atmosphere Monitoring Service (CAMS) (ECMWF, 2019). Figure 4.5 shows the lowest concentration of background NO_2 is located to the north east.

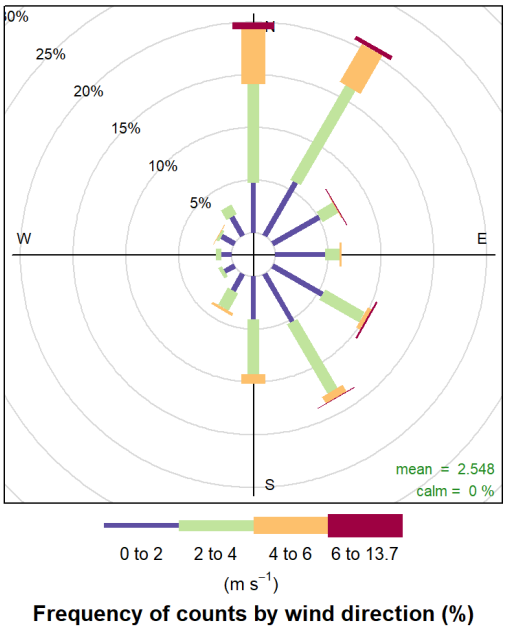

Figure 4.4 Annual average wind rose of hourly wind speed and direction in 2017 in Guangzhou using data from ERA5 (ECMWF, 2019) for the area delineated by the latitude and longitude coordinates: 23.94°/112.95°/22.73°/114.05°. Data are summarized by direction by 30 degrees and by different wind speed categories. Wind speeds are represented by different width "paddles". The plots show the proportion (as a percentage) of time that the wind is from a certain angle and wind speed range.

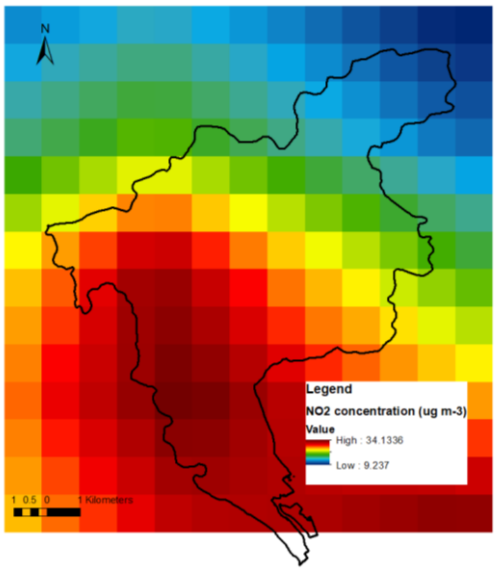

Figure 4.5 Annual-mean concentrations of NO_2 (in µg m^{-3}) at 0.1° (~11 km) spatial resolution obtained from the Copernicus Atmosphere Monitoring Service (CAMS) (ECMWF, 2019). The lowest concentration of background NO_2 is located to the north east, upwind for the prevailing wind direction as shown in Figure 4.4.

4.4 Selection of the ADMS-Urban virtual receptor sites

As the main purpose of modelling NO_2 concentrations is to estimate NO_2 where people live, the virtual sites were primarily selected to be proportionally located across the residential areas of Guangzhou. The six districts have a large range in population (Table 4.6) so site selection was first stratified across the six districts so as to ensure that sites in the virtual network were located across all districts. Centroids of each cell of population data (100 m $\times$ 100 m) (Worldpop, 2013) were extracted as potential virtual receptor sites. Three types of virtual sites were defined for each district so as also to span the range in anticipated NO_2 concentration:

- ***Background site:*** centroid of the population cell with greatest distance to the nearest road.
- ***Roadside sites:*** centroids of the population cells with a distance to nearest road of no more than 5 m.
- ***Residential sites:*** centroids of the population cells with the highest population density.

In each district, residential sites were selected first, with number of residential sties proportional to the relative proportion of the total Guangzhou population in that district (the specific number is given in Table 4.6). One residential site in two districts also fitted the definition of roadside site (see Table 4.6), but these were retained under the category of residential. All other sites that satisfied the definition of roadside site (17 across the six districts, Table 4.6) were selected as receptor locations within the roadside site category. A background site was selected in each district. An additional overarching criterion was a minimum distance of 300 m between any pair of sites in each district to ensure that all sites were distributed across the range of localities in the study area. The locations of the 83 sites are shown in Figure 4.6. ADMS-Urban was used to simulate annual-mean NO_2 concentrations at these locations at a height of 1.5 m above local surface level.

Table 4.6 Population of each district, the number of residential and roadside sites selected and the number residential sites also satisfying the definition of roadside site.

District	Population	No. of residential sites	No. of residential sites also fitting roadside definition	No. of roadside sites
Conghua	596,816	3	0	1
Guangzhou city centre	7,909,399	37	1	6
Huaxian	916,916	4	1	2
Nansha	110,923	1	0	1
Panyu	1,986,223	10	0	5
Zengcheng	1,120,186	5	0	2

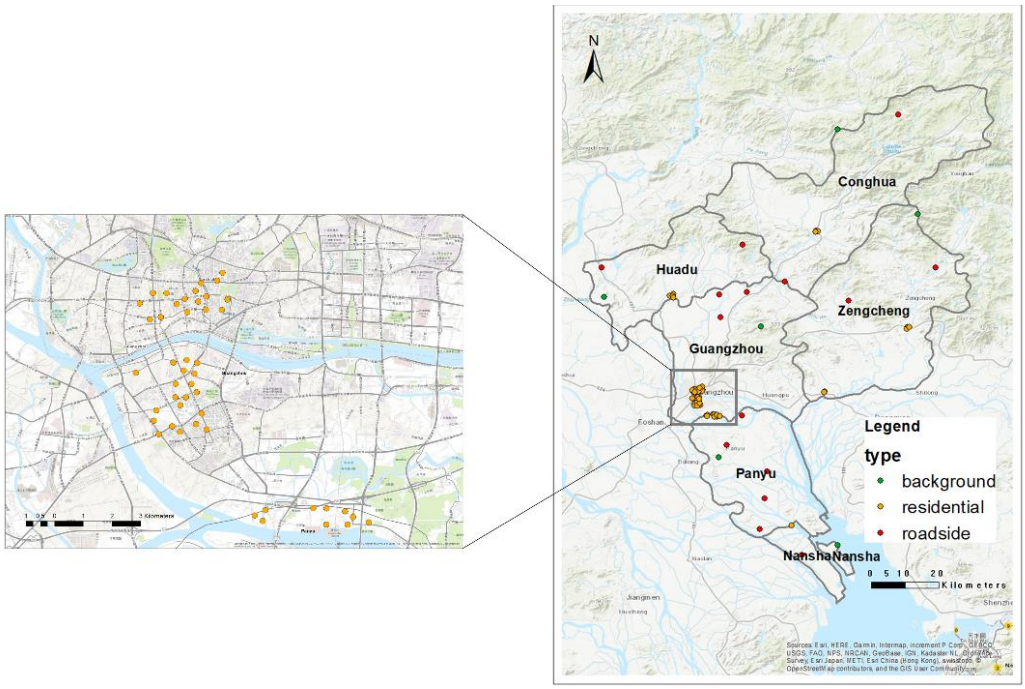

Figure 4.6 The locations of 83 virtual receptor sites for the dispersion modelling, which were stratified into the six districts of Guangzhou indicated by the boundaries. The basemap is from Word Topographic Map.

4.5 Development of the LUR model

4.5.1 LUR model predictor variables

Sources of data used to develop the LUR model are given Table 3.4 and potential predictor variables for the LUR model are listed in Table 4.7. Road lengths in a buffer had to be used as surrogates for traffic flow and fleet composition, as neither of these data are publicly available for Guangzhou. The variables of number of people and artificial (i.e. non-natural) area within a buffer do not directly affect NO_2 concentration, but they are indirectly related to road transport emissions and to domestic, industrial and electrical generation emissions which contribute to total NO_x emission in Guangzhou (Figure 4.8). Distance to nearest port and its derivates were included as non-buffer variables to account for the impacts of shipping, Guangzhou is close to the South China Sea, and is a major port, with ship activities significantly contributing to total NO_x emissions in the southern part of the model domain (Johansson et al., 2017; H. Liu et al., 2016) (Figure 4.8). A maximum distance of 35,000 m was specified for the distance to port variable as the dispersion modelling at the virtual sites indicated that NO_2 concentration decreased to urban background level at this distance from nearest port as shown in Figure 4.7. The reasons for having a cap on shipping is that, shipping effects are represented as a variable without buffers (which shows the areas this variable can affect). A scatter plot of NO_2 concentration at “virtual sites” and distance to the nearest port is shown in Figure 4.7 and it shows that the concentration dropped most dramatically at distance before 20,000 m but it still decrease with the distance increase and it’s unclear which number gives best model predictability. Sensitivity tests of different models with various cap distances were conducted and and the one with highest R^2 is 35,000 m. Green, i.e. not built-up, areas are assumed to mitigate NO_2 concentration since they are not sources of NO_2 and also act as areas over which NO_2 concentrations disperse and dilute (and deposit), hence the *a priori* direction of effect of the green area

variable is negative (Jim and Chen, 2008). Coordinates and altitude were included to reflect physical geography influence and wind speed and direction proxies.

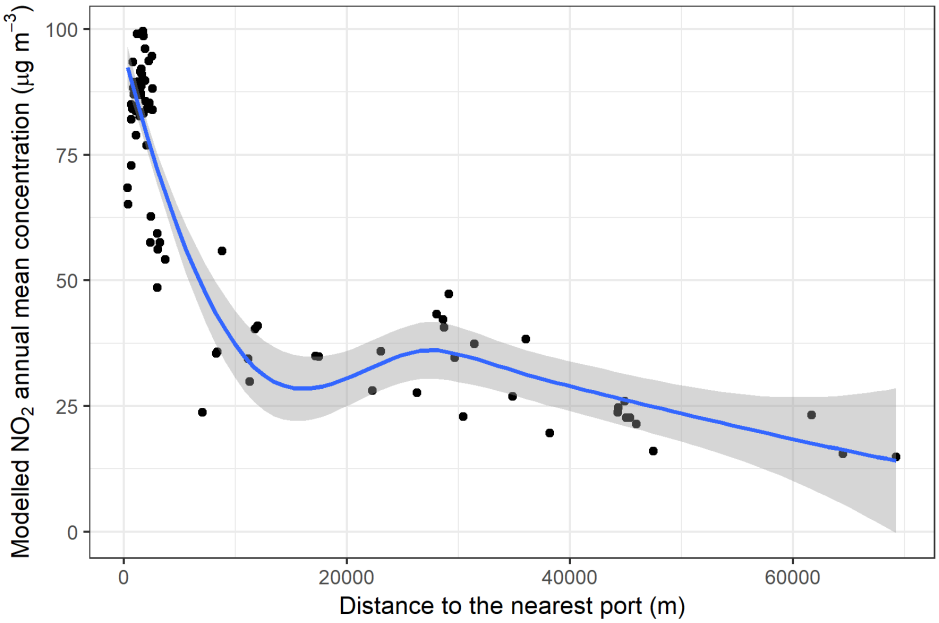

Figure 4.7 Concentration of ADMS-Urban modelled NO_2 at the 83 'virtual sites' (black dots) as a function of distance to the nearest port. The blue line is a smoothed conditional mean of the data and is presented only to guide the eye.

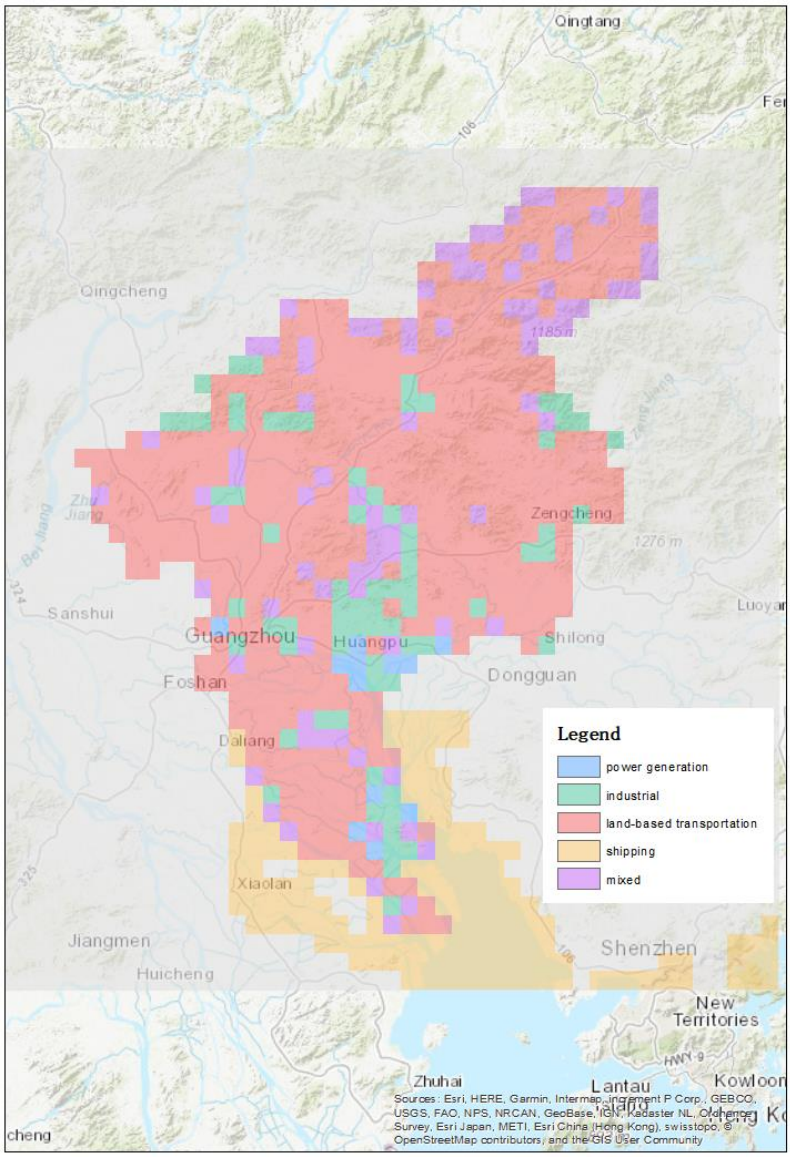

Figure 4.8 The dominant NO_x emission source for each emission grid cell in Guangzhou. A cell is designated as mixed when no single source contributes >50% of total emissions. Data from MEIC (Zheng et al., 2018a) and MarcoPolo-Panda (2017).

Table 4.7 Predictor variables and buffer sizes included in LUR model development, and a priori anticipated direction of effect of variable on NO_2 concentration. The road categories assigned as being major or minor are the names of the OpenStreetMap road types indicated in the table.

Variable	Abbreviation	Unit	Buffer radius (m)	*A priori* sign of effect
all road length	all_len	m	25, 50, 100, 300, 500, 1,000	+
major road length (motor, trunk, primary)	maj_len	m	25, 50, 100, 300, 500, 1,000	+
minor road length (secondary+tertiary)	min_len	m	25, 50, 100, 300, 500, 1,000	+
motorway (link)	mot_len	m	25, 50, 100, 300, 500, 1,000	+
trunk (link)	tru_len	m	25, 50, 100, 300, 500, 1,000	+
primary (link)	pri_len	m	25, 50, 100, 300, 500, 1,000	+
Secondary	sec_len	m	25, 50, 100, 300, 500, 1,000	+
tertiary	ter_len	m	25, 50, 100, 300, 500, 1,000	+
distance to the nearest road length	dis_all	m	N/A	–
distance to the nearest major road length (motor, trunk, primary)	dis_maj	m	N/A	–
distance to the nearest minor road length (secondary+tertiary)	dis_min	m	N/A	–

distance to the nearest motorway (link)	dis_mot	m	N/A	–
distance to the nearest trunk (link)	dis_tru	m	N/A	–
distance to the nearest primary (link)	dis_pri	m	N/A	–
distance to the nearest secondary road	dis_sec	m	N/A	–
distance to the nearest tertiary road	dis_ter	m	N/A	–
distance to the nearest port	dis_por	m	N/A	–
square distance to the nearest port	sq_dis_port	m^2	N/A	–
distance to coast	dis_cst	m	N/A	–
distance to river	dis_riv	m	N/A	–
number of people	Pop	N/A	100, 300, 500, 1,000, 5,000	+
artificial area	art_area	m^2	100, 300, 500, 1,000, 5,000	+
altitude	Alt	m	N/A	–
latitude, longitude	lat, lon	°	N/A	N/A
green area	gre_area	m^2	100, 300, 500, 1,000, 5,000	–
district indicator	Conghua, Guangzhou city centre, Huaxian, Nansha, Panyu, Zengcheng	N/A	N/A	N/A

4.5.2 LUR model development and evaluation

A stepwise multiple regression approach was used to select the potential predictor variables and the details are in Section 2.3.3. First, all predictor variables were individually regressed against the dependent variable data (annual-mean NO_2 concentrations modelled by ADMS-urban at the 83 receptor sites). The predictor variable which explained the most NO_2 concentration variation (highest R^2) and with a coefficient in the *a priori*-defined direction (Table 4.7) formed the initial model. The univariate linear regression process was repeated with the remaining variables followed the criteria on adjusted R^2 , *p*-value, and coefficients of variables (Section 2.3.3). Diagnostic tests were then performed to check multicollinearity and influential observations. In this study, no observation was removed. The model was evaluated using both the measurement and virtual site concentration data.

4.6 Health burden calculation

The association with all-cause mortality of 2.45% (95% CI: 2.34%, 2.58%) per 10 μg m^{-3} elevation of NO_2 reported by Zhang *et al.* (2011) were used, since it was derived from data in Shenyang, a province in China. The number of deaths in 2017 in Guangzhou was 60,900 (Guangzhou Statistics Bureau, 2018). The population data (100 m × 100 m) was resampled to the resolution of the concentration map (25 m × 25 m). The population-weighted average concentration (E) for NO_2 across the whole of Guangzhou was calculated as follows:

$$\textbf{Equation 4.2} \qquad \mathbf{E} = \frac{\mathbf{1}}{\mathbf{Pop}} \sum_{\mathbf{i}} \mathbf{C_i}\, \mathbf{Pop_i}$$

where C_i and Pop_i are the concentration and the number of people in each cell *i* of the concentration map.

The attributable deaths from exposure to ambient NO_2 in Guangzhou was calculated by multiplying the AF by number of all-cause deaths (Equation 2.5, Equation 2.10 and Equation 2.11). Details are in Section 2.6.2.

4.7 Model Evaluation

4.7.1 ADMS-Urban model evaluation

The ADMS-Urban model showed good statistical performance against the annual-mean NO_2 concentrations at the 11 monitoring sites in Guangzhou (Figure 4.9A). The model explains 72% of the spatial variation in the measured NO_2, with an RMSE of 17.7 μg m^{-3}, albeit with a tendency to overpredict NO_2 concentrations (MB = 11.2 μg m^{-3}, NMB = 0.22). A likely explanation for the general overprediction is that the precise height of each monitoring site is unknown. The only information provided to us is that they range in elevation from 2–20 m, which is consistent with anecdotal information that pollutant monitoring sites in Chinese cities are often situated on tops of buildings, and thus at higher elevation (where NO_2 concentrations would be lower) than the receptor height used in the model. The greatest model overprediction at site 1354A (Figure 4.9A) is likely explained by the fact that this site is located in a park in the city centre and is surrounded by dense vegetation whose effects on NO_2 concentration (through dispersion, deposition, and temperature reduction) are not sufficiently captured by the model. As the distance to nearest road for all 11 monitoring sites is greater than 5 m, the observed data can not verify the model for roadside locations where highest NO_2 concentrations are anticipated, but at the other end of the concentration range the model predicted well the background site 1355A which is located in an area of natural land cover (Maofengshan). It is also important to recognise that the observational data have uncertainty. It has not been feasible to robustly quantify uncertainty for the NO_2 measurements in Guangzhou within the scope of this study, as documentation of the processes applied for data quality control and assurance

(QA/QC) and the operating principles at each monitoring site is not publicly available (Section 2.5).

4.7.1 Hybrid LUR model and evaluation

The final LUR model contained three variables (Table 4.8): *pop_5,000* (the number of people within a 5,000 m buffer) *sq_dis_port* (the squared distance to the nearest port), and *all_len_25* (the length of all type of roads within a 25 m buffer). The three variables respectively represent the influence of people (indirectly related to residential, industrial, and traffic emission, and inversely related to green space), shipping emissions, and traffic emissions. Table 4.9 summarizes the results of hybrid LUR model evaluation against both the 83 virtual sites and the 11 monitoring sites and Figure 4.9B shows the scatter plot for the LUR model predictions at the 11 monitoring sites.

Against the 83 virtual sites, LOOCV evaluation shows the hybrid LUR model explains 96% of the spatial variation of NO_2 concentration with an RMSE of 5.64 μg m^{-3}. The NO_2 concentrations at the monitoring site provide an additional evaluation of the hybrid LUR model independent of the NO_2 data used to construct the model (Table 4.9 and Figure 4.9B). For this plot, R^2 = 0.63 and MB = 9.08 μg m^{-3}, which corresponds to an NMB of 18.2%. These statistical uncertainties seem reasonable for intra-urban modelling/mapping of a domain of this size and with the paucity of detailed emissions data to support modelling. Figure 4.9B shows that the hybrid model slightly overestimates NO_2 concentrations, which as discussed earlier is likely the consequence of the model predicting NO_2 concentration at 1.5 m height, which is lower than the height of most monitoring sites (2 – 20 m). Closer inspection of Figure 4.9B shows that the model generally over-predicts more at locations with higher NO_2 concentrations which can be rationalised because these are the locations most affected by local traffic emissions for which there is insufficiently detailed input

data. As noted above, it is also important to recognise that there is uncertainty in the observed values.

Table 4.8 The final LUR model variables and their coefficients and standard errors.

Variable	Definition	Coefficient	Standard Error ($\mu g\ m^{-3}$)
Intercept ($\mu g\ m^{-3}$)	/	33.09	1.77
pop_5,000	number of people within a 5,000 m buffer	2.875×10^{-5} ($\mu g\ m^{-3}$)	1.087×10^{-6}
sq_dis_port (m^2)	squared distance to the nearest port	-9.543×10^{-9} ($m^{-2}\ \mu g\ m^{-3}$)	1.832×10^{-9}
all_len_25 (m)	length of all type of roads within a 25 m buffer	6.362×10^{-2} ($m^{-1}\ \mu g\ m^{-3}$)	1.261×10^{-2}

Table 4.9 LUR model performance evaluated by training (R^2 and RMSE), LOOCV (R^2 and RMSE), and observation (R^2 and RMSE).

Evaluation method	R^2	RMSE ($\mu g\ m^{-3}$)
Using 83 virtual sites	0.96	5.48
LOOCV using 83 virtual sites	0.96	5.64
Using measurement at 11 monitoring sites	0.63	18.0

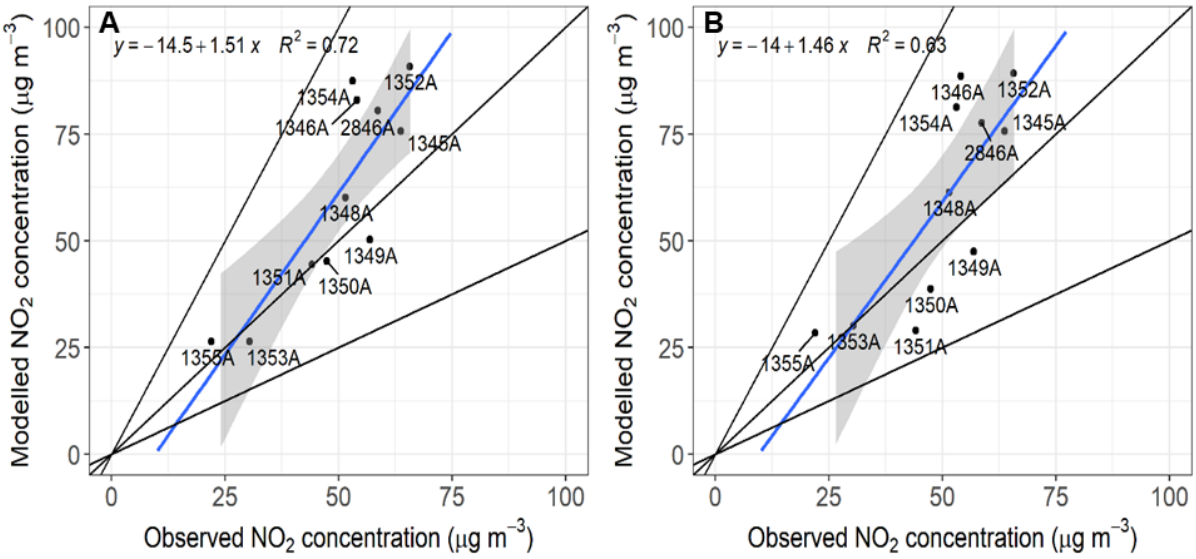

Figure 4.9 (A) Dispersion model NO_2 concentrations versus observed NO_2 concentrations. (B) Hybrid LUR and dispersion model NO_2 concentrations versus observed NO_2 concentrations.

4.8 Concentration map and premature attributable deaths

Figure 4.10 shows the spatial distribution of NO_2 concentration across Guangzhou in 2017. Modelled concentrations vary between 21.5 μg m^{-3} in the most rural areas in the north of the domain to 99.7 μg m^{-3} in the most polluted district of Guangzhou city centre. The map indicates that, as expected, concentrations of NO_2 are highest on road links, particularly those with heavy traffic as shown on the expanded map of the city centre. The model NO_2 concentration show high values at the boundary of Nansha, which is likely due to shipping (Figure 4.8). The population-weighted annual-mean concentration of NO_2 across Guangzhou is 52.5 μg m^{-3}. This population-weighted concentration exceeds the Chinese air quality standard and WHO guideline of 40 μg m^{-3} (Ministry of Ecology and Environment, 2012; WHO, 2006), and Figure 4.10 indicates that, in large areas of Guangzhou, concentrations of NO_2 are substantially in excess of this value.

The modelled number of premature deaths attributable to long-term exposure to NO_2 in Guangzhou in 2017 was 7,270 (6,960–7,620; range based only on the 95% CI for the health risk coefficient). For comparison, the total number of deaths from road-traffic accidents in Guangzhou was 847 in 2015 (Guangzhou Municipal Public Security Bureau, 2016). Approximately 60% of people in Guangzhou experienced NO_2 concentration above the China air quality standard/WHO guideline of 40 μg m^{-3}. The air quality plan (2016-2025) published by the Guangzhou government to combat air pollution problems sets the target of meeting the NO_2 air quality standard of 40 μg m^{-3} by 2020 (Guangzhou Government, 2017). Our model predicts that if all areas with NO_2 concentrations greater than 40 μg m^{-3} were reduced to the air quality standard, the number of lives saved would be 1,900 (1,820–1,980) compared to the 2017 estimate. Walton *et al.* (2015) estimated the mortality burden of NO_2 in London in 2010. The AF in various boroughs in London ranged from 9.8% to 20% with an average of 13.3% and the concentration-response coefficient used in the study was 1.06. The AF values reported in London are comparable to 11.9% using 1.0245 as the coefficient in Guangzhou in our study. Carnell *et al.* (2019) calculated AF values for all-cause mortality in the UK associated with NO_2 using 1.023 as the coefficient. The AF values from 1970 to 2010 ranged from 2.96 % to 5.76%, which are lower than those in London and in Guangzhou. The lower AF values are likely due to areas with much lower concentration of NO_2 than London and Guangzhou included in the calculation for the whole UK.

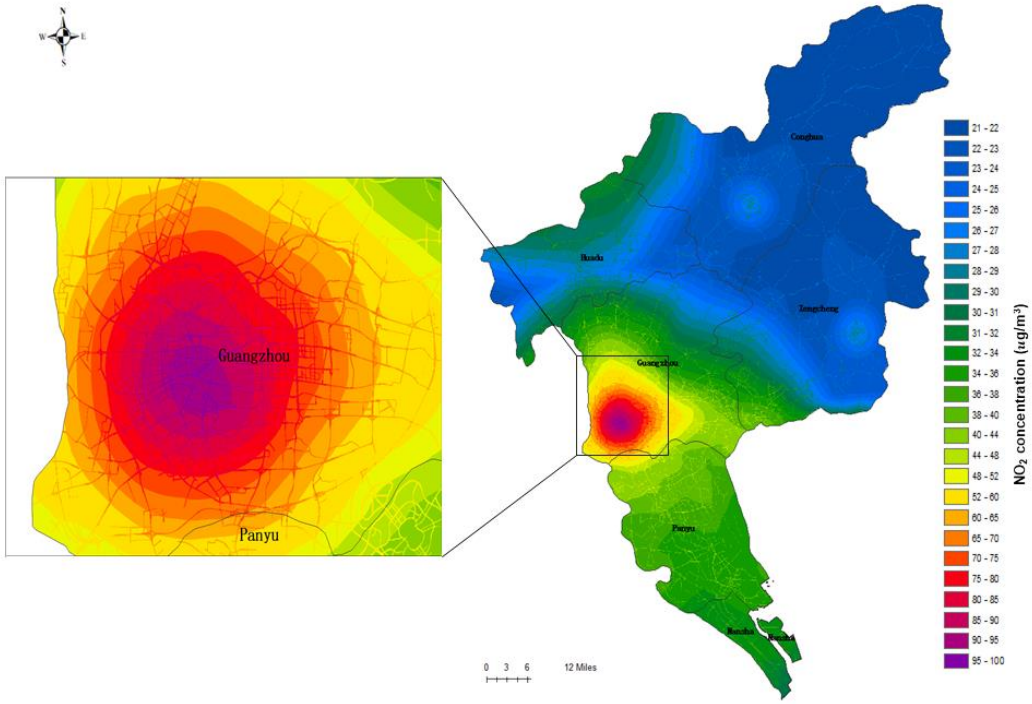

Figure 4.10 The final hybrid dispersion-LUR model of NO_2 concentrations in Guangzhou. The most polluted district is Guangzhou city center. NO_2 concentrations are higher at locations around the road links, industrial areas, and close to the ports (in the southern part of the model domain).

4.9 Advantages and limitations of the hybrid model

4.9.1 Advantages of the hybrid modelling approach

The challenge of high spatial resolution air pollution modelling has driven integrated data and modelling approaches (Beevers et al., 2012; Hao et al., 2016; Hood et al., 2018; Johnson et al., 2010; Xue et al., 2019; Yang et al., 2017). For megacities of large area like Guangzhou, without additional monitoring data, our solution for simulation of an NO_2 concentration map has been to derive a hybrid modelling approach that uses a virtual network of receptor locations for dispersion and LUR modelling. This approach gives flexibility to choose the input sites (such as weighting towards residential population (around 60% of the receptors are in Guangzhou city centre) and number of sites (83 receptor sites). It also takes less time to generate a high-

resolution map over a large domain compared with dispersion modelling only. In this hybrid approach, dispersion modelling is used to conduct scenario analysis and LUR is used for interpolating the spatial trends. This approach can be easily used to derive concentration maps to calculate health burdens (including for future scenarios) or for epidemiological studies.

4.9.2 Limitations of the study

There are of course uncertainties, as for any modelling approach. Even though we have sought to play to the strengths of the available data for Guangzhou, data accessibility and quality are generally an issue for China (He et al., 2018). For example, detailed industrial emissions as point sources for the dispersion model are not accessible in Guangzhou. Similarly, detailed traffic flow and speed are not available, hence road length was used as a proxy in the LUR model. Also daily vehicle NO_x emissions on different road types in Beijing had to be used to estimate emissions on different roads in Guangzhou. Since detailed land-use data are not available, satellite observation derived data Globeland30 were used (Globeland30, 2010). It is extremely difficult to get access to monitoring data in Guangzhou; several websites provide real time data (AQICN, 2019; CNEMC, 2019), but historical data are not available for download from official sites and the detailed location and environment of the monitoring sites are unclear. State-controlled sites were used in this study, but no information about monitoring site heights was available other than they range in elevation from 2–20 m. The quality of monitoring data is unknown. ADMS requires concentrations of NO and NO_2 background concentrations but only NO_2 was reported at each monitoring site, therefore ECMWF-CAMS re-analysis data was used for the boundary concentration. No roadside monitoring sites were available, so neither the dispersion nor the LUR model simulations could be validated at highest NO_2 concentrations. Since the LUR model used ADMS-Urban modelled concentrations as input, the hybrid model inevitably transmits any bias in the dispersion modelling to the final model.

In terms of the health burden calculation, detailed census data is not available and UN modelled population data (Worldpop, 2013) were used instead. A health risk coefficient from a single-pollutant model was used which may overestimate the actual effects due to NO_2 (COMEAP, 2018). In common with studies of this kind, population data at residential address was used. An assessment of the impact of work location on population level of exposure requires additional information on population distributions at different times (Reis et al., 2018).

4.10 Conclusions

Given the current challenges related to data availability, accessibility and quality in Chinese megacities, and their large spatial area, a single model struggles to provide high spatio-temporal resolution air pollution maps for the whole city. In this work, a combined dispersion and LUR model approach to simulate annual average NO_2 for health burden assessments was demonstrated for the megacity of Guangzhou. Ambient concentrations of NO_2 simulated by the ADMS-Urban dispersion model at 83 'virtual' monitoring sites, selected to span both the range of NO_2 concentration and weighting by population density, were used to develop a highly spatial resolved LUR model. To our knowledge, this is the first attempt to apply this approach to maximize the advantages of both modelling approaches and to overcome data shortcomings in relation to data availability in China. This method can be employed in other cities in China, or globally, to model ambient NO_2 concentration at high spatial resolution to investigate the effectiveness of potential mitigation policies. The dispersion model simulates the effect of different emissions scenarios on concentrations at the network of receptor locations, from which LUR modelled maps are constructed to estimate future concentrations and health burdens across the whole domain.

Chapter 5 Modelling public health benefits of various emission control options to reduce NO_2 concentrations in Guangzhou

This chapter is based on a research paper submitted in 'Environmental Research Letters' (He, B.; Heal, M.R.; Reis, S Modelling public health benefits of various emission control options to reduce NO_2 concentrations in Guangzhou) I, in discussion with Stefan.Reis and Mathew Heal, conceived the aims and methodology of the research. I undertook the modelling, mapping and calculations, plus all table and figure presentations. I wrote the full first draft of the paper. Other co-authors supplied further suggestions and revisions to the text.

5.1 Introduction

Guangzhou is an example of many cities in China that do not currently meet the Chinese air quality standards (GB 3095-2012) (Ministry of Ecology and Environment, 2012). Consequently, as required under both the Chinese national laws cited above the Guangzhou Municipal People's Government has developed the Guangzhou Ambient Air Quality Compliance Plan (2016-2025) (People's Government of Guangzhou Municipality, 2017). The Chinese air quality standard for NO_2 is currently set equal to the World Health Organization (WHO) air quality guideline, at 40 μg m^{-3} as an annual average, and the Guangzhou aspiration is to achieve this by 2020 (and also to achieve an annual average NO_2 concentration of 38 μg m^{-3} by 2025) (People's Government of Guangzhou Municipality, 2017).

NO_2 derives primarily from NO_x (NO and NO_2) emitted from road transport, domestic, commercial and industrial combustion, and shipping (Ding et al., 2018; Fu et al., 2017; Liu et al., 2017; MEIC, 2016). Due to the ubiquitous nature of combustion sources and the relatively short lifetime of NO_2, its concentrations are highly spatially variable (Beirle et al., 2011; Cyrys et al., 2012; Gurung et al., 2017). However, although the Guangzhou Ambient Air Quality Compliance Plan states that the NO_2 target needs to be met in all areas in Guangzhou, it is not defined how compliance is to be evaluated, for instance

whether this includes at locations without monitoring stations. Furthermore, because the ultimate aim of setting an NO_2 concentration target is to alleviate the negative impacts on health, the estimation of potential city-wide population health gains from policy interventions that target NO_2 emission reductions from local sources also requires highly spatially resolved NO_2 concentration data.

The hybrid modelling approach (Chapter 4) were applied in Guangzhou and can be used to derive spatially-explicit maps of NO_2 concentrations for the whole domain under alternative future emissions scenarios that are underpinned by process-based dispersion simulations. The aim of the study in this chapter is two-fold. First, the modelling approach (He et al., 2019) is used to investigate the ability of a range of example emission reduction scenarios to meet the Guangzhou Ambient Air Quality Compliance Plan target of 40 μg m^{-3} annual-average NO_2 concentration. Since it is not clear what constitutes compliance with the target, we present results that illustrate the emissions reductions required for modelled concentrations to meet the following interpretations of a 40 μg m^{-3} target:

- Target Interpretation 1: the average of the annual average concentrations at all current NO_2 monitoring sites meets the target (TI1).
- Target Interpretation 2: the annual average concentration at all current NO_2 monitoring sites meet the target (TI2).
- Target Interpretation 3: the population-weighted annual average concentration in Guangzhou meets the target (TI3).
- Target Interpretation 4: the annual average concentration everywhere in Guangzhou meets the target (TI4).

Secondly, the modelled NO_2 concentrations are used to determine the changes in population exposure to NO_2, and the associated population premature mortality avoided. These data are used to illustrate that the use of a concentration threshold as a policy metric can fail to convey to policy-makers

and the public the extent of population health gain achieved across a range of potential emissions reductions even where reductions fail to deliver the concentration target (and the continuing public health gain for reductions that go beyond meeting the concentration target).

The study does not set out to simulate real-world proposed policy measures, but to illustrate an approach to identifying the scale of the mitigation challenge to achieve city-wide concentration standards set under existing policy targets and what their associated potential health gains may be. Economic costs and benefits are not evaluated. Whilst the results are based on consistent model results for the specific situation in Guangzhou, they provide relevant evidence to decision makers designing effective air pollution control policies in other fast-growing megacities in China and elsewhere globally.

5.2 Method

5.2.1 A hybrid modelling approach

The final LUR model variables and the evaluation statistics for the LUR model for 2017 ('base case') NO_2 concentrations, as reported previously in He *et al.* (2019) and Chapter 4 , are summarised in Table 4.8 and Table 4.9, respectively. The spatial resolution of the final modelled NO_2 concentrations is 25 m. The same method here to develop spatial maps of NO_2 concentration for each of the emission reductions scenarios described in the following section. The use of the dispersion model means that NO_2 concentrations at the set of 83 receptor locations for different emissions reductions scenarios are derived from a process-based model. The variables selected for the subsequent LUR models for the different scenarios are listed in Table 5.1. Because road length was used as a proxy of traffic, and therefore cannot reflect the proportion change of traffic emission, the final model might

underestimate the impacts of traffic emission reduction. The ADMS-Urban model was also used to derive NO_2 concentrations at each of the 11 NO_2 monitor locations in order to address target interpretations TI1 and TI2 of compliance with a Guangzhou NO_2 target.

Table 5.1 The variables selected in the final LUR models for the different emissions reductions scenarios modelled in this study. (*pop_5,000*: population with 5,000 meter buffer, *sq_dis_port:* squared distance to the port*)*

Scenarios	Variables selected
$A_{10\text{-}50}$, $B_{10\text{-}90}$	*pop_5,000, sq_dis_port*
$A_{60\text{-}90}$	*pop_5,000*

5.2.2 Modelling scenarios

To explore the scale of emissions reductions required to meet the Guangzhou NO_2 concentration target of 40 μg m^{-3}, the following different scenarios were simulated using ADMS-Urban to derive concentrations at the 83 pre-selected receptor locations.

1) Base case: 2017 emissions
2) Scenarios A_x: reductions of NO_x and VOCs emission in all source sectors equally by 10% decrements (x) between 10% and 90%
3) Scenarios B_x: reductions of NO_x and VOCs emission in the road transport sector by 10% decrements (x) between 10% and 90%

Traffic is a dominant NO_x emission source in Guangzhou (Figure 4.8) (MEIC, 2016) and is explicitly modelled in ADMS-Urban (CERC, 2017), so the B_x scenarios were undertaken to demonstrate the change of NO_2 concentration if interventions focusing only on reductions of NO_x and VOCs emissions from road traffic were to be implemented.

Under the base case scenario (2017), the total annual NO_x and VOCs emissions are 180.2 kt and 357.3 kt, respectively (Table 5.2). Emissions reductions are substantially larger under the A_x scenarios than the B_x scenarios. Scenario B_{90}, the reduction of NO_x and VOCs emissions from road transport by 90%, results in reductions of about 34 kt NO_x and 45 kt VOC. Scenario A_{90}, which reduces all sector emissions by 90%, corresponds to reductions in NO_x and VOC of 162 kt and 322 kt respectively (Table 5.2).

Emissions reductions in VOCs as well as NO_x in the model simulations were included since VOCs are the other class of primary emissions that can impact on the gas-phase NO_x chemistry. The same percentage reductions in VOCs and NO_x were applied, although equal reductions of each is probably not a realistic outcome of particular policy measures. However, the VOCs reductions imposed in the model scenarios in fact impact relatively little on the results of our study which investigates the impacts of emissions reductions in the Guangzhou domain on intraurban levels of NO_2 in the Guangzhou domain. To demonstrate this, a sensitivity simulation with the dispersion model of NO_2 concentrations at the 11 monitoring sites in Guangzhou for a scenario with 50% reduction in NO_x emissions but baseline VOCs emissions was conducted. The results from this simulation are compared in Figure 5.1 with those for the simulation with baseline NO_x and VOCs emissions and for the scenario where both NO_x and VOC emissions are reduced by 50%. Figure 5.1 shows that the inclusion or not of 50% VOC emissions reductions alongside the 50% reductions in NO_x emissions has very little impact on the NO_2 concentrations at these locations (across a range of absolute NO_2 concentrations) compared with the change in NO_2 concentrations brought about by the reductions in NO_x emissions. The average change (increase) in NO_2 concentration for the scenario with 50% NO_x emissions reduction and no VOCs reductions compared with the scenario where both VOCs and NOx emissions are reduced by 50% is only 1.1 µg m^{-3}, which equates to only a 2.5% change in the mean of the NO_2 concentrations across the 11 sites under these scenarios (43 µg m^{-}

^{3}). In comparison, the 50% reduction in the NO_x emissions causes an average change across the 11 sites of more than 18 µg m^{-3}.

Meteorological variability can have a significant influence on air quality by affecting the advection, diffusion, and deposition of air pollutants, although less so for annual average concentrations compared with shorter averaging times. The magnitude of inter-annual meteorological variability on annual average NO_2 in Guangzhou was explored by also running the dispersion model for the 11 monitoring sites using the Guangzhou meteorology for each of the years 2013 to 2016. Emissions were maintained at the 2017 base case year. The ranges in the annual averages of the meteorological variables input into the dispersion model across these five years are shown in Table 5.3.

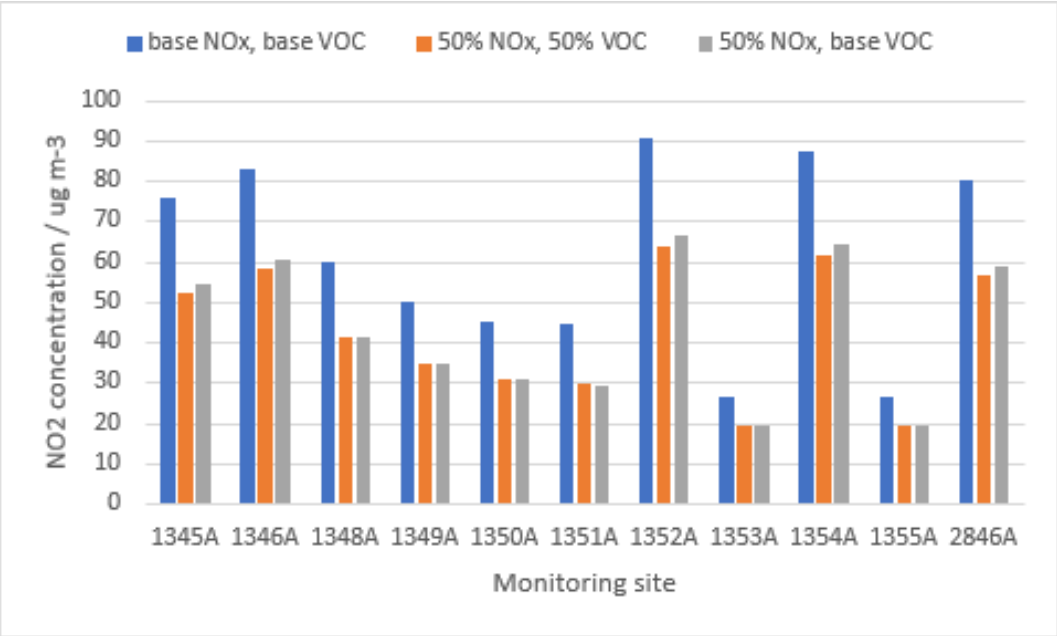

Figure 5.1 Dispersion model simulations of NO_2 concentrations at the 11 monitoring sites in Guangzhou for the baseline scenario (blue), for 50% reductions in NO_x and VOC emissions, as included in the manuscript (orange), and for 50% reductions in NO_x emissions but zero reductions in VOC emissions (grey).

Table 5.2 Total NO_x (as kt-NO_2) and VOCs (as kt-VOCs) emissions, and their corresponding reductions compared with the base-case scenario, for the different emissions reductions scenarios modelled in this study.

Scenarios	NO_x emission (kt[1])	NO_x reduction (kt)	VOCs emission (kt)	VOCs reduction (kt)
Base	180.2	NA	357.3	NA
A_{10}	162.2	18.0	321.6	35.7
A_{20}	144.2	36.0	285.8	71.5
A_{30}	126.2	54.1	250.1	107.2
A_{40}	108.1	72.1	214.4	142.9
A_{50}	90.1	90.1	178.7	178.7
A_{60}	72.1	108.1	142.9	214.4
A_{70}	54.1	126.2	107.2	250.1
A_{80}	36.0	144.2	71.5	285.8
A_{90}	18.0	162.2	35.7	321.6
B_{10}	176.4	3.8	352.3	5.0
B_{20}	172.6	76.7	347.3	10.0
B_{30}	168.7	11.5	342.4	14.9
B_{40}	164.9	15.3	337.4	19.9
B_{50}	161.1	19.2	332.4	24.9
B_{60}	157.2	23.0	327.4	29.9
B_{70}	153.4	26.8	322.4	34.9
B_{80}	149.6	30.7	317.4	39.9
B_{90}	145.7	34.5	312.5	44.8

[1] kilotonne (10^3 tonne)

Table 5.3 Annual averages for 2013-2017 of the hourly meteorological variables needed as input to the dispersion model.

Year	Sensible heat flux (W m^{-2})	Boundary Layer (m)	T (°C)	Cloud cover	Wind Speed (m s^{-1})	Wind direction (°)
2,013	13.2	446.0	22.8	0.65	2.6	65.5
2,014	15.2	441.4	23.0	0.67	2.4	74.1
2,015	13.6	444.2	23.6	0.71	2.6	79.4
2,016	10.4	440.5	23.1	0.71	2.7	59.8
2,017	12.1	434.9	23.3	0.69	2.5	52.6

5.3 Modelled NO_2 concentrations

5.3.1 NO_2 concentrations at monitoring sites

The Guangzhou Ambient Air Quality Compliance Plan does not specify whether modelling is to be used for compliance assessment. Without modelling, compliance can only be evaluated using the monitor data. The NO_2 concentrations simulated using the ADMS-Urban dispersion model at the 11 monitoring sites for the base case and the 18 emissions reduction scenarios are summarized in Figure 5.2. For comparison, the NO_2 concentrations simulated at the 11 monitor sites for the base case for the five meteorological years tested are shown in Figure 5.3. The latter figure shows that NO_2 concentrations at a given receptor varied relatively little for the different meteorological scenarios (at most a few µg m^{-3}) compared with the changes associated with the emissions reduction scenarios shown in Figure 5.2.

As expected, concentrations at monitoring sites under A_x scenarios, which reduce emissions across all sectors equally, are lower than those under B_x scenarios, which only reduce emissions from road transport (Figure 5.2). It is notable that the range in NO_2 concentrations across the 11 sites gets smaller as emissions reductions become greater. Concentrations at sites with the highest concentrations, which are located nearer to main roads, fall off faster than at sites with the lowest concentrations, which are background sites. This is because NO_2 concentrations are strongly influenced by local NO_x emission sources, so locations closer to strong sources, particularly roads, are more immediately impacted by reductions in emissions from those sources. This effect is greater for the A_x emissions reduction scenarios (Figure 5.2) since these also include reductions in domestic and other local NO_x sources, not just traffic sources. As a consequence of the relatively greater effect of emissions reductions on higher concentration locations, there is a smaller reduction in the average NO_2 concentrations for the scenarios with smaller reductions in emissions (toward the left side of each panel in Figure 5.2) compared with the reductions in the average NO_2 concentration when emissions reductions are already substantial (toward the right side of each panel in Figure 5.2).

Figure 5.2 suggests that to attain an average annual-average NO_2 concentration across all monitoring sites of 40 µg m^{-3} (TI1) would require a 60% reduction of emissions in all sectors (A_{60}). (We note here that since our emissions reductions scenarios go in 10% increments it is more strictly accurate to state that TI1 would be reached with a scenario somewhere between A_{50} and A_{60}, and likewise for other statements below referring to emissions reductions required to meet certain target interpretations.) To attain 40 µg m^{-3} or less at all 11 monitoring sites individually (TI2) would require a 80% reduction from all emitting sectors (A_{80}). Figure 5.2 further suggests that neither of the Target Interpretations 1 or 2 are attainable if interventions aiming at emission reductions only from road transport are implemented.

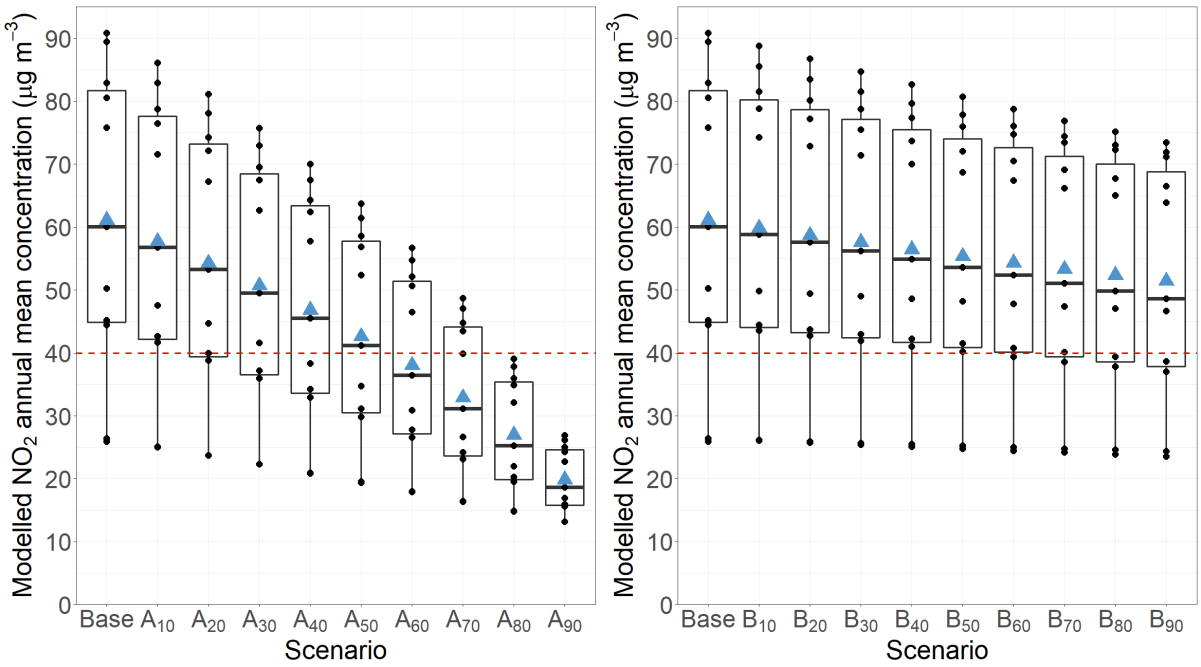

Figure 5.2 Modelled NO_2 concentrations at the 11 monitoring sites under (left) emissions reduction scenarios A_x, in which emissions are reduced by 10% - 90% across all sectors equally, and (right) emissions reduction scenarios B_x, in which only traffic emissions are reduced by 10% - 90%. The box plots summarise the range in NO_2 concentrations across the 11 sites, which are shown individually as the black dots, whilst the blue triangle shows the average concentration across all 11 sites. The horizontal red line on each panel demarcates 40 μg m^{-3}, the WHO NO_2 guideline and Guangzhou 2020 target. The lower and upper hinges correspond to the first and third quartiles (the 25th and 75th percentiles). The upper whisker extends from the hinge to the largest value no further than 1.5 x IQR from the hinge (where IQR is the inter-quartile range, or distance between the first and third quartiles). The lower whisker extends from the hinge to the smallest value at most 1.5 x IQR of the hinge. Data beyond the end of the whiskers are outliers and are plotted individually.

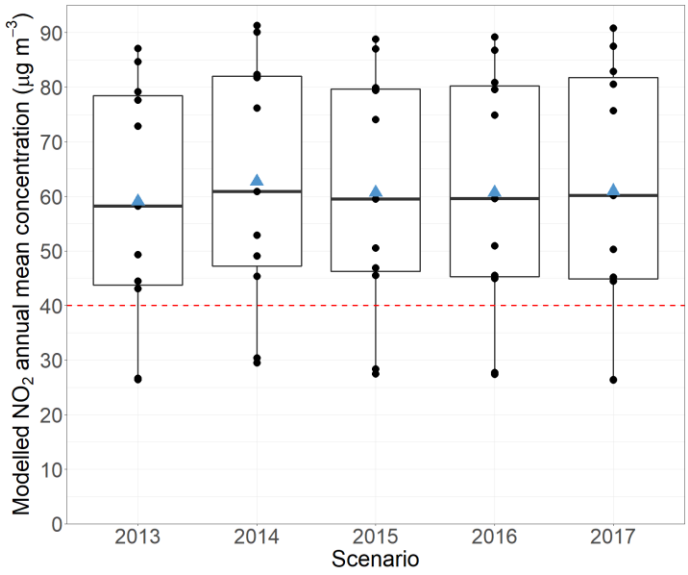

Figure 5.3 Box plots of dispersion modelled NO_2 concentrations at the 11 monitoring sites for the base case emissions using meteorology for years 2013-2017. Individual sites are shown as black dots, whilst the grey triangle is the average concentration across all 11 sites. The horizontal red line on each set of plots demarcate 40 µg m^{-3}, the WHO NO_2 guideline and Guangzhou 2020 target.

5.3.2 NO_2 concentration maps

The data presented in Section 4.3.1 show modelled concentrations of NO_2 under emissions reductions scenarios only for the 11 locations in Guangzhou that currently have NO_2 monitoring, yet compliance with the Guangzhou NO_2 target may be required at non-monitor locations. Furthermore, 11 monitoring locations in a city the size of Guangzhou cannot capture the full extent of variation in population exposure to NO_2. Our hybrid dispersion-LUR model maps of the spatial variation in NO_2 concentration across Guangzhou for six examples of the 18 emissions reductions scenarios are shown in Figure 5.4. For all scenarios, concentrations of NO_2 remain highest in the city centre where most people live and lowest in the north of the city domain. Figure 5.5 illustrates the spatial patterns the change of NO_2 concentration against the base-case scenario for the same emissions reduction scenarios presented in Figure 5.4. As the finer spatial structure of the changes in NO_2 concentration

cannot be visualised in Figure 5.5, Figure 5.6 shows a magnification of the changes in NO_2 concentration in the city centre for the A_{50} and B_{50} scenarios (using a different colour scale compared with Figure 5.5).

The A_x scenarios show more substantive reductions in annual average concentrations of NO_2 (Figure 5.4 and Figure 5.5) than the B_x scenarios, given the larger absolute emissions reductions applied in the former set. In terms of the spatial variation, the modelled annual average NO_2 concentrations under the A_{90} scenario ranged from 13.0 to 27.8 µg m^{-3} while under the B_{90} scenario they ranged from 20.0 to 78.4 µg m^{-3} (Figure 5.4). In the base case they ranged from 21.5 to 99.7 µg m^{-3} (He et al., 2019). Figure 4.5 illustrates the substantial spatial structure to the changes in NO_2 concentration that is difficult to discern in the maps of Figure 5.5 that present the changes for the entire Guangzhou city area. The NO_2 reductions are greatest near roads in both A and B scenarios but Figure 5.6 illustrates that the A scenarios also lead to larger reductions in NO_2 away from roads than the B scenarios. Nevertheless, these simulations suggest that only the most stringent emissions reduction scenario simulated (A_{90}) would result in NO_2 concentrations of less than 40 µg m^{-3} in all locations, including in the city centre, i.e. would meet Target Interpretation TI4. This target interpretation would not be achieved even with complete elimination of road traffic emissions, without reductions in other sources as well.

Figure 5.5 shows that under small and moderate emissions reductions the annual average NO_2 concentration are simulated to increase slightly in some areas of Guangzhou. This is most apparent for the B_{10} scenario, under which the maximum simulated increase in NO_2 concentration is 2.59 µg m^{-3}. There are two explanations for the small increases in NO_2 when emissions are reduced. First, it reflects errors in simulated NO_2 concentration inherent in the two different LUR models being subtracted; when the effect of emissions reductions in an area are small the subtraction of surfaces of roughly similar

concentration can lead to a positive value. These positive values of a couple of µg m^{-3} provide an indication of model surface uncertainty. There is also potentially an atmospheric chemistry contribution. Where NO_x emissions are large, the concentrations of O_3 are low, and rate of oxidation of NO emissions to NO_2 is suppressed (Section 1.1.2); therefore as the NO_x emissions are initially lowered more O_3 is available to convert NO to NO_2. The effect is proportionally greater where NO_2 concentrations are lower.

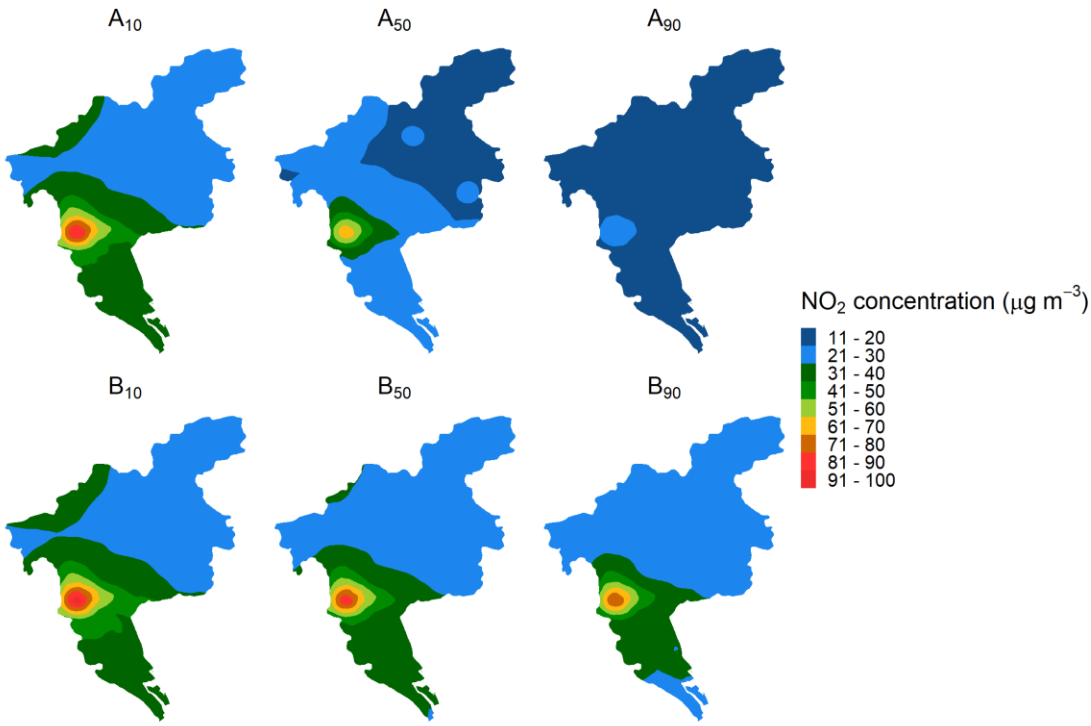

Figure 5.4 Hybrid dispersion-LUR modelled maps of annual-average NO_2 concentrations in Guangzhou under the A_{10}, A_{50}, A_{90}, B_{10}, B_{50}, and B_{90} emission reduction scenarios. Highest concentrations occur in Guangzhou city centre.

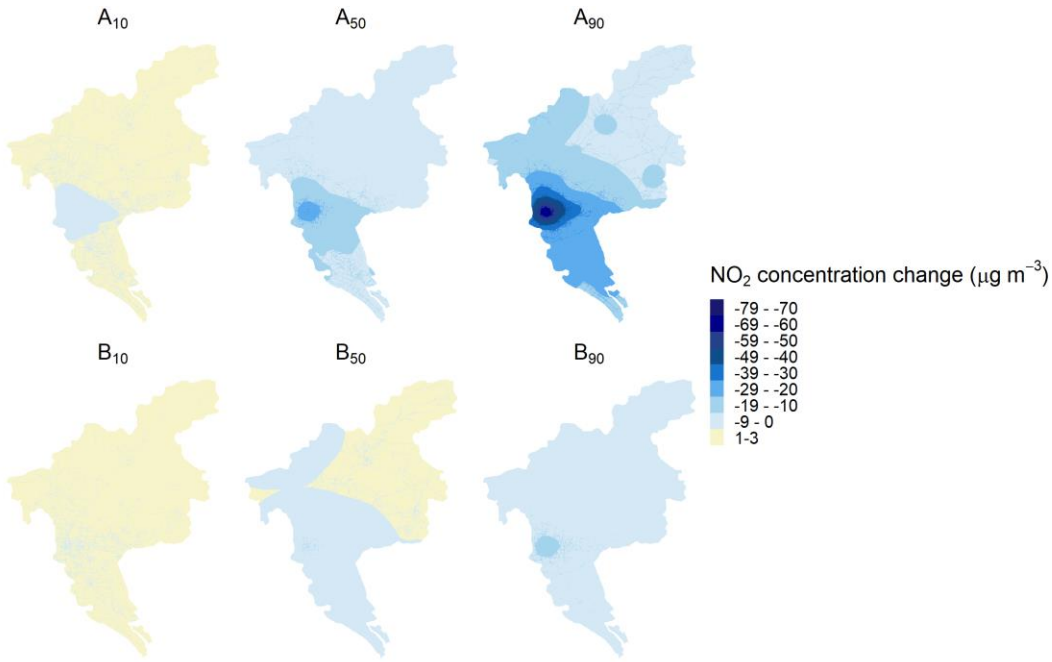

Figure 5.5 Changes in modelled annual-average NO_2 concentrations in Guangzhou for the A_{10}, A_{50}, A_{90}, B_{10}, B_{50}, and B_{90} emission reduction scenarios compared with the 2,017 base case.

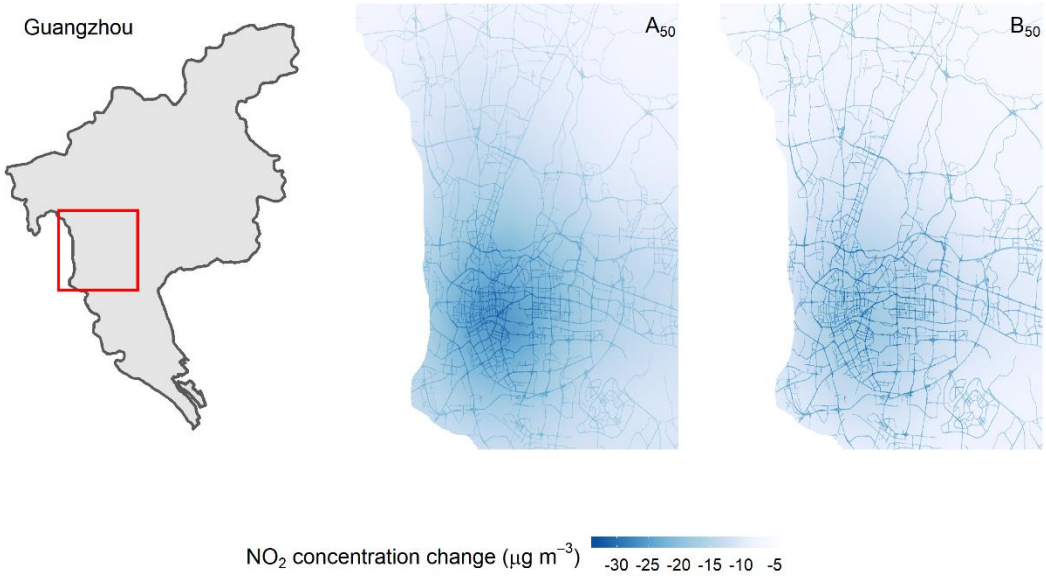

Figure 5.6 Changes in modelled annual-average NO_2 concentrations in Guangzhou for the A_{50} (centre) and B_{50} (right) emissions reduction scenarios compared with the 2017 base case for a magnification of the city centre area (shown by the red box on the map) to illustrate the spatial gradients in NO_2 change. Note that the colour scale is different to that used in Figure 4 for the equivalent maps for the whole of Guangzhou. The road network is apparent from the spatial gradients in the NO_2 concentration changes.

5.4 Modelled potential health gains

Table 5.4 presents, for each scenario, the population-weighted NO_2 concentration, the percentage of the Guangzhou population living at locations where NO_2 concentration exceeds 40 μg m^{-3}, the number of NO_2-attributable premature deaths, and the number of NO_2-attributable premature deaths avoided compared with the base case. Under A_x scenarios, the number of premature deaths avoided is almost three times that of the equivalent percentage NO_x and VOCs reductions under B_x scenarios, which is due to the greater absolute emission reductions in A_x scenarios than in B_x scenarios. Under the A_x scenarios, no part of the population is exposed to concentrations exceeding 40 μg m^{-3} when the emissions reductions reach 90% (Table 5.4). Under the B_x scenarios, even for the B_{90} scenario nearly half (48.6%) of the population resides in locations where modelled NO_2 concentrations still exceed 40 μg m^{-3}. The corresponding population-weighted NO_2 concentration for A_{90} and B_{90} emissions reduction scenarios are 18.0 μg m^{-3} and 43.5 μg m^{-3} respectively. However, although the population-weighted NO_2 concentration for the A_{90} emissions reduction scenario is less than 40 μg m^{-3}, the modelled number of NO_2-attributable premature deaths under A_{90} is still 2,594 [2,481, 2,727].

Table 5.4 Summary for each modelled emissions reduction scenario of the population-weighted annual-average NO_2 concentration, the percentage of people living at locations with annual average NO_2 concentration above 40 μg m^{-3}, the number of NO_2-attributable premature deaths, and the number of NO_2-attributable lives saved compared with the base case. The ranges given for the numbers of attributable premature deaths reflect the confidence interval given for the health response coefficient used in the calculation.

Scenario	Population-weighted NO_2 concentration (μg m-3)	Proportion of population at locations with NO_2 concentration >40 μg m^{-3} (%)	Number of NO_2-attributable premature deaths	Reduction in number of NO_2-attributable premature deaths c.f. base case
Base	52.5	60.0	7,270 [6,960–7,620]	n.a.
Emission reductions – all sources				
A_{10}	49.9	58.6	6,932 [6,642,7,273]	338 [318, 347]
A_{20}	46.9	52.5	6,539 [6,264,6,861]	731[696,759]
A_{30}	43.8	48.8	6,122 [5,863,6,425]	1,148 [1,096,1,195]
A_{40}	40.4	44.4	5,676 [5,436,5,959]	1,594 [1,524,1,661]
A_{50}	36.8	37.8	5,195 [4,974,5,454]	2,075 [1,986,2,165]
A_{60}	32.2	28.5	4,567 [4,371,4,796]	2,703 [2,589,2,824]
A_{70}	28.1	18.8	4,008 [3,836,421]	3,262 [3,124,3,409]
A_{80}	23.5	1.73	3,365 [3,219, 3,536]	3,905 [3,741,4,084]
A_{90}	18.0	0	2,594 [2,481, 2,727]	4,676 [4,479,4,893]
Emission reductions – traffic sources only				
B_{10}	51.7	63.4	7,167 [6,868, 7,519]	103 [92,101]
B_{20}	50.7	60.7	7,030 [6,736, 7,375]	240 [224,245]
B_{30}	49.6	58.2	6,891 [6,602, 7,229]	379 [358,391]
B_{40}	48.5	55.4	6,752 [6,469, 7,084]	518 [491,536]

B_{50}	47.5	53.5	6,615 [6,337, 6,941]	655 [623,679]
B_{60}	46.5	52.1	6,479 [6,207, 6,799]	791 [753,821]
B_{70}	45.5	50.9	6,345 [6,078, 6,658]	925 [882,962]
B_{80}	44.5	49.7	6,215 [5,953, 6,523]	1,055 [1,007,1,097]
B_{90}	43.5	48.6	6,087 [5,831, 6,389]	1,183 [1,129,1,231]

5.5 Discussion of policy targets

5.5.1 The scale of emissions reductions needed to satisfy different interpretations of the NO_2 concentration target

We have found that different interpretations of the Guangzhou Municipal People's Government's target to attain an NO_2 concentration of 40 μg m^{-3} can lead to different amounts of emissions reduction required. These are illustrated in Figure 5.7. If modelling is not used, then compliance can only be assessed via the concentrations measured at the 11 sites in Guangzhou that monitor levels of NO_2 (our target interpretations TI1 and TI2). Our simulations suggest that the scenario in which NO_x and VOC emissions from all source sectors are reduced by 80% (the A_{80} scenario) would achieve the goal of reducing NO_2 concentrations at all monitor sites to ≤40 μg m^{-3} (TI2). The slightly smaller reductions in emissions required to reach this interpretation of the target, compared with the A_{90} scenario that is required to satisfy the interpretation that NO_2 concentrations must not exceed 40 μg m^{-3} everywhere (TI4), and which can only be evaluated through modelling, is because there are no monitors at the 'hotspots' simulated in the spatial model to have the highest concentrations. If an interpretation of the target is that the average NO_2 concentration across the 11 monitor sites is to be ≤40 μg m^{-3} (TI1), then this is met with the A_{60} scenario. A population-weighted concentration of ≤40 μg m^{-3} (TI3) is met under scenario A_{50}, but this scenario still leaves 37.8% of the

Guangzhou population living in locations where NO_2 concentration exceeds 40 µg m^{-3} (Table 5.4 and Figure 5.7).

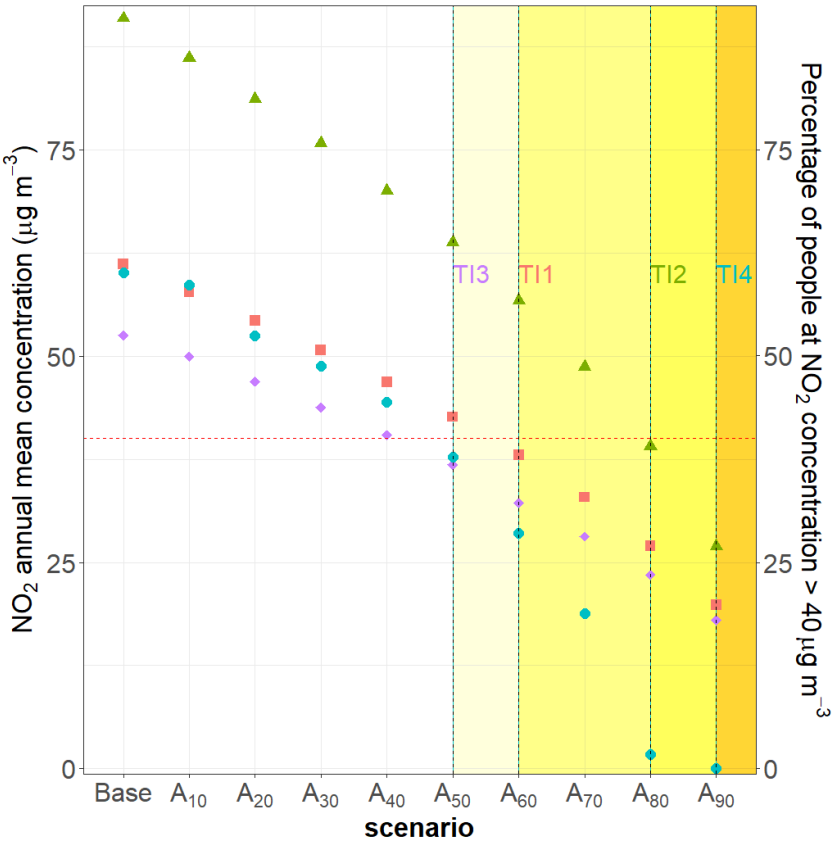

Figure 5.7 Changes as a function of the A set of emissions reduction scenarios in different metrics of quantifying NO_2 concentration and associated population health gains in Guangzhou. Red squares show the average NO_2 concentration for the 11 monitor sites. Green triangles show the maximum NO_2 concentration across the 11 monitor sites. Purple diamonds show the population-weighted NO_2 concentration. Blue dots show the percentage of population in locations where NO_2 exceeds 40 µg m^{-3}. The horizontal red line demarcates 40 µg m^{-3}, the WHO NO_2 guideline and Guangzhou 2,020 target. The four vertical dotted lines marked TI*n* indicate at what point of A_x scenario emission reductions each of our four target interpretations (TI) of the Guangzhou target of 40 µg m^{-3} are met. TI1, the average concentration at the 11 monitoring sites is below 40 µg m^{-3}, is met under scenario A_{60} (and greater emissions reductions). TI2, the concentration at all 11 monitoring sites is below 40 µg m^{-3}, is met under scenario A_{80} (and greater emissions reductions). TI3, the population-weighted concentration is below 40 µg m^{-3}, is met under scenario A_{50}. TI4, the concentration everywhere is below 40 µg m^{-3}, is met only under scenario A_{90}. The yellow-orange shadings indicates the scenarios under which a given TI is met.

Our simulations illustrate the enormous challenge to reduce NO_2 concentrations to 40 μg m^{-3}, whatever way compliance with this target may be assessed, via actions on emissions sources in Guangzhou alone. Although NO_2 concentrations reduce more rapidly with emissions reductions at locations where the concentrations are high initially, because these are the locations closest to local emissions of NO_x (e.g. heavily trafficked roads) huge efforts are still required to reduce these 'hotspot' concentrations to ≤40 μg m^{-3}. These hotspots also tend to be the places where most people live. None of the scenarios reducing emission from road traffic sector alone (the B_x scenarios) can achieve any of the four interpretations of the 40 μg m^{-3} target (Table 5.4). Thus only substantial overall emissions reductions across all sectors will be viable to make progress towards attaining the limit values. In fact, our simulations show that only a scenario in which NO_x and VOC emissions from all source sectors are reduced by 90% (the A_{90} scenario) results in annual average NO_2 concentrations ≤40 μg m^{-3} everywhere in Guangzhou. This scenario equates to emission reductions of 162.2 kt for NO_x and 321.5 kt for VOC (Table 5.2). Specific interventions targeted at very high concentration areas may be a more practical approach to avoid such locations dominating the overall attainment of limit values.

5.5.2 The use of NO_2 concentration threshold as a policy target

Given the scale of the emissions reductions required that are illustrated by our model simulations, one could argue that a 40 μg m^{-3} objective for NO_2 concentration over a megacity is unattainable through actions in that city alone, as long as internal combustion engines and combustion in stationary sources are the predominant source of NO_x emissions in cities. For example, since the 1980s, the UK government has committed to reducing NO_2 concentration; but despite the continuous improvement, in many larger cities in the UK it is still a challenge to meet the current limit value for annual average NO_2 concentrations of 40 μg m^{-3} (Carnell et al., 2019). The same is true for many

cities across other European countries (Fuller, 2018). Overall behavioural change (Vardoulakis et al., 2018) and measures attenuating negative health impacts (Lucock et al., 2017; Stevens et al., 2019) might need to be explored alongside traditional policy interventions aiming to reduce NO_2 concentration levels.

On the other hand it is important to remember that NO_2 concentration targets within cities are driven by the desire to improve adverse health outcomes associated with the NO_2, and in this context using a specific concentration target to assess progress towards improvement in air quality can underplay the actual extent of gains made in improving population health outcome. For example, it is important to note that, even for our 'softer' interpretations of attainment of the Guangzhou target (TI1 and TI3), substantial reductions in the number of NO_2-attributable premature deaths compared to the base case are anticipated: 2,703 [2,589,2,824] for TI1 and 2,075 [1,986,2,165] for TI3. These represent reductions in attributable mortality of 37% and 29%, respectively, relative to the 7,270 NO_2-attributable deaths associated with the base case (in comparison, the reductions in NO_2-attributable premature deaths for TI2 and TI4 are 3,905 [3,741,4,084] and 4,676 [4,479,4,893] respectively), but with substantially less stringent emissions reductions than needed to attain TI2 or TI4.

The use of a concentration threshold as a policy target to deliver health protection against NO_2 has further shortcoming in that the 40 μg m^{-3} concentration does not constitute a no-effect threshold for NO_2, and in fact current epidemiological evidence is that there is no zero-effect threshold for exposure to NO_2 (Beelen et al., 2014; COMEAP, 2018). In other words, there are health gains if concentrations go down in locations irrespective of whether the concentrations are above or below the target value. Therefore what is fundamentally relevant in relation to potential policy measures is not the change in proportion of locations with NO_2 concentrations ≤40 μg m^{-3}, nor the

change in the numbers of people in locations with NO_2 concentrations ≤40 μg m^{-3}, but by how much the cumulative population exposure changes. Quantification of the latter shows that there are greater rates of population health gain as emissions are reduced than is implied by considering only the rates of change of number of people with NO_2 exposure brought below 40 μg m^{-3}. This point is clearly illustrated in Figure 5.8 for our Guangzhou example emissions reduction scenarios. The gradient of the plot of the number of NO_2-attribuable deaths saved (compared to base case) for the set of A emissions reduction scenarios is steeper than the plot of the percentage of population at locations with NO_2 ≤40 μg m^{-3}. The message is particularly obvious for the smallest emissions reduction scenario simulated (the A_{10} scenario), which makes almost no difference to the number of people in locations with concentrations ≤40 μg m^{-3} compared with the base case (and which might therefore be deemed to be having no effect), but yet delivers health gains of 338 attributable deaths avoided. The need to consider cumulative population health exposure rather than progress against a concentration target is again graphically apparent in Figure 5.8 at the other end of the scale of emissions reductions: further emissions reductions beyond the A_{90} scenario will not lead to more people living at locations with NO_2 concentration ≤40 μg m^{-3}, since 100% of the population would then already do so, but further emissions reductions would continue to deliver additional NO_2-attributable deaths avoided.

The use of attainment of a specific concentration as a policy target actually has the potential to promote a detrimental effect on policy ambition levels (Fuller and Font, 2019), since there might be a perception that once a 40 μg m^{-3} is reached that is ‘job done’; or worse, to encourage the perception that it doesn’t matter if previously low concentrations are allowed to increase as long as they still remain below 40 μg m^{-3}. This may lead to situations where compliance may be achieved, but more pronounced public health impacts could be attained at lower cost, or irrespective of individual locations being in exceedance. The data we present for our example modelling in Guangzhou

illustrate the quantitative evidence on population health gain for different scenarios (as opposed to evidence just on NO_2 concentrations) that needs to be fed into policy decisions related to costs and benefits associated with attaining a concentration target in any large city.

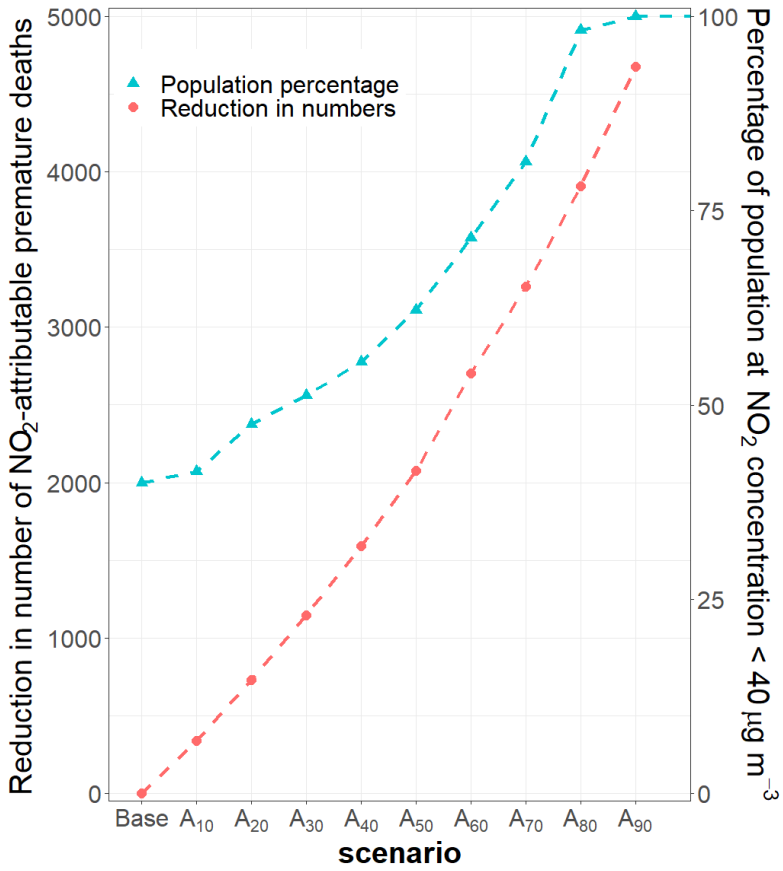

Figure 5.8 The percentage of population in locations where NO_2 is ≤40 µg m^{-3} (blue triangles) and the reduction in the number of NO_2-attributable premature deaths compared with the base case (red dots) under the A_x set of scenarios.

5.5.3 Benefits of wider emissions reductions

The reduction scenarios investigated here only represent reductions in emissions within the Guangzhou city domain. Emissions reductions in the region surrounding Guangzhou will contribute to lowering background NO_2

concentrations coming into Guangzhou, which would likely enable the city to attain air quality limit values for NO_2 with less additional emissions reductions within Guangzhou itself than simulated here. In addition, emissions reductions within Guangzhou will have the additional benefit of lowering NO_2 concentrations, with consequent gains in health, in areas surrounding and downwind of Guangzhou, in addition to the health gains calculated here for Guangzhou alone. As studies in both Europe and China have pointed out, joint emissions controls within both the target area and surrounding areas are most effective for improving air quality holistically (Ou et al., 2016; Reis et al., 2012; Xue et al., 2014; Yu et al., 2019); although Yu *et al.* (2019) found that local emissions control was more helpful in the reduction of the concentrations of SO_2, NO_2, $PM_{2.5}$, and PM_{10} in Guangzhou compared with surrounding area emissions control.

The benefits of emissions reductions in Guangzhou calculated as reductions in NO_2-attributable premature death presented in this paper also represent only part of the overall benefits. Emission reductions have important additional health and environmental benefits other than those directly experienced through NO_2 on health. For instance, NO_x emission reductions will also contribute to reducing the formation of secondary inorganic aerosols and hence $PM_{2.5}$ concentrations, and also reduce dry and wet deposition of reactive nitrogen on terrestrial ecosystems (Gao et al., 2015; Guo et al., 2018; Kanakidou, 2019; Qiao et al., 2019; Zhu et al., 2018). Measures to reduce NO_x emissions will also often lead to reductions in co-emitted pollutants such as primary particulate matter and black carbon. Therefore, instead of focusing on attaining regulatory concentration targets only, a focus on rate of change and accounting for the integrated benefits from emission reduction might be more appropriate. This paper only focuses on NO_2, but benefits from emission reduction need to be assessed along with other pollutants including $PM_{2.5}$ and O_3. For instance, O_3 concentrations have been reported to be highest at the regional background sites, decreasing at urban background sites and lowest at traffic sites in both cities. This is explained by the rapid reaction between

NO and O_3 close to the points of emission. At traffic sites, the dominant NO_x emission from vehicle exhaust is NO. A consequence of the reaction between NO and O_3 is that O_3 is consumed and O_3 levels here are lower (Hagenbjörk et al., 2017). Therefore, the reduction of NO_x can cause increase of O_3 short time (Li et al., 2013) .

5.6 Conclusions

We used a hybrid dispersion and land-use regression model to explore the impact of all-sector vs transport-sector-only emission reductions within Guangzhou city on annual-average NO_2 concentrations in relation to the 2020 policy target of 40 µg m^{-3}. We also explored the effect of these emissions reductions on estimated NO_2-attributable premature mortality. From our model results we derive the following conclusions:

1. An explicit definition of the compliance assessment criteria for the policy target would clarify the most appropriate emissions reductions that should be implemented.
2. Regardless of our interpretation of compliance, reductions from traffic emissions alone will not be able to meet the target, and substantial reductions in all-sector emissions will be required to meet the objective.

The ultimate goal to improve urban air quality is gains in population health. As adverse health impacts are still observed at concentration levels far below current limit values, any population exposure reduction will yield public health benefits. A more specific target focusing on health gain (such as population weighted concentration, or attributable pre-mature death avoided) is more appropriate compared to setting a threshold. Even if the target value of 40 µg m^{-3} was achieved, which can only be obtained in Guangzhou by very pronounced emission reductions (>80% of all NO_x emissions), a large

population across the city would still be exposed to NO_2 concentrations and no evidence for any zero-effect threshold for it (Beelen et al., 2014; COMEAP, 2018). Evidence from other studies (Qiao et al., 2019; Yu et al., 2019; Zhong et al., 2013) suggests that integrated emission control at regional level may make it easier to attain concentration targets in an urban area embedded in the region. To what degree this applies to Guangzhou should be investigated in further studies. Whilst the results of the model simulations we present are for the specific situation in Guangzhou, the methodology we use and our discussion in relation to limitations of an NO_2 concentration target for assessing effectiveness of air pollutant emissions policies, are relevant to decision makers in other fast-growing megacities in China and elsewhere globally.

Chapter 6 Conclusions and future work

6.1 Overview of the thesis outputs

The aim of this PhD was to develop and implement a novel method for estimation of highly spatially resolved human exposure to atmospheric pollutants for health burden calculation in cities in China, given the obstacles in availability of monitor data, emission inventories, and other highly spatially resolved data, and the challenges in applying high spatially resolved models in large domains (Chapter 3). The approach that has been developed and applied combines the advantages of two widely-used methods: dispersion modelling and LUR modelling. The model was developed for the exemplar city of Guangzhou because it is one of the largest cities in China, and for NO_2 as the pollutant because of the large intra-urban variability of NO_2 and the current widespread exceedance of its associated target concentration (Chapter 4). Ambient concentrations of NO_2 simulated by the ADMS-Urban dispersion model at 83 'virtual' monitoring sites, selected to span both the range of NO_2 concentration and weighted by population density, were used to develop a LUR model of 2,017 annual-mean NO_2 across Guangzhou at 25 m × 25 m spatial resolution. This hybrid model successfully simulated current highly spatially variable NO_2 concentrations over a megacity and predicted concentrations under different scenarios. The model was used to explore the impact of all-sector vs transport-sector-only emission reductions within Guangzhou city on annual-average NO_2 concentrations in relation to the 2020 policy target of 40 μg m^{-3} (Chapter 5).

6.2 Implications

6.2.1 Current obstacles in modelling NO_2 concentrations in cities in China

The application of urban-scale modelling in Chinese cities is constrained by the scarcity of data. Table 2.1 and Table 2.3 and summarize the input data required for applying dispersion models and LUR models (Chapter 2). Table 3.4 lists the data used in this study. The most widely-used emission inventory, MEIC, provides monthly gridded emission data from 2008-2016 (2 year intervals) at a spatial resolution of 4 km for the whole of China, for the power, industry, residential, transportation, and agriculture sectors, but detailed and consistent emission data with updated emission factors and activity are not available for dispersion modelling. LUR modelling has often been used, but the quality of LUR models are also constrained by the scarcity of input data, especially monitoring pollution data and higher spatial resolution proxy data for urban emissions, particularly in respect of traffic-related variables. Not enough monitor data makes constructing and validating LUR models a challenge, and the resultant model regressions can be subject to overfitting issues. There is an urgent need for accessible archives of quality-assured measurement data and for higher spatial resolution proxy data for urban emissions, particularly in respect of traffic-related variables. Other challenges particularly in China are the massive scale of cities and the rapidly changing urban landscape. It is more computational demanding to simulate the physical and chemical processes in a city domain because cities in China are larger, denser and more complex. The rapidly evolving nature of the Chinese urban landscape makes maintaining up-to-date land-use and urban morphology datasets difficult.

6.2.2 Applicability of the hybrid model

The hybrid approach used simulated concentrations of NO_2 from dispersion models as 'virtual receptors' for LUR models. Gridded emissions of NO_x and VOCs for the year 2016 were obtained from MEIC and shipping emissions for 2014 were obtained from MarcoPolo-Panda. OpenstreetMap was used to explicitly model road emissions and gridded emission from MEIC was assigned to each road. Meteorological data from ECMWF-ERA5 and background concentration from CAMS were also used to run the dispersion model (ADMS-Urban) (Table 3.4). The model was validated with 11 monitor data in Guangzhou and the model explains 72% of the spatial variation in the measured NO_2, with an RMSE of 17.7 μg m^{-3}.

The key to develop an appropriate LUR model is to select receptors based on the study aim. In some studies, researchers collect campaign data themselves in order to ensure that receptor sites cover the whole domain as well as capture the concentration variation, but this is time and money consuming. Campaign data also often span only a few weeks which may not accurately represent the annual averages that long-term health burden studies require. Therefore, in this work to estimate human exposure, virtual locations were selected to meet the minimum number requirement of sites (n > 40), weighting towards population, and stratified across all districts within the city for developing LUR models. The selection of buffers and variables were based on the expectation that emission sources, dispersion, and physical geography may contribute to NO_2 concentration variation in urban areas. The final LUR model was validated against the ADMS-Urban results as well as the monitor concentrations. The final LUR model contained three variables: *pop_5,000* (the number of people within a 5,000 m buffer), *sq_dis_port* (the squared distance to the nearest port) and *all_len_25* (the length of all type of roads within a 25 m buffer). Against the 83 virtual sites, LOOCV evaluation showed the hybrid LUR model explained 96% of the spatial variation of NO_2 concentration with an RMSE of

5.64 μg m^{-3}. The NO_2 concentrations at the monitoring sites provided an additional evaluation of the hybrid LUR model independent of the NO_2 data used to construct the model (R^2 = 0.63 and MB = 9.08 μg m^{-3}, which corresponds to an NMB of 18.2%).

6.2.3 Advantages of the hybrid model

This study demonstrates a practical approach to simulating annual-average concentrations of NO_2 in a Chinese megacity in which the advantages of both dispersion and LUR modelling are combined. ADMS-Urban-simulated concentrations at receptor sites are used instead of limited monitor sites in this approach. The advantages are summarised here:

(1) It overcomes the issues associated with overfitting arising from too few monitor sites, and the location of each monitor site can be chosen to optimize the results rather than reliance only on the sites in the CNEMC national monitoring network which do not capture the full concentration range.

(2) LUR modelling permits much easier and faster simulation of concentrations over a large domain, compared with applying a process-based dispersion model on the scale of Chinese cities.

(3) Since users can select predictors in the LUR model to explain the concentration variability, LUR can be adapted to each city by adding new variables (for example, in China, variables representing fireworks during Chinese New Year were included in some studies and shipping proxy variables and green space variables are included in the model for Guangzhou).

(4) Integration of the two models can also help to simulate different scenarios for testing policy effectiveness which LUR modelling alone cannot achieve.

(5) To develop this hybrid model, only a dispersion model and open data sources (summarised in Table 4.2) are required, so this approach can be easily transferred to cities both in China and elsewhere.

6.2.4 Implications from model results

This hybrid model simulates the spatial distribution of annual-mean NO_2 concentration across Guangzhou in 2017 and 22 different emission reduction and meteorological scenarios. Modelled concentrations in 2017 vary between 21.5 μg m^{-3} in the most rural areas in the north of the domain to 99.7 μg m^{-3} in the most polluted district of Guangzhou city centre. In large areas of Guangzhou, concentrations of NO_2 are substantially in excess of the Chinese air quality standard and WHO guideline of 40 μg m^{-3}. The population-weighted annual-mean concentration of NO_2 across Guangzhou is 52.5 μg m^{-3}. The modelled number of premature deaths attributable to long-term exposure to NO_2 in Guangzhou in 2017 was 7,270 (6,960–7,620; range based only on the 95% CI for the health risk coefficient). As expected, model results from simulating different emission reduction scenarios show number of NO_2-attributable premature deaths reduce dramatically when NO_x and VOCs emissions are cut from all sectors, but to bring concentrations for everyone in Guangzhou below the WHO guideline of 40 μg m^{-3}, emissions reduction in all sectors in Guangzhou by ~90% are required, which roughly equates to 162.2 kt NO_x reduction and 321.6 kt VOCs reduction. Emissions reductions from the transport sector alone cannot achieve this target. Compared with effects from emission controls, meteorological variation is not the major factor contributing to concentration change in Guangzhou. Based on MEIC data, in Guangdong province, total NO_x emission has only reduced ~24% from 2010 to 2016. This suggests the hard work needed to reduce NO_x emission further for a relatively healthy atmospheric environment.

The local governments set targets of a threshold based on the 13th Five-Year Plan (2016-2020) on air quality, and the Guangzhou aspiration is to achieve this by 2020 (and also to achieve an annual average NO_2 concentration of 38 μg m^{-3} by 2025). However, it is not clear what constitutes compliance with the target, different emission reduction scenarios were simulated to test different interpretation of compliance. Regardless of the interpretation of compliance, reductions from traffic emissions alone will not be able to meet the target, and substantial reductions in all-sector emissions will be required to meet the target.

There is no zero-effect threshold for exposure to NO_2 found in epidemiological studies and the ultimate goal of improvement in urban air quality is gains in population health. Any population exposure reduction will yield public health benefits, but the use of attainment of a specific concentration as a policy target cannot directly promote population exposure reduction. A more specific target focus on health gain is more appropriate compared to setting a threshold.

6.3 Future work

In this section, future work related to modelling air pollutant concentrations in Chinese megacities for health impacts estimation and effectiveness of policy intervention are explored.

6.3.1 Improvement of data quality/accessibility

Despite rapid expansion of the CNEMC monitoring network across China, the number of monitor sites are still not enough to construct and validate LUR model results and represent human exposure. The CNEMC monitoring network is not designed for these purposes. There is therefore a need to

expand the monitoring network as well as to carefully plan the new monitoring locations. Real-time concentration data are published on the National Air Quality Publication Platform (http://106.37.208.233:20,035/) but are not for archived historical data. Historical data are also collected and archived elsewhere by private companies without validation and detailed documentation. Therefore, formal archived historical data available to the public, together with nationally-applied QA/QC approaches to improve data quality, are still urgently needed.

Emission inventories are key to drive air quality dispersion models. However, discrepancies exist between the inventories at both national and local scales. Complete emission sources such as burning biomass predominantly in rural areas, residential emissions, or often uncontrolled local emission sources (e.g. small, cottage industries) are needed to be collected as well as updated emission factors and activity data since the government regulations being implemented. In order to accurately estimate human exposure, detailed population and activity data are needed in the future.

6.3.2 Improvement of urban-scale air pollution modelling

Urban-scale air pollution modelling can be improved in the following areas:

- Coupling urban-scale dispersion model with regional-scale atmospheric transport models. Urban-scale models normally use rural background concentrations to represent long-range transport. Combining regional modelling with urban local modelling takes into account both short range and long-range transport and chemistry effects. It can simulate climate change related scenarios and the local effects of regional emissions changes. It can be used to investigate emission control at regional level and its effects on attaining concentration targets in an urban area within the region. Attempts have been made to couple local-

scale atmospheric dispersion models with regional-scale atmospheric chemical transport models, such as CMAQ-urban (the regional scale CMAQ coupled with ADMS road) (Beevers et al., 2012), CAMx (a chemical and transport Eulerian model) coupled with AUSTAL2,000 (a local scale Lagrangian dispersion model) (Pepe et al., 2016), EMEP4UK coupled with ADMS-Urban (Hood et al., 2018) and uEMEP (Denby, 2020). These coupled models have not been applied in cities in China.

- Incorporating urban climate effects (urban heat island and complex boundary-layer structures) in modelling air pollutants. Examples are WRF/Chem with MICROSYS (a CFD model) (San José et al., 2018) and WRF. Urban-scale climate model such as WRF-urban (Chen et al., 2011; Yang et al., 2015) can also be used.
- Application of spatial data mining in modelling spatiotemporal variation of air pollutants. The empirical modelling approach LUR intrinsically is a supervised learning approach which assumes the relationships between concentrations of pollutants and predictor variables are linear. LUR efforts to find a linear function to model the data with the least error and considers the spatial pattern constant. It therefore can only model annual average concentration. This limitation does not exist in spatial data mining methods. Spatial data mining approach can find relations between air pollution and affecting parameters and considers air pollution patterns as moving objects during space and time (Akbari et al., 2015).

6.3.3 Improvement of human exposure assessment

The current model only calculates impacts of annual average NO_2 concentration no attributable pre-mature deaths, however, short-term NO_2 health impacts also needs to be assessed, therefore models explain NO2

spatiotemporal variability needs to be developed. n terms of the impact of air pollutant exposure on human health, it is critical to better understand: (1) pollutant exposures at the level of individual and (2) cofactors that have a bearing on health at the level of individual. All air pollutants are correlated with each other, these needed to be considered holistically and so as the policy decisions.

Urban-scale air pollution models do not take account of exposure within the home, at work/school, and in different microenvironments. Future models need to capture the difference between personal and outdoor exposures (Reis et al., 2018). One example is LHEM (London Hybrid Exposure Model) which estimates outdoors, as well as in-building, in-vehicle, and walking and cycling exposures (Smith et al., 2016). Recent progress in environmental sensing and the corresponding increasing measurements taken by citizens and researchers make it possible to explore personal exposure and to incorporate 'Big Data' from sensors and health-related datasets (Reis et al., 2015). Data collected at different spatiotemporal scale can be used to calibrate and validate models.

References

Aguilera, I., Sunyer, J., Fernández-Patier, R., Hoek, G., Aguirre-Alfaro, A., Meliefste, K., Bomboi-Mingarro, M.T., Nieuwenhuijsen, M.J., Herce-Garraleta, D., Brunekreef, B., 2007. Estimation of outdoor NO x, NO2, and BTEX exposure in a cohort of pregnant women using land use regression modeling. Environ. Sci. Technol. 42, 815–821. https://doi.org/10.1021/es0715492

Akbari, M., Samadzadegan, F., Weibel, R., 2015. A generic regional spatio-temporal co-occurrence pattern mining model: a case study for air pollution. J. Geogr. Syst. 17, 249–274. https://doi.org/10.1007/s10109-015-0216-4

Anand, J.S., Monks, P.S., 2017. Estimating daily surface NO2 concentrations from satellite data – a case study over Hong Kong using land use regression models. Atmospheric Chem. Phys. 17, 8211–8230. https://doi.org/10.5194/acp-17-8211-2017

AQICN, 2019. 中国空气污染：实时空气质量指数地图 [WWW Document]. URL https://aqicn.org/map/china/cn/#@g/39.5901/88.9673/5z (accessed 4.23.19).

Ashmore, M.R., 2005. Assessing the future global impacts of ozone on vegetation. Plant Cell Environ. 28, 949–964. https://doi.org/10.1111/j.1365-3040.2005.01341.x

Babatola, S.S., 2018. Global burden of diseases attributable to air pollution. J. Public Health Afr. 9. https://doi.org/10.4081/jphia.2018.813

Basagaña, X., Rivera, M., Aguilera, I., Agis, D., Bouso, L., Elosua, R., Foraster, M., de Nazelle, A., Nieuwenhuijsen, M., Vila, J., Künzli, N., 2012. Effect of the number of measurement sites on land use regression models in estimating local air pollution. Atmos. Environ. 54, 634–642. https://doi.org/10.1016/j.atmosenv.2012.01.064

Beelen, R., Hoek, G., Vienneau, D., Eeftens, M., Dimakopoulou, K., Pedeli, X., Tsai, M.-Y., Künzli, N., Schikowski, T., Marcon, A., Eriksen, K.T., Raaschou-Nielsen, O., Stephanou, E., Patelarou, E., Lanki, T., Yli-Tuomi, T., Declercq, C., Falq, G., Stempfelet, M., Birk, M., Cyrys, J., von Klot, S., Nádor, G., Varró, M.J., Dėdelė, A., Gražulevičienė, R., Mölter, A., Lindley, S., Madsen, C., Cesaroni, G., Ranzi, A., Badaloni, C., Hoffmann, B., Nonnemacher, M., Krämer, U., Kuhlbusch, T., Cirach, M., de Nazelle, A., Nieuwenhuijsen, M., Bellander, T., Korek, M., Olsson, D., Strömgren, M., Dons, E., Jerrett, M., Fischer, P., Wang, M., Brunekreef, B., de Hoogh, K., 2013. Development of NO_2 and NO_x land use regression models for estimating air pollution exposure in 36 study areas in Europe – The ESCAPE project. Atmos. Environ. 72, 10–23. https://doi.org/10.1016/j.atmosenv.2013.02.037

Beelen, R., Raaschou-Nielsen, O., Stafoggia, M., Andersen, Z.J., Weinmayr, G., Hoffmann, B., Wolf, K., Samoli, E., Fischer, P., Nieuwenhuijsen, M., Vineis, P., Xun, W.W., Katsouyanni, K., Dimakopoulou, K., Oudin, A., Forsberg, B., Modig, L., Havulinna, A.S., Lanki, T., Turunen, A., Oftedal, B., Nystad, W., Nafstad, P., Faire, U.D., Pedersen, N.L., Östenson, C.-G., Fratiglioni, L., Penell, J., Korek, M., Pershagen, G., Eriksen, K.T., Overvad, K., Ellermann, T., Eeftens, M., Peeters, P.H., Meliefste, K., Wang, M., Bueno-de-Mesquita,

B., Sugiri, D., Krämer, U., Heinrich, J., Hoogh, K. de, Key, T., Peters, A., Hampel, R., Concin, H., Nagel, G., Ineichen, A., Schaffner, E., Probst-Hensch, N., Künzli, N., Schindler, C., Schikowski, T., Adam, M., Phuleria, H., Vilier, A., Clavel-Chapelon, F., Declercq, C., Grioni, S., Krogh, V., Tsai, M.-Y., Ricceri, F., Sacerdote, C., Galassi, C., Migliore, E., Ranzi, A., Cesaroni, G., Badaloni, C., Forastiere, F., Tamayo, I., Amiano, P., Dorronsoro, M., Katsoulis, M., Trichopoulou, A., Brunekreef, B., Hoek, G., 2014. Effects of long-term exposure to air pollution on natural-cause mortality: an analysis of 22 European cohorts within the multicentre ESCAPE project. The Lancet 383, 785–795. https://doi.org/10.1016/S0140-6736(13)62158-3

Beevers, S.D., Kitwiroon, N., Williams, M.L., Carslaw, D.C., 2012. One way coupling of CMAQ and a road source dispersion model for fine scale air pollution predictions. Atmospheric Environ. Oxf. Engl. 1994 59, 47–58. https://doi.org/10.1016/j.atmosenv.2012.05.034

Beirle, S., Boersma, K.F., Platt, U., Lawrence, M.G., Wagner, T., 2011. Megacity emissions and lifetimes of nitrogen oxides probed from space. Science 333, 1737–1739. https://doi.org/10.1126/science.1207824

Brasseur, G.P., Jacob, D.J., 2017. Modeling of Atmospheric Chemistry. Cambridge University Press. https://doi.org/10.1017/9781316544754

Briggs, D.J., Collins, S., Elliott, P., Fischer, P., Kingham, S., Lebret, E., Pryl, K., Van Reeuwijk, H., Smallbone, K., Van Der Veen, A., 1997. Mapping urban air pollution using GIS: a regression-based approach. Int. J. Geogr. Inf. Sci. 11, 699–718. https://doi.org/10.1080/136588197242158

Brunekreef, B., Holgate, 2002. Air pollution and health. The Lancet 360, 1233–1242. https://doi.org/10.1016/S0140-6736(02)11274-8

Cai, H., Xie, S., 2011. Traffic-related air pollution modeling during the 2008 Beijing Olympic Games: The effects of an odd-even day traffic restriction scheme. Sci. Total Environ. 409, 1935–1948. https://doi.org/10.1016/j.scitotenv.2011.01.025

Cai Yuanyuan, Zhang Bo, Ke Weixia, Feng Baixiang, Lin Hualiang, Xiao Jianpeng, Zeng Weilin, Li Xing, Tao Jun, Yang Zuyao, Ma Wenjun, Liu Tao, 2016. Associations of Short-Term and Long-Term Exposure to Ambient Air Pollutants With Hypertension. Hypertension 68, 62–70. https://doi.org/10.1161/HYPERTENSIONAHA.116.07218

Carnell, E., Vieno, M., Vardoulakis, S., Beck, R., Heaviside, C., Tomlinson, S., Dragosits, U., Heal, M.R., Reis, S., 2019. Modelling public health improvements as a result of air pollution control policies in the UK over four decades—1970 to 2010. Environ. Res. Lett. 14, 074001. https://doi.org/10.1088/1748-9326/ab1542

Carruthers, D.J., Edmunds, H.A., Lester, A.E., McHugh, C.A., Singles, R.J., 2000. Use and validation of ADMS-Urban in contrasting urban and industrial locations. Int. J. Environ. Pollut. 14, 364. https://doi.org/10.1504/IJEP.2000.000558

Carruthers, D.J., Stocker, J.R., Ellis, A., Seaton, M.D., Smith, S.E., 2017. Evaluation of an explicit NOx chemistry method in AERMOD. J. Air Waste Manag. Assoc. 1995 67, 702–712. https://doi.org/10.1080/10962247.2017.1280096

Center for Earth System Science, 2012. MEIC model [WWW Document]. URL http://www.meicmodel.org/ (accessed 2.27.17).

CERC, 2017. ADMS-Urban User Guide [WWW Document]. URL https://www.cerc.co.uk/environmental-software/assets/data/doc_userguides/CERC_ADMS-Urban4.1.1_User_Guide.pdf (accessed 5.21.19).

Chen, C.-H., Kan, H.-D., Huang, C., Li, L., Zhang, Y.-H., Chen, R.-J., Chen, B.-H., 2009. Impact of Ambient Air Pollution on Public Health under Various Traffic Policies in Shanghai, China. Biomed. Environ. Sci. 22, 210–215. https://doi.org/10.1016/S0895-3988(09)60047-7

Chen, F., Kusaka, H., Bornstein, R., Ching, J., Grimmond, C.S.B., Grossman-Clarke, S., Loridan, T., Manning, K.W., Martilli, A., Miao, S., Sailor, D., Salamanca, F.P., Taha, H., Tewari, M., Wang, X., Wyszogrodzki, A.A., Zhang, C., 2011. The integrated WRF/urban modelling system: development, evaluation, and applications to urban environmental problems. Int. J. Climatol. 31, 273–288. https://doi.org/10.1002/joc.2158

Chen, L., Bai, Z., Kong, S., Han, B., You, Y., Ding, X., Du, S., Liu, A., 2010a. A land use regression for predicting NO2 and PM10 concentrations in different seasons in Tianjin region, China. J. Environ. Sci. 22, 1364–1373. https://doi.org/10.1016/S1001-0742(09)60263-1

Chen, L., Du, S., Bai, Z., Shao-fei, K., Yan, Y., Bin, H., Dao-wen, H., Li, Z., 2010b. Application of land use regression for estimating concentrations of major outdoor air pollutants in Jinan, China. J. Zhejiang Univ.-Sci. A 11, 857–867. https://doi.org/10.1631/jzus.A1000092

Chen, L., Ng, E., An, X., Ren, C., Lee, M., Wang, U., He, Z., 2012. Sky view factor analysis of street canyons and its implications for daytime intra-urban air temperature differentials in high-rise, high-density urban areas of Hong Kong: a GIS-based simulation approach. Int. J. Climatol. 32, 121–136. https://doi.org/10.1002/joc.2243

Chen, R., Kan, H., Chen, B., Huang, W., Bai, Z., Song, G., Pan, G., 2012. Association of Particulate Air Pollution With Daily MortalityThe China Air Pollution and Health Effects Study. Am. J. Epidemiol. 175, 1173–1181. https://doi.org/10.1093/aje/kwr425

Chen, R., Peng, R.D., Meng, X., Zhou, Z., Chen, B., Kan, H., 2013a. Seasonal variation in the acute effect of particulate air pollution on mortality in the China Air Pollution and Health Effects Study (CAPES). Sci. Total Environ. 450, 259–265. https://doi.org/10.1016/j.scitotenv.2013.02.040

Chen, R., Yin, P., Meng, X., Liu, C., Wang, L., Xu, X., Ross, J.A., Tse, L.A., Zhao, Z., Kan, H., Zhou, Maigeng, 2017. Fine Particulate Air Pollution and Daily Mortality: A Nationwide Analysis in 272 Chinese Cities. Am. J. Respir. Crit. Care Med. 196, 73–81.

Chen, R., Zhang, Y., Yang, C., Zhao, Z., Xu, X., Kan, H., 2013b. Acute Effect of Ambient Air Pollution on Stroke Mortality in the China Air Pollution and Health Effects Study. Stroke 44, 954–960. https://doi.org/10.1161/STROKEAHA.111.673442

Chen, X., Zhang, Li-wen, Huang, J., Song, F., Zhang, Luo-ping, Qian, Z., Trevathan, E., Mao, H., Han, B., Vaughn, M., Chen, K., Liu, Y., Chen, J., Zhao, B., Jiang, G., Gu, Q., Bai, Z., Dong, G., Tang, N., 2016. Long-term exposure to

urban air pollution and lung cancer mortality: A 12-year cohort study in Northern China. Sci. Total Environ. 571, 855–861. https://doi.org/10.1016/j.scitotenv.2016.07.064

Chen, Y., Ebenstein, A., Greenstone, M., Li, H., 2013. Evidence on the impact of sustained exposure to air pollution on life expectancy from China's Huai River policy. Proc. Natl. Acad. Sci. 110, 12936–12941. https://doi.org/10.1073/pnas.1300018110

Chen, Y., Jin, G.Z., Kumar, N., Shi, G., 2012. Gaming in Air Pollution Data? Lessons from China. BE J. Econ. Anal. Policy 12. https://doi.org/10.1515/1935-1682.3227

China National Environmental Monitoring Centre, 2016. Air Quality Report of 74 cities in November 2016 [WWW Document]. China Natl. Environ. Monit. Cent. URL http://www.cnemc.cn/publish/totalWebSite/news/news_50607.html (accessed 2.26.17).

Chiusolo, M., Cadum, E., Stafoggia, M., Galassi, C., Berti, G., Faustini, A., Bisanti, L., Vigotti, M.A., Dessì, M.P., Cernigliaro, A., Mallone, S., Pacelli, B., Minerba, S., Simonato, L., Forastiere, F., 2011. Short-Term Effects of Nitrogen Dioxide on Mortality and Susceptibility Factors in 10 Italian Cities: The EpiAir Study. Environ. Health Perspect. 119, 1233–1238. https://doi.org/10.1289/ehp.1002904

Cimorelli, A.J., Perry, S.G., Venkatram, A., Weil, J.C., Paine, R.J., Wilson, R.B., Lee, R.F., Peters, W.D., Brode, R.W., 2005. AERMOD: A Dispersion Model for Industrial Source Applications. Part I: General Model Formulation and Boundary Layer Characterization. J. Appl. Meteorol. 44, 682–693. https://doi.org/10.1175/JAM2227.1

CNEMC, 2019. 实时数据-中国环境监测总站 [WWW Document]. URL http://www.cnemc.cn/sssj/ (accessed 4.23.19).

CNEMC, 2017. 大气环境-中国环境监测总站 [WWW Document]. URL http://www.cnemc.cn/zzjj/jcwl/dqjcwl/201711/t20171108_645109.shtml (accessed 12.9.19).

Cohen, A.J., Brauer, M., Burnett, R., Anderson, H.R., Frostad, J., Estep, K., Balakrishnan, K., Brunekreef, B., Dandona, L., Dandona, R., Feigin, V., Freedman, G., Hubbell, B., Jobling, A., Kan, H., Knibbs, L., Liu, Y., Martin, R., Morawska, L., Pope, C.A., Shin, H., Straif, K., Shaddick, G., Thomas, M., Dingenen, R. van, Donkelaar, A. van, Vos, T., Murray, C.J.L., Forouzanfar, M.H., 2017. Estimates and 25-year trends of the global burden of disease attributable to ambient air pollution: an analysis of data from the Global Burden of Diseases Study 2015. The Lancet 389, 1907–1918. https://doi.org/10.1016/S0140-6736(17)30505-6

COMEAP, 2018. Associations of long-term average concentrations of nitrogen dioxide with mortality.

Crouse, D.L., Peters, P.A., Hystad, P., Brook, J.R., van Donkelaar, A., Martin, R.V., Villeneuve, P.J., Jerrett, M., Goldberg, M.S., Pope, C.A., Brauer, M., Brook, R.D., Robichaud, A., Menard, R., Burnett, R.T., 2015. Ambient $PM_{2.5}$, O_3, and NO_2 Exposures and Associations with Mortality over 16 Years of Follow-Up in the Canadian Census Health and Environment Cohort

(CanCHEC). Environ. Health Perspect. 123. https://doi.org/10.1289/ehp.1409276

Cyrys, J., Eeftens, M.R., Heinrich, J., Ampe, C., Armengaud, A., Beelen, R., Bellander, T., Beregszaszi, T., Birk, M., Cesaroni, G., Cirach, M., de Hoogh, K., de Nazelle, A., de Vocht, F., Declercq, C., Dėdelė, A., Dimakopoulou, K., Eriksen, K., Galassi, C., Grąulevičienė, R., Grivas, G., Gruzieva, O., Gustafsson, A.H., Hoffmann, B., Iakovides, M., Ineichen, A., Krämer, U., Lanki, T., Lozano, P., Madsen, C., Meliefste, K., Modig, L., Mölter, A., Mosler, G., Nieuwenhuijsen, M., Nonnemacher, M., Oldenwening, M., Peters, A., Pontet, S., Probst-Hensch, N., Quass, U., Raaschou-Nielsen, O., Ranzi, A., Sugiri, D., Stephanou, E.G., Taimisto, P., Tsai, M.-Y., Vaskövi, É., Villani, S., Wang, M., Brunekreef, B., Hoek, G., 2012. Variation of NO_2 and NO_x concentrations between and within 36 European study areas: Results from the ESCAPE study. Atmos. Environ. https://doi.org/10.1016/j.atmosenv.2012.07.080

de Hoogh, K., Gulliver, J., Donkelaar, A. van, Martin, R.V., Marshall, J.D., Bechle, M.J., Cesaroni, G., Pradas, M.C., Dedele, A., Eeftens, M., Forsberg, B., Galassi, C., Heinrich, J., Hoffmann, B., Jacquemin, B., Katsouyanni, K., Korek, M., Künzli, N., Lindley, S.J., Lepeule, J., Meleux, F., de Nazelle, A., Nieuwenhuijsen, M., Nystad, W., Raaschou-Nielsen, O., Peters, A., Peuch, V.-H., Rouil, L., Udvardy, O., Slama, R., Stempfelet, M., Stephanou, E.G., Tsai, M.Y., Yli-Tuomi, T., Weinmayr, G., Brunekreef, B., Vienneau, D., Hoek, G., 2016. Development of West-European PM2.5 and NO2 land use regression models incorporating satellite-derived and chemical transport modelling data. Environ. Res. 151, 1–10. https://doi.org/10.1016/j.envres.2016.07.005

De Visscher, A., 2013. Air Dispersion Modeling: Foundations and Applications | Wiley.

Delfino Ralph J., Staimer Norbert, Gillen Dan, Tjoa Thomas, Sioutas Constantinos, Fung Kochy, George Steven C., Kleinman Michael T., 2006. Personal and Ambient Air Pollution is Associated with Increased Exhaled Nitric Oxide in Children with Asthma. Environ. Health Perspect. 114, 1736–1743. https://doi.org/10.1289/ehp.9141

Demographia, 2019. World Urban Areas [WWW Document]. URL http://demographia.com/db-worldua.pdf (accessed 4.9.19).

Denby, B.R., 2020. metno/uEMEP. Norwegian Meteorological Institute.

Di Sabatino, S., Buccolieri, R., Pulvirenti, B., Britter, R., 2007. Simulations of pollutant dispersion within idealised urban-type geometries with CFD and integral models. Atmos. Environ. 41, 8316–8329. https://doi.org/10.1016/j.atmosenv.2007.06.052

Ding, J., A, R.J. van der, Mijling, B., Jalkanen, J.-P., Johansson, L., Levelt, P.F., 2018. Maritime NO_x emissions over Chinese seas derived from satellite observations. Geophys. Res. Lett. 45, 2031–2037. https://doi.org/10.1002/2017GL076788

Duncan, B.N., Prados, A.I., Lamsal, L.N., Liu, Y., Streets, D.G., Gupta, P., Hilsenrath, E., Kahn, R.A., Nielsen, J.E., Beyersdorf, A.J., Burton, S.P., Fiore, A.M., Fishman, J., Henze, D.K., Hostetler, C.A., Krotkov, N.A., Lee, P., Lin, M., Pawson, S., Pfister, G., Pickering, K.E., Pierce, R.B., Yoshida,

Y., Ziemba, L.D., 2014. Satellite data of atmospheric pollution for U.S. air quality applications: Examples of applications, summary of data end-user resources, answers to FAQs, and common mistakes to avoid. Atmos. Environ. 94, 647–662. https://doi.org/10.1016/j.atmosenv.2014.05.061

ECMWF, 2019. ECMWF | Public Datasets [WWW Document]. URL https://apps.ecmwf.int/datasets/ (accessed 3.30.19).

EPA, 2017. Environmental Protection Department of Anhui Province [WWW Document]. URL http://www.aepb.gov.cn/pages/Aepb15_SJZX_List.aspx?CityCode=340100&LX=5 (accessed 11.24.17).

EPG, 2017. Environmental Protection of Guangdong Province [WWW Document]. URL http://www.gdep.gov.cn/hjjce/kqjc/ (accessed 11.24.17).

EPW, 2017. Environmental Protection Department of Wuhan [WWW Document]. URL http://www.whepb.gov.cn/viewAirDarlyForestWaterInfohistory.jspx (accessed 11.24.17).

Erisman, J.W., Galloway, J.N., Dise, N.B., Sutton, M.A., Bleeker, A., Grizzetti, B., Leach, A.M., Vries, W. de, 2015. Nitrogen : too much of a vital resource : Science Brief. WWF Netherlands, Zeist, The Netherlands.

ESCAPE, 2010. ESCAPE_Exposure-manual [WWW Document]. URL http://www.escapeproject.eu/manuals/ESCAPE_Exposure-manualv9.pdf (accessed 6.29.17).

ESCAPE, 2008. ESCAPE study manual [WWW Document]. URL http://www.escapeproject.eu/manuals/ESCAPE-Study-manual_x007E_final.pdf (accessed 5.21.19).

Faustini, A., Rapp, R., Forastiere, F., 2014. Nitrogen dioxide and mortality: review and meta-analysis of long-term studies. Eur. Respir. J. 44, 744–753. https://doi.org/10.1183/09031936.00114713

Feng, Z., Hu, E., Wang, X., Jiang, L., Liu, X., 2015. Ground-level O3 pollution and its impacts on food crops in China: A review. Environ. Pollut. 199, 42–48. https://doi.org/10.1016/j.envpol.2015.01.016

Fu, M., Liu, H., Jin, X., He, K., 2017. National- to port-level inventories of shipping emissions in China. Environ. Res. Lett. 12, 114024. https://doi.org/10.1088/1748-9326/aa897a

Fuller, G., 2018. The Invisible Killer: The Rising Global Threat of Air Pollution - and How We Can Fight Back. Melville House UK.

Fuller, G.W., Font, A., 2019. Keeping air pollution policies on track. Science 365, 322–323. https://doi.org/10.1126/science.aaw9865

Gabel, J., Shehadi, A., Ursini, S., Gerometta, M., 2016. CTBUH Year in Review: Tall Trends of 2016. The Council on Tall Buildings and Urban Habitat (CTBUH).

GADM, 2019. GADM [WWW Document]. GADM Maps Data. URL https://gadm.org/ (accessed 10.10.19).

Gao, J., Tian, H., Cheng, K., Lu, L., Zheng, M., Wang, S., Hao, J., Wang, K., Hua, S., Zhu, C., Wang, Y., 2015. The variation of chemical characteristics of $PM_{2.5}$ and PM_{10} and formation causes during two haze pollution events in urban Beijing, China. Atmos. Environ. 107, 1–8. https://doi.org/10.1016/j.atmosenv.2015.02.022

Gerboles, M., Lagler, F., Rembges, D., Brun, C., 2003. Assessment of uncertainty of NO2 measurements by the chemiluminescence method and discussion of the quality objective of the NO2 European Directive. J. Environ. Monit. JEM 5, 529–540. https://doi.org/10.1039/b302358c

Ghanem, D., Zhang, J., 2014. 'Effortless Perfection:' Do Chinese cities manipulate air pollution data? J. Environ. Econ. Manag. 68, 203–225. https://doi.org/10.1016/j.jeem.2014.05.003

Gilbert, N.L., Goldberg, M.S., Beckerman, B., Brook, J.R., Jerrett, M., 2005. Assessing Spatial Variability of Ambient Nitrogen Dioxide in Montréal, Canada, with a Land-Use Regression Model. J. Air Waste Manag. Assoc. 55, 1059–1063. https://doi.org/10.1080/10473289.2005.10464708

Gillespie, J., Beverland, I.J., Hamilton, S., Padmanabhan, S., 2016. Development, Evaluation, and Comparison of Land Use Regression Modeling Methods to Estimate Residential Exposure to Nitrogen Dioxide in a Cohort Study. Environ. Sci. Technol. 50, 11085–11093. https://doi.org/10.1021/acs.est.6b02089

Globeland30, 2010. GLC30 information service [WWW Document]. URL http://www.globallandcover.com/GLC30Download/index.aspx (accessed 5.19.19).

Gong, J., Hu, Y., Liu, M., Bu, R., Chang, Y., Bilal, M., Li, C., Wu, W., Ren, B., 2016. Land Use Regression Models Using Satellite Aerosol Optical Depth Observations and 3D Building Data from the Central Cities of Liaoning Province, China. Pol. J. Environ. Stud. 25, 1015–1026. https://doi.org/10.15244/pjoes/61261

Guangzhou Government, 2017. Environmental air quality standardization plan of Guangzhou city (2016-2025) [WWW Document]. Website Guangzhou Gov. URL http://www.gz.gov.cn/gzgov/s2811/201712/57727a1d77354f5dbc22bb5831aa7d93.shtml (accessed 9.25.18).

Guangzhou Municipal Public Security Bureau, 2016. The number of deaths in Guangzhou traffic accidents has dropped for 13 consecutive years [WWW Document]. URL http://www.gzjd.gov.cn/gzjd/gaxw_ztbd_ctgc/201602/67b06e82303f4f1bb3e6f7225f187552.shtml (accessed 5.21.19).

Guangzhou Statistics Bureau, 2018. Guangzhou Statistics Bureau [WWW Document]. URL http://www.gzstats.gov.cn/gzstats/tjgb_qtgb/201802/cf533209a9cc46d08da1f6070a65067e.shtml (accessed 4.15.19).

Guo, H., Gu, X., Ma, G., Shi, S., Wang, W., Zuo, X., Zhang, X., 2019. Spatial and temporal variations of air quality and six air pollutants in China during 2015–2017. Sci. Rep. 9, 1–11. https://doi.org/10.1038/s41598-019-50655-6

Guo, H., Otjes, R., Schlag, P., Kiendler-Scharr, A., Nenes, A., Weber, R.J., 2018. Effectiveness of ammonia reduction on control of fine particle nitrate. Atmospheric Chem. Phys. 18, 12241–12256. https://doi.org/10.5194/acp-18-12241-2018

Gurung, A., Levy, J.I., Bell, M.L., 2017. Modeling the intraurban variation in nitrogen dioxide in urban areas in Kathmandu Valley, Nepal. Environ. Res. 155, 42–48. https://doi.org/10.1016/j.envres.2017.01.038

Hagenbjörk, A., Malmqvist, E., Mattisson, K., Sommar, N.J., Modig, L., 2017. The spatial variation of O3, NO, NO2 and NOxand the relation between them in two Swedish cities. Environ. Monit. Assess. 189, 161. https://doi.org/10.1007/s10661-017-5872-z

Hao, W., Reis, S., Lin, C., Heal, M.R., 2016. Effect of monitoring network design on land use regression models for estimating residential NO_2 concentration 149, 24–33. https://doi.org/10.1016/j.atmosenv.2016.11.014

He, B., Heal, M.R., Humstad, K.H., Yan, L., Zhang, Q., Reis, S., 2019. A hybrid model approach for estimating health burden from NO2 in megacities in China: a case study in Guangzhou. Environ. Res. Lett. 14, 124019. https://doi.org/10.1088/1748-9326/ab4f96

He, B., Heal, M.R., Reis, S., 2018. Land-use regression modelling of intra-urban air pollution variation in China: current status and future needs. Atmosphere 9, 134. https://doi.org/10.3390/atmos9040134

He, K., Huo, H., Zhang, Q., 2002. Urban Air Pollution in China: Current Status, Characteristics, and Progress. Annu. Rev. Energy Environ. 27, 397–431. https://doi.org/10.1146/annurev.energy.27.122001.083421

Ho, C.-C., Chan, C.-C., Cho, C.-W., Lin, H.-I., Lee, J.-H., Wu, C.-F., 2015. Land use regression modeling with vertical distribution measurements for fine particulate matter and elements in an urban area. Atmos. Environ. 104, 256–263. https://doi.org/10.1016/j.atmosenv.2015.01.024

Hoek, G., Beelen, R., de Hoogh, K., Vienneau, D., Gulliver, J., Fischer, P., Briggs, D., 2008. A review of land-use regression models to assess spatial variation of outdoor air pollution. Atmos. Environ. 42, 7561–7578. https://doi.org/10.1016/j.atmosenv.2008.05.057

Hoek, G., Krishnan, R.M., Beelen, R., Peters, A., Ostro, B., Brunekreef, B., Kaufman, J.D., 2013. Long-term air pollution exposure and cardio-respiratory mortality: a review. Environ. Health 12, 43. https://doi.org/10.1186/1476-069X-12-43

Hood, C., MacKenzie, I., Stocker, J., Johnson, K., Carruthers, D., Vieno, M., Doherty, R., 2018. Air quality simulations for London using a coupled regional-to-local modelling system. Atmos. Chem. Phys. 18, 11221–11245. https://doi.org/doi.org/10.5194/acp-18-11221-2018

Huang, L., Zhang, C., Bi, J., 2017. Development of land use regression models for PM2.5 , SO2 , NO2 and O3 in Nanjing, China. Environ. Res. 158, 542–552. https://doi.org/10.1016/j.envres.2017.07.010

Humstad, K.H., 2018. Developing a land use regression model for NO2 concentrations in Guangzhou, China.

International Council on Clean Transportation, 2017. China's Stage 6 Emission Standard for New Light-Duty Vehicles (Final Rules) [WWW Document]. URL https://theicct.org/sites/default/files/publications/China-LDV-Stage-6_Policy-Update_ICCT_20032017_vF_corrected.pdf

Jerrett, M., Arain, A., Kanaroglou, P., Beckerman, B., Potoglou, D., Sahsuvaroglu, T., Morrison, J., Giovis, C., 2005. A review and evaluation of intraurban air pollution exposure models. J. Expo. Anal. Environ. Epidemiol. 15, 185–204. https://doi.org/10.1038/sj.jea.7500388

Jiang, Y., Niu, Y., Xia, Y., Liu, C., Lin, Z., Wang, W., Ge, Y., Lei, X., Wang, C., Cai, J., Chen, R., Kan, H., 2019. Effects of personal nitrogen dioxide

exposure on airway inflammation and lung function. Environ. Res. 177, 108620. https://doi.org/10.1016/j.envres.2019.108620

Jim, C.Y., Chen, W.Y., 2008. Assessing the ecosystem service of air pollutant removal by urban trees in Guangzhou (China). J. Environ. Manage. 88, 665–676. https://doi.org/10.1016/j.jenvman.2007.03.035

Jin, Y., Andersson, H., Zhang, S., 2016. Air Pollution Control Policies in China: A Retrospective and Prospects. Int. J. Environ. Res. Public. Health 13. https://doi.org/10.3390/ijerph13121219

Jing, B., Wu, L., Mao, H., Gong, S., He, J., Zou, C., Song, G., Li, X., Wu, Z., 2016. Development of a vehicle emission inventory with high temporal – spatial resolution based on NRT traffic data and its impact on air pollution in Beijing – Part 1 : Development and evaluation of vehicle emission inventory. Atmos. Chem. Phys. 16, 3161–3170. https://doi.org/Atmos. Chem. Phys., 16, 3161-3170, 2016 https://doi.org/10.5194/acp-16-3161-2016

Johansson, L., Jalkanen, J.-P., Kukkonen, J., 2017. Global assessment of shipping emissions in 2015 on a high spatial and temporal resolution. Atmos. Environ. 167, 403–415. https://doi.org/10.1016/j.atmosenv.2017.08.042

Johnson, M., Isakov, V., Touma, J.S., Mukerjee, S., Özkaynak, H., 2010. Evaluation of land-use regression models used to predict air quality concentrations in an urban area 44, 3660–3668. https://doi.org/doi.org/10.1016/j.atmosenv.2010.06.041

Kan, H., Chen, B., Hong, C., 2009. Health Impact of Outdoor Air Pollution in China: Current Knowledge and Future Research Needs. Environ. Health Perspect. 117, A187–A187. https://doi.org/10.1289/ehp.12737

Kanakidou, M., 2019. China's nitrogen management. Nat. Geosci. 12, 403–404. https://doi.org/10.1038/s41561-019-0358-y

Kleffmann, J., Tapia, G.V., Bejan, I., Kurtenbach, R., Wiesen, P., 2013. NO2 Measurement Techniques: Pitfalls and New Developments, in: Barnes, I., Rudziński, K.J. (Eds.), Disposal of Dangerous Chemicals in Urban Areas and Mega Cities, NATO Science for Peace and Security Series C: Environmental Security. Springer Netherlands, Dordrecht, pp. 15–28. https://doi.org/10.1007/978-94-007-5034-0_2

Kloog, I., Koutrakis, P., Coull, B.A., Lee, H.J., Schwartz, J., 2011. Assessing temporally and spatially resolved PM2.5 exposures for epidemiological studies using satellite aerosol optical depth measurements. Atmos. Environ. 45, 6267–6275. https://doi.org/10.1016/j.atmosenv.2011.08.066

Kloog, I., Nordio, F., Coull, B.A., Schwartz, J., 2012. Incorporating Local Land Use Regression And Satellite Aerosol Optical Depth In A Hybrid Model Of Spatiotemporal PM2.5 Exposures In The Mid-Atlantic States. Environ. Sci. Technol. 46, 11913–11921. https://doi.org/10.1021/es302673e

Lee, J.-H., Wu, C.-F., Hoek, G., de Hoogh, K., Beelen, R., Brunekreef, B., Chan, C.-C., 2014. Land use regression models for estimating individual NOx and NO2 exposures in a metropolis with a high density of traffic roads and population. Sci. Total Environ. 472, 1163–1171. https://doi.org/10.1016/j.scitotenv.2013.11.064

Lee, M., Brauer, M., Wong, P., Tang, R., Tsui, T.H., Choi, C., Cheng, W., Lai, P.-C., Tian, L., Thach, T.-Q., Allen, R., Barratt, B., 2017. Land use regression modelling of air pollution in high density high rise cities: A case study in

Hong Kong. Sci. Total Environ. 592, 306–315. https://doi.org/10.1016/j.scitotenv.2017.03.094

Li, X., Liu, W., Chen, Z., Zeng, G., Hu, C., León, T., Liang, J., Huang, G., Gao, Z., Li, Z., Yan, W., He, X., Lai, M., He, Y., 2015. The application of semicircular-buffer-based land use regression models incorporating wind direction in predicting quarterly NO2 and PM10 concentrations. Atmos. Environ. 103, 18–24. https://doi.org/10.1016/j.atmosenv.2014.12.004

Li, Y., Lau, A.K.H., Fung, J.C.H., Zheng, J., Liu, S., 2013. Importance of NOx control for peak ozone reduction in the Pearl River Delta region. J. Geophys. Res. Atmospheres 118, 9428–9443. https://doi.org/10.1002/jgrd.50659

Lin, C., Feng, X., Heal, M.R., 2016. Temporal persistence of intra-urban spatial contrasts in ambient NO2, O3 and Ox in Edinburgh, UK. Atmospheric Pollut. Res. 7, 734–741. https://doi.org/10.1016/j.apr.2016.03.008

Lin, C., Masey, N., Wu, H., Jackson, M., Carruthers, D.J., Reis, S., Doherty, R.M., Beverland, I.J., Heal, M.R., 2017. Practical Field Calibration of Portable Monitors for Mobile Measurements of Multiple Air Pollutants. Atmosphere 8, 231. https://doi.org/10.3390/atmos8120231

Liu, C., Henderson, B.H., Wang, D., Yang, X., Peng, Z., 2016. A land use regression application into assessing spatial variation of intra-urban fine particulate matter (PM2.5) and nitrogen dioxide (NO2) concentrations in City of Shanghai, China. Sci. Total Environ. 565, 607–615. https://doi.org/10.1016/j.scitotenv.2016.03.189

Liu, F., Beirle, S., Zhang, Q., van der A, R.J., Zheng, B., Tong, D., He, K., 2017. NO_x emission trends over Chinese cities estimated from OMI observations during 2005 to 2015. Atmospheric Chem. Phys. 17, 9261–9275. https://doi.org/10.5194/acp-17-9261-2017

Liu, H., Fu, M., Jin, X., Shang, Y., Shindell, D., Faluvegi, G., Shindell, C., He, K., 2016. Health and climate impacts of ocean-going vessels in East Asia. Nat. Clim. Change 6, 1037–1041. https://doi.org/10.1038/nclimate3083

Liu, J., Diamond, J., 2005. China's environment in a globalizing world. Nature 435, 1179–1186. https://doi.org/10.1038/4351179a

Liu, J., Kuang, W., Zhang, Z., Xu, X., Qin, Y., Ning, J., Zhou, W., Zhang, S., Li, R., Yan, C., Wu, S., Shi, X., Jiang, N., Yu, D., Pan, X., Chi, W., 2014. Spatiotemporal characteristics, patterns, and causes of land-use changes in China since the late 1980s. J. Geogr. Sci. 24, 195–210. https://doi.org/10.1007/s11442-014-1082-6

Liu, W., Li, X., Chen, Z., Zeng, G., León, T., Liang, J., Huang, G., Gao, Z., Jiao, S., He, X., Lai, M., 2015. Land use regression models coupled with meteorology to model spatial and temporal variability of NO2 and PM10 in Changsha, China. Atmos. Environ. 116, 272–280. https://doi.org/10.1016/j.atmosenv.2015.06.056

Lokwani, R., Wark, P.A.B., Baines, K.J., Barker, D., Simpson, J.L., 2019. Hypersegmented airway neutrophils and its association with reduced lung function in adults with obstructive airway disease: an exploratory study. BMJ Open 9, e024330. https://doi.org/10.1136/bmjopen-2018-024330

Lucock, M., Jones, P., Veysey, M., Beckett, E., 2017. B vitamins and pollution, an interesting, emerging, yet incomplete picture of folate and the exposome.

Proc. Natl. Acad. Sci. 114, E3878–E3879. https://doi.org/10.1073/pnas.1704662114

Ma, J., Yi, H., Tang, X., Zhang, Y., Xiang, Y., Pu, L., 2013. Application of AERMOD on near future air quality simulation under the latest national emission control policy of China: A case study on an industrial city. J. Environ. Sci. 25, 1608–1617. https://doi.org/10.1016/S1001-0742(12)60245-9

Ma, X., Longley, I., Gao, J., Kachhara, A., Salmond, J., 2019. A site-optimised multi-scale GIS based land use regression model for simulating local scale patterns in air pollution. Sci. Total Environ. 685, 134–149. https://doi.org/10.1016/j.scitotenv.2019.05.408

MarcoPolo-Panda, 2017. MarcoPolo Emission Inventory | MarcoPolo – Panda. URL http://www.marcopolo-panda.eu/products/toolbox/emission-data/marcopolo-emission-inventory/ (accessed 3.30.19).

McHugh, C. a., Carruthers, D. j., Edmunds, H. a., 1997. ADMS–Urban: an air quality management system for traffic, domestic and industrial pollution. Int. J. Environ. Pollut. 8, 666–674. https://doi.org/10.1504/IJEP.1997.028218

McHugh, C., Xiangyu, S., Carruthers, D., 2005. Using ADMS models for Air Quality Assessment and Management in China. Chin. J. Popul. Resour. Environ. 3, 3–10. https://doi.org/10.1080/10042857.2005.10677419

MEIC, 2016. Multi-resolution Emission Inventory (MEIC) [WWW Document]. URL http://meicmodel.org/ (accessed 3.30.19).

Melli, P., Runca, E., 1979. Gaussian Plume Model Parameters for Ground-Level and Elevated Sources Derived from the Atmospheric Diffusion Equation in a Neutral Case. J. Appl. Meteorol. 18, 1216–1221. https://doi.org/10.1175/1520-0450(1979)018<1216:GPMPFG>2.0.CO;2

Meng, X., Fu, Q., Ma, Z., Chen, L., Zou, B., Zhang, Y., Xue, W., Wang, J., Wang, D., Kan, H., Liu, Y., 2016. Estimating ground-level PM10 in a Chinese city by combining satellite data, meteorological information and a land use regression model. Environ. Pollut. 208, 177–184. https://doi.org/10.1016/j.envpol.2015.09.042

MEP, 2016. Law of the People's Republic of China on the Prevention and Control of Atmospheric Pollution[1] [WWW Document]. URL http://english.court.gov.cn/2016-04/15/content_24565639.htm (accessed 12.7.19).

Mills, G., Harmens, H., Wagg, S., Sharps, K., Hayes, F., Fowler, D., Sutton, M., Davies, B., 2016. Ozone impacts on vegetation in a nitrogen enriched and changing climate. Environ. Pollut. 208, 898–908. https://doi.org/10.1016/j.envpol.2015.09.038

Mills, G., Sharps, K., Simpson, D., Pleijel, H., Broberg, M., Uddling, J., Jaramillo, F., Davies, W.J., Dentener, F., Berg, M.V. den, Agrawal, M., Agrawal, S.B., Ainsworth, E.A., Büker, P., Emberson, L., Feng, Z., Harmens, H., Hayes, F., Kobayashi, K., Paoletti, E., Dingenen, R.V., 2018. Ozone pollution will compromise efforts to increase global wheat production. Glob. Change Biol. 24, 3560–3574. https://doi.org/10.1111/gcb.14157

Ministry of Ecology and Environment, 2018. Report on the State of the Environment in China [WWW Document]. URL http://english.mee.gov.cn/Resources/Reports/soe/ (accessed 12.7.19).

Ministry of Ecology and Environment, 2012. Ambient air quality standards [WWW Document]. URL http://bz.mee.gov.cn/bzwb/dqhjbh/dqhjzlbz/201203/t20120302_224165.shtml (accessed 5.21.19).

Ministry of Ecology and Environment of the People's Republic of China, 2018. 中华人民共和国大气污染防治法（Law of the People's Republic of China on the Prevention and Control of Atmospheric Pollution） [WWW Document]. Minist. Ecol. Environ. Peoples Repub. China. URL http://zfs.mee.gov.cn/fl/201811/t20181113_673567.shtml (accessed 11.3.19).

Ministry of Environmental Protection, 2018a. Report on the State of the Environment in China [WWW Document]. URL http://english.mee.gov.cn/Resources/Reports/soe/ (accessed 4.9.19).

Ministry of Environmental Protection, 2018b. 环境空气气态污染物（SO2、NO2、O3、CO）连续自动监测系统技术要求及检测方法 Specifications and Test Procedures for Ambient Air Quality Continuous Automated Monitoring System for SO2、NO2、O3 and CO [WWW Document]. URL http://kjs.mee.gov.cn/hjbhbz/bzwb/jcffbz/201308/t20130802_256853.shtml (accessed 10.13.19).

Mölter, A., Lindley, S., de Vocht, F., Simpson, A., Agius, R., 2010. Modelling air pollution for epidemiologic research — Part I: A novel approach combining land use regression and air dispersion. Sci. Total Environ., Special Section: Integrating Water and Agricultural Management Under Climate Change 408, 5862–5869. https://doi.org/10.1016/j.scitotenv.2010.08.027

National Bureau of Statistics of China, 2016a. China Statistical Yearbook-2016 [WWW Document]. URL http://www.stats.gov.cn/tjsj/ndsj/2016/indexeh.htm (accessed 11.17.17).

National Bureau of Statistics of China, 2016b. National Data- National Bureau of Statistics of China [WWW Document]. URL http://data.stats.gov.cn/english/easyquery.htm?cn=C01 (accessed 1.20.18).

National Bureau of Statistics of China, 2012. China Statistical Yearbook 2012 [WWW Document]. URL http://www.stats.gov.cn/tjsj/ndsj/2012/indexeh.htm (accessed 11.17.17).

Nieuwenhuijsen, M. (Ed.), 2015. Exposure Assessment in Environmental Epidemiology, Exposure Assessment in Environmental Epidemiology. Oxford University Press.

Novotny, E.V., Bechle, M.J., Millet, D.B., Marshall, J.D., 2011. National Satellite-Based Land-Use Regression: NO2 in the United States. Environ. Sci. Technol. 45, 4407–4414. https://doi.org/10.1021/es103578x

O'brien, R.M., 2007. A Caution Regarding Rules of Thumb for Variance Inflation Factors. Qual. Quant. 41, 673–690. https://doi.org/10.1007/s11135-006-9018-6

Olive, D.J., 2017. Multiple Linear Regression, in: Olive, D.J. (Ed.), Linear Regression. Springer International Publishing, Cham, pp. 17–83. https://doi.org/10.1007/978-3-319-55252-1_2

OMI Team, 2012. Ozone Monitoring Instrument (OMI) Data User's Guide [WWW Document]. URL https://docserver.gesdisc.eosdis.nasa.gov/repository/Mission/OMI/3.3_Scienc

eDataProductDocumentation/3.3.2_ProductRequirements_Designs/README.OMI_DUG.pdf (accessed 1.10.18).

OpenStreetMap, 2018. OpenStreetMap [WWW Document]. OpenStreetMap. URL https://www.openstreetmap.org/ (accessed 5.19.19).

Ou, J., Yuan, Z., Zheng, J., Huang, Z., Shao, M., Li, Z., Huang, X., Guo, H., Louie, P.K.K., 2016. Ambient Ozone Control in a Photochemically Active Region: Short-Term Despiking or Long-Term Attainment? Environ. Sci. Technol. 50, 5720–5728. https://doi.org/10.1021/acs.est.6b00345

Owen, B., Edmunds, H.A., Carruthers, D.J., Singles, R.J., 2000. Prediction of total oxides of nitrogen and nitrogen dioxide concentrations in a large urban area using a new generation urban scale dispersion model with integral chemistry model. Atmos. Environ. 34, 397–406. https://doi.org/10.1016/S1352-2310(99)00332-5

Palmes, E.D., Gunnison, A.F., DiMattio, J., Tomczyk, C., 1976. Personal sampler for nitrogen dioxide. Am. Ind. Hyg. Assoc. J. 37, 570–577. https://doi.org/10.1080/0002889768507522

People's Government of Guangzhou Municipality, 2017. 广州市人民政府门户网站 - 广州市人民政府关于印发广州市环境空气质量达标规划（2016－2025年）的通知 [WWW Document]. Guangzhou Munic. Environ. Air Qual. Plan 2016-2025. URL https://www.gz.gov.cn/gzgov/s2811/201712/57727a1d77354f5dbc22bb5831aa7d93.shtml (accessed 5.14.19).

Pepe, N., Pirovano, G., Lonati, G., Balzarini, A., Toppetti, A., Riva, G.M., Bedogni, M., 2016. Development and application of a high resolution hybrid modelling system for the evaluation of urban air quality. Atmos. Environ. 141, 297–311. https://doi.org/10.1016/j.atmosenv.2016.06.071

Qi, J., Zheng, B., Li, M., Yu, F., Chen, C., Liu, F., Zhou, X., Yuan, J., Zhang, Q., He, K., 2017. A high-resolution air pollutants emission inventory in 2013 for the Beijing-Tianjin-Hebei region, China. Atmos. Environ. 170, 156–168. https://doi.org/10.1016/j.atmosenv.2017.09.039

Qiao, X., Guo, H., Tang, Y., Wang, P., Deng, W., Zhao, X., Hu, J., Ying, Q., Zhang, H., 2019. Local and regional contributions to fine particulate matter in the 18 cities of Sichuan Basin, southwestern China. Atmospheric Chem. Phys. 19, 5791–5803. https://doi.org/10.5194/acp-19-5791-2019

Qiu, J., 2012. Megacities pose serious health challenge. Nat. News. https://doi.org/10.1038/nature.2012.11495

Reis, S., Grennfelt, P., Klimont, Z., Amann, M., ApSimon, H., Hettelingh, J.-P., Holland, M., LeGall, A.-C., Maas, R., Posch, M., Spranger, T., Sutton, M.A., Williams, M., 2012. From Acid Rain to Climate Change. Science 338, 1153–1154. https://doi.org/10.1126/science.1226514

Reis, S., Liška, T., Vieno, M., Carnell, E.J., Beck, R., Clemens, T., Dragosits, U., Tomlinson, S.J., Leaver, D., Heal, M.R., 2018. The influence of residential and workday population mobility on exposure to air pollution in the UK. Environ. Int. 121, 803–813. https://doi.org/10.1016/j.envint.2018.10.005

Reis, S., Seto, E., Northcross, A., Quinn, N.W.T., Convertino, M., Jones, R.L., Maier, H.R., Schlink, U., Steinle, S., Vieno, M., Wimberly, M.C., 2015. Integrating modelling and smart sensors for environmental and human health.

Environ. Model. Softw. 74, 238–246. https://doi.org/10.1016/j.envsoft.2015.06.003

Ridley, B.A., Carroll, M.A., Gregory, G.L., Sachse, G.W., 1988. NO and NO2 in the troposphere: Technique and measurements in regions of a folded tropopause. J. Geophys. Res. Atmospheres 93, 15813–15830. https://doi.org/10.1029/JD093iD12p15813

Righi, S., Lucialli, P., Pollini, E., 2009. Statistical and diagnostic evaluation of the ADMS-Urban model compared with an urban air quality monitoring network. Atmos. Environ. 43, 3850–3857. https://doi.org/10.1016/j.atmosenv.2009.05.016

Rosenthal, G., Rosenthal, J.A., 2011. Statistics and Data Interpretation for Social Work. Springer Publishing Company.

Samoli, E., Aga, E., Touloumi, G., Nisiotis, K., Forsberg, B., Lefranc, A., Pekkanen, J., Wojtyniak, B., Schindler, C., Niciu, E., Brunstein, R., Fikfak, M.D., Schwartz, J., Katsouyanni, K., 2006. Short-term effects of nitrogen dioxide on mortality: an analysis within the APHEA project. Eur. Respir. J. 27, 1129–1138. https://doi.org/10.1183/09031936.06.00143905

San José, R., Pérez, J.L., Pérez, L., Gonzalez Barras, R.M., 2018. Effects of climate change on the health of citizens modelling urban weather and air pollution. Energy 165, 53–62. https://doi.org/10.1016/j.energy.2018.09.088

Schraufnagel, D.E., Balmes, J.R., Cowl, C.T., Matteis, S.D., Jung, S.-H., Mortimer, K., Perez-Padilla, R., Rice, M.B., Riojas-Rodriguez, H., Sood, A., Thurston, G.D., To, T., Vanker, A., Wuebbles, D.J., 2019a. Air Pollution and Noncommunicable Diseases: A Review by the Forum of International Respiratory Societies' Environmental Committee, Part 1: The Damaging Effects of Air Pollution. CHEST 155, 409–416. https://doi.org/10.1016/j.chest.2018.10.042

Schraufnagel, D.E., Balmes, J.R., Cowl, C.T., Matteis, S.D., Jung, S.-H., Mortimer, K., Perez-Padilla, R., Rice, M.B., Riojas-Rodriguez, H., Sood, A., Thurston, G.D., To, T., Vanker, A., Wuebbles, D.J., 2019b. Air Pollution and Noncommunicable Diseases: A Review by the Forum of International Respiratory Societies' Environmental Committee, Part 2: Air Pollution and Organ Systems. CHEST 155, 417–426. https://doi.org/10.1016/j.chest.2018.10.041

Seinfeld, J.H., Pandis, S.N., 2016. Atmospheric Chemistry and Physics: From Air Pollution to Climate Change, 3rd ed. Wiley.

Seinfeld, J.H., Pandis, S.N., 1998. Atmospheric Chemistry and Physics: From Air Pollution to Climate Change, 3rd ed. Wiley.

Shi, Y., Lau, K.K.-L., Ng, E., 2017. Incorporating wind availability into land use regression modelling of air quality in mountainous high-density urban environment. Environ. Res. 157, 17–29. https://doi.org/10.1016/j.envres.2017.05.007

Shi, Y., Lau, K.K.-L., Ng, E., 2016. Developing Street-Level PM2.5 and PM10 Land Use Regression Models in High-Density Hong Kong with Urban Morphological Factors. Environ. Sci. Technol. 50, 8178–8187. https://doi.org/10.1021/acs.est.6b01807

Smith, J.D., Mitsakou, C., Kitwiroon, N., Barratt, B.M., Walton, H.A., Taylor, J.G., Anderson, H.R., Kelly, F.J., Beevers, S.D., 2016. London Hybrid Exposure

Model: Improving Human Exposure Estimates to NO2 and PM2.5 in an Urban Setting. Environ. Sci. Technol. 50, 11760–11768. https://doi.org/10.1021/acs.est.6b01817

Song, C., Wu, L., Xie, Y., He, J., Chen, X., Wang, T., Lin, Y., Jin, T., Wang, A., Liu, Y., Dai, Q., Liu, B., Wang, Y., Mao, H., 2017. Air pollution in China: Status and spatiotemporal variations. Environ. Pollut. 227, 334–347. https://doi.org/10.1016/j.envpol.2017.04.075

Stevens, C.J., Thompson, K., Grime, J.P., Long, C.J., Gowing, D.J.G., 2010. Contribution of acidification and eutrophication to declines in species richness of calcifuge grasslands along a gradient of atmospheric nitrogen deposition. Funct. Ecol. 24, 478–484. https://doi.org/10.1111/j.1365-2435.2009.01663.x

Stevens, E.L., Rosser, F., Forno, E., Peden, D., Celedón, J.C., 2019. Can the effects of outdoor air pollution on asthma be mitigated? J. Allergy Clin. Immunol. 143, 2016-2018.e1. https://doi.org/10.1016/j.jaci.2019.04.011

Stoerk, T., 2016. Statistical corruption in Beijing's air quality data has likely ended in 2012. Atmos. Environ. 127, 365–371. https://doi.org/10.1016/j.atmosenv.2015.12.055

Su, J.G., Jerrett, M., Beckerman, B., 2009. A distance-decay variable selection strategy for land use regression modeling of ambient air pollution exposures. Sci. Total Environ., Thematic Issue - BioMicroWorld Conference 407, 3890–3898. https://doi.org/10.1016/j.scitotenv.2009.01.061

Sutton, M.A., Howard, C.M., Erisman, J.W., Billen, G., Bleeker, A., Grennfelt, P., Grinsven, H. van, Grizzetti, B., 2011. The European Nitrogen Assessment: Sources, Effects and Policy Perspectives. Cambridge University Press.

The Royal Society, 2008. Ground-level ozone in the 21st century: future trends, impacts and policy implications | Royal Society.

Tonnesen, S., Jeffries, H.E., 1994. Inhibition of odd oxygen production in the carbon bond four and generic reaction set mechanisms. Atmos. Environ. 28, 1339–1349. https://doi.org/10.1016/1352-2310(94)90281-X

UN Environment, 2019. A review of 20 Years' Air Pollution Control in Beijing [WWW Document]. UNEP. URL http://www.unenvironment.org/resources/report/review-20-years-air-pollution-control-beijing (accessed 8.30.19).

United Nations, 2017. The World's Cities in 2016 [WWW Document]. URL http://www.un.org/en/development/desa/population/publications/pdf/urbanization/the_worlds_cities_in_2016_data_booklet.pdf (accessed 1.25.18).

Vallero, D., 2014. Fundamentals of Air Pollution, 5th ed. Elsevier. https://doi.org/10.1016/C2012-0-01172-6

Vardoulakis, S., Kettle, R., Cosford, P., Lincoln, P., Holgate, S., Grigg, J., Kelly, F., Pencheon, D., 2018. Local action on outdoor air pollution to improve public health. Int. J. Public Health 63, 557–565. https://doi.org/10.1007/s00038-018-1104-8

Vekemans, O., Chaouki, J., 2016. Municipal Solid Waste Cofiring in Coal Power Plants: Combustion Performance. Dev. Combust. Technol. https://doi.org/10.5772/63940

Venkatram, A., Karamchandani, P., Pai, P., Goldstein, R., 1994. The development and application of a simplified ozone modeling system (SOMS). Atmos. Environ. 28, 3665–3678. https://doi.org/10.1016/1352-2310(94)00190-V

Vennemo, H., Aunan, K., Lindhjem, H., Seip, H.M., 2009. Environmental Pollution in China: Status and Trends. Rev. Environ. Econ. Policy 3, 209–230. https://doi.org/10.1093/reep/rep009

Vienneau, D., de Hoogh, K., Bechle, M.J., Beelen, R., van Donkelaar, A., Martin, R.V., Millet, D.B., Hoek, G., Marshall, J.D., 2013. Western European Land Use Regression Incorporating Satellite- and Ground-Based Measurements of NO2 and PM10. Environ. Sci. Technol. 47, 13555–13564. https://doi.org/10.1021/es403089q

Walton, H., Dajnak, D., Beevers, S., Williams, M., Watkiss, P., Hunt, A., 2015. Understanding the health impacts of air pollution in London.

Wang, H., Zhang, Yanxu, Zhao, H., Lu, X., Zhang, Yanxia, Zhu, W., Nielsen, C.P., Li, X., Zhang, Q., Bi, J., McElroy, M.B., 2017. Trade-driven relocation of air pollution and health impacts in China. Nat. Commun. 8, 1–7. https://doi.org/10.1038/s41467-017-00918-5

Wang, M., Beelen, R., Eeftens, M., Meliefste, K., Hoek, G., Brunekreef, B., 2012. Systematic Evaluation of Land Use Regression Models for NO2. Environ. Sci. Technol. 46, 4481–4489. https://doi.org/10.1021/es204183v

Wang, S., Hao, J., 2012. Air quality management in China: issues, challenges, and options. J. Environ. Sci. China 24, 2–13. https://doi.org/10.1016/S1001-0742(11)60724-9

Wang, T., Xue, L., Brimblecombe, P., Lam, Y.F., Li, L., Zhang, L., 2017. Ozone pollution in China: A review of concentrations, meteorological influences, chemical precursors, and effects. Sci. Total Environ. 575, 1582–1596. https://doi.org/10.1016/j.scitotenv.2016.10.081

Watson, A.Y., Bates, R.R., Kennedy, D., 1988. Atmospheric Transport and Dispersion of Air Pollutants Associated with Vehicular Emissions. National Academies Press (US).

Weinmayr, G., Romeo, E., De Sario, M., Weiland, S.K., Forastiere, F., 2010. Short-Term Effects of PM_{10} and NO_2 on Respiratory Health among Children with Asthma or Asthma-like Symptoms: A Systematic Review and Meta-Analysis. Environ. Health Perspect. 118, 449–457. https://doi.org/10.1289/ehp.0900844

WHO, 2018. Air pollution [WWW Document]. URL https://www.who.int/news-room/fact-sheets/detail/ambient-(outdoor)-air-quality-and-health (accessed 12.5.19).

WHO, 2013. Review of evidence on health aspects of air pollution- REVIHAAP Project Technical Report.

WHO (Ed.), 2006. Air quality guidelines: global update 2005: particulate matter, ozone, nitrogen dioxide, and sulfur dioxide. World Health Organization, Copenhagen, Denmark.

WHO, 2005. WHO | Air quality guidelines - global update 2005 [WWW Document]. URL https://www.who.int/phe/health_topics/outdoorair/outdoorair_aqg/en/ (accessed 7.25.19).

Worldpop, 2013. China 100m Population. https://doi.org/10.5258/SOTON/WP00055

Wu, C.-D., Chen, Y.-C., Pan, W.-C., Zeng, Y.-T., Chen, M.-J., Guo, Y.L., Lung, S.-C.C., 2017. Land-use regression with long-term satellite-based greenness

index and culture-specific sources to model PM2.5 spatial-temporal variability. Environ. Pollut. 224, 148–157. https://doi.org/10.1016/j.envpol.2017.01.074

Wu, C.-F., Lin, H.-I., Ho, C.-C., Yang, T.-H., Chen, C.-C., Chan, C.-C., 2014. Modeling horizontal and vertical variation in intraurban exposure to PM2.5 concentrations and compositions. Environ. Res. 133, 96–102. https://doi.org/10.1016/j.envres.2014.04.038

Wu, H., Reis, S., Lin, C., Beverland, I., Heal, M., 2015. Identifying drivers for the intra-urban spatial variability of airborne particulate matter components and their interrelationships. Atmos. Environ. 112, 306–316. https://doi.org/10.1016/j.atmosenv.2015.04.059

Wu, H., Reis, S., Lin, C., Heal, M.R., 2017. Effect of monitoring network design on land use regression models for estimating residential NO_2 concentration. Atmos. Environ. 149, 24–33. https://doi.org/10.1016/j.atmosenv.2016.11.014

Wu, J., Li, J., Peng, J., Li, W., Xu, G., Dong, C., 2015. Applying land use regression model to estimate spatial variation of PM2.5 in Beijing, China. Environ. Sci. Pollut. Res. 22, 7045–7061. https://doi.org/10.1007/s11356-014-3893-5

Xie, X., Semanjski, I., Gautama, S., Tsiligianni, E., Deligiannis, N., Rajan, R.T., Pasveer, F., Philips, W., 2017. A Review of Urban Air Pollution Monitoring and Exposure Assessment Methods. ISPRS Int. J. Geo-Inf. 6, 389. https://doi.org/10.3390/ijgi6120389

Xu, G., Jiao, L., Zhao, S., Yuan, M., Li, X., Han, Y., Zhang, B., Dong, T., 2016. Examining the Impacts of Land Use on Air Quality from a Spatio-Temporal Perspective in Wuhan, China. Atmosphere 7, 62. https://doi.org/10.3390/atmos7050062

Xu, Z., Wang, T., Xue, L.K., Louie, P.K.K., Luk, C.W.Y., Gao, J., Wang, S.L., Chai, F.H., Wang, W.X., 2013. Evaluating the uncertainties of thermal catalytic conversion in measuring atmospheric nitrogen dioxide at four differently polluted sites in China. Atmos. Environ., Improving Regional Air Quality over the Pearl River Delta and Hong Kong: from Science to Policy 76, 221–226. https://doi.org/10.1016/j.atmosenv.2012.09.043

Xue, L., Wang, T., Louie, P.K.K., Luk, C.W.Y., Blake, D.R., Xu, Z., 2014. Increasing External Effects Negate Local Efforts to Control Ozone Air Pollution: A Case Study of Hong Kong and Implications for Other Chinese Cities. Environ. Sci. Technol. 48, 10769–10775. https://doi.org/10.1021/es503278g

Xue, T., Zheng, Y., Tong, D., Zheng, B., Li, X., Zhu, T., Zhang, Q., 2019. Spatiotemporal continuous estimates of $PM_{2.5}$ concentrations in China, 2000–2016: A machine learning method with inputs from satellites, chemical transport model, and ground observations. Environ. Int. 123, 345–357. https://doi.org/10.1016/j.envint.2018.11.075

Yang, J., Wang, Z.-H., Chen, F., Miao, S., Tewari, M., Voogt, J.A., Myint, S., 2015. Enhancing Hydrologic Modelling in the Coupled Weather Research and Forecasting–Urban Modelling System. Bound.-Layer Meteorol. 155, 87–109. https://doi.org/10.1007/s10546-014-9991-6

Yang, X., Zheng, Y., Geng, G., Liu, H., Man, H., Lv, Z., He, K., de Hoogh, K., 2017. Development of $PM_{2.5}$ and NO_2 models in a LUR framework incorporating satellite remote sensing and air quality model data in Pearl River Delta

region, China. Environ. Pollut. 226, 143–153. https://doi.org/10.1016/j.envpol.2017.03.079

Yin, P., Brauer, M., Cohen, A., Burnett, R.T., Liu, J., Liu, Y., Liang, R., Wang, W., Qi, J., Wang, L., Zhou, M., 2017. Long-term Fine Particulate Matter Exposure and Nonaccidental and Cause-specific Mortality in a Large National Cohort of Chinese Men. Environ. Health Perspect. 125. https://doi.org/10.1289/EHP1673

Yu, M., Zhu, Y., Lin, C.-J., Wang, S., Xing, J., Jang, C., Huang, Jizhang, Huang, Jinying, Jin, J., Yu, L., 2019. Effects of air pollution control measures on air quality improvement in Guangzhou, China. J. Environ. Manage. 244, 127–137. https://doi.org/10.1016/j.jenvman.2019.05.046

Yue, X., Wu, Y., Hao, J., Pang, Y., Ma, Y., Li, Y., Li, B., Bao, X., 2015. Fuel quality management versus vehicle emission control in China, status quo and future perspectives. Energy Policy 79, 87–98. https://doi.org/10.1016/j.enpol.2015.01.009

Yuyu, C., Zhe, J.G., Naresh, K., Guang, S., 2012. Gaming in Air Pollution Data? Lessons from China. BE J. Econ. Anal. Policy 13, 1–43.

Zannetti, P., 1990. Dry and Wet Deposition, in: Zannetti, P. (Ed.), Air Pollution Modeling: Theories, Computational Methods and Available Software. Springer US, Boston, MA, pp. 249–262. https://doi.org/10.1007/978-1-4757-4465-1_10

Zhang, B., Cao, C., Gu, J., Liu, T., 2016. A New Environmental Protection Law, Many Old Problems? Challenges to Environmental Governance in China. J. Environ. Law 28, 325–335. https://doi.org/10.1093/jel/eqw014

Zhang, F., Sha, M., Wang, G., Li, Z., Shao, Y., 2017. Urban Aerodynamic Roughness Length Mapping Using Multitemporal SAR Data [WWW Document]. Adv. Meteorol. https://doi.org/10.1155/2017/8958926

Zhang, J., Mauzerall, D.L., Zhu, T., Liang, S., Ezzati, M., Remais, J.V., 2010. Environmental health in China: progress towards clean air and safe water. The Lancet 375, 1110–1119. https://doi.org/10.1016/S0140-6736(10)60062-1

Zhang, P., Dong, G., Sun, B., Zhang, L., Chen, X., Ma, N., Yu, F., Guo, H., Huang, H., Lee, Y.L., Tang, N., Chen, J., 2011. Long-term exposure to ambient air pollution and mortality due to cardiovascular disease and cerebrovascular disease in Shenyang, China. PLoS ONE 6. https://doi.org/10.1371/journal.pone.0020827

Zhang, Q., He, K., Huo, H., 2012. Cleaning China's air. Nature 484, 161–162. https://doi.org/10.1038/484161a

Zheng, Y., Xue, T., Zhang, Q., Geng, G., Tong, D., Li, X., He, K., 2017. Air quality improvements and health benefits from China's clean air action since 2013. Environ. Res. Lett. 12, 114020. https://doi.org/10.1088/1748-9326/aa8a32

Zhong, L., Louie, P.K.K., Zheng, J., Yuan, Z., Yue, D., Ho, J.W.K., Lau, A.K.H., 2013. Science–policy interplay: Air quality management in the Pearl River Delta region and Hong Kong. Atmos. Environ., Improving Regional Air Quality over the Pearl River Delta and Hong Kong: from Science to Policy 76, 3–10. https://doi.org/10.1016/j.atmosenv.2013.03.012

Zhu, Y., Huang, L., Li, J., Ying, Q., Zhang, H., Liu, X., Liao, H., Li, N., Liu, Z., Mao, Y., Fang, H., Hu, J., 2018. Sources of particulate matter in China:

Insights from source apportionment studies published in 1987-2017. Environ. Int. 115, 343–357. https://doi.org/10.1016/j.envint.2018.03.037

Ziemba, L.D., Lee Thornhill, K., Ferrare, R., Barrick, J., Beyersdorf, A.J., Chen, G., Crumeyrolle, S.N., Hair, J., Hostetler, C., Hudgins, C., Obland, M., Rogers, R., Scarino, A.J., Winstead, E.L., Anderson, B.E., 2013. Airborne observations of aerosol extinction by in situ and remote-sensing techniques: Evaluation of particle hygroscopicity. Geophys. Res. Lett. 40, 417–422. https://doi.org/10.1029/2012GL054428